USAFTPS-TIM-19B-03

A LIMITED CHARACTERIZATION OF AN OPPORTUNISTIC NAVIGATION SYSTEM USING CELLUAR SIGNALS

(Project Have SNIFFER)

USAFTPS

STEVEN T. WACHTEL, Capt, USAF
Project Manager, Flight Test Engineer

RACHEL L. QUIRARTE, Capt, USAF
Test Plans Chief, Project Test Pilot

ZACHARY W. HOEFFNER, Capt, USAF
Data Management Chief, Project Flight Test Engineer

JACOB Z. DUEDE, Capt, USAF
Budget/Logistics Chief, Project Test Pilot

THOMAS P. HULSEY, Capt, USAF
Safety Chief, Project Flight Test Engineer

RUN XUAN TAY, Capt, RSAF
Reporting Chief, Project Test Pilot

JUNE 2020
FINAL TECHNICAL INFORMATION MEMORANDUM

UNITED STATES AIR FORCE TEST PILOT SCHOOL
AIR FORCE TEST CENTER
EDWARDS AIR FORCE BASE, CALIFORNIA
AIR FORCE MATERIEL COMMAND
UNITED STATES AIR FORCE

This technical information memorandum (USAFTPS-TIM-19B-03, Project Have SNIFFER Limited Characterization of an Opportunistic Navigation System Using Cellular Signals) was submitted under job order number MT19B700 by the Commandant, USAF Test Pilot School, Edwards AFB, California 93524-6485.

Prepared by:

WACHTEL.STEVEN.T.1398910865 Digitally signed by WACHTEL.STEVEN.T.1398910865 Date: 2020.06.04 12:49:35 -07'00'

STEVEN T. WACHTEL
Captain, USAF
Project Manager / Flight Test Engineer

QUIRARTE.RACHEL.LYNN.1262671328 Digitally signed by QUIRARTE.RACHEL.LYNN.1262671328 Date: 2020.06.04 16:48:09 -07'00'

RACHEL L. QUIRARTE
Captain, USAF
Project Test Pilot

HOEFFNER.ZACHARY.WILLIAM.1385304230 Digitally signed by HOEFFNER.ZACHARY.WILLIAM.1385304230 Date: 2020.06.04 17:18:16 -07'00'

ZACHARY W. HOEFFNER
Captain, USAF
Project Flight Test Engineer

DUEDE.JACOB.ZEBEDIAH.1286920736 Digitally signed by DUEDE.JACOB.ZEBEDIAH.1286920736 Date: 2020.06.04 11:10:11 -07'00'

JACOB Z. DUEDE
Captain, USAF
Project Test Pilot

HULSEY.THOMAS.P.1292834418 Digitally signed by HULSEY.THOMAS.P.1292834418 Date: 2020.06.04 06:17:28 -07'00'

THOMAS P. HULSEY
Captain, USAF
Project Flight Test Engineer

Digitally signed by TAY.RUNXUAN.1396649159
Date: 2020.06.03 22:17:45 -07'00'

RUN XUAN TAY
Captain, RSAF
Project Test Pilot

This memorandum has been reviewed and is approved for publication:

JURADO.JUAN.D.1272700300 Digitally signed by JURADO.JUAN.D.1272700300 Date: 2020.06.05 12:49:11 -07'00'

JUAN D. JURADO
Lieutenant Colonel, USAF
Staff Advisor / Director of Education
USAF Test Pilot School

LEE.CHIAWEI.NMN.1300514088 Digitally signed by LEE.CHIAWEI.NMN.1300514088 Date: 2020.06.11 16:03:19 -07'00'

CHIA WEI LEE
NH-III, DAF
Test Management Program Director
USAF Test Pilot School

VANHOY.DAVID.L.1229799688 Digitally signed by VANHOY.DAVID.L.1229799688 Date: 2020.06.12 13:31:31 -07'00'

DAVID L. VANHOY
NH-IV, DAF
Technical Director
USAF Test Pilot School

BLAKE.RYAN.D.1129274553 Digitally signed by BLAKE.RYAN.D.1129274553 Date: 2020.06.12 09:51:15 -07'00'

RYAN D. BLAKE
Colonel, USAF
Commandant
USAF Test Pilot School

REPORT DOCUMENTATION PAGE

Form Approved
OMB No. 0704-0188

1. REPORT DATE *(DD-MM-YYYY)*	2. REPORT TYPE	3. DATES COVERED *(From - Through)*
08-06-2020	Final Technical Information Memorandum	09 March - 13 March 2020

4. TITLE AND SUBTITLE

Project Have SNIFFER
Limited Characterization of an Opportunistic Navigation System Using Cellular Signals

5A. CONTRACT NUMBER
N/A

5B. GRANT NUMBER
N/A

5C. PROGRAM ELEMENT NUMBER
N/A

6. AUTHOR(S)
Wachtel, Steven, T, Captain, USAF
Quirarte, Rachel, L, Captain, USAF
Hoeffner, Zachary, W, Captain, USAF
Duede, Jacob, Z, Captain, USAF
Hulsey, Thomas, P, Captain, USAF
Tay, Run Xuan, Captain, RSAF

5D. PROJECT NUMBER
MT19B700

5E. TASK NUMBER
N/A

5F. WORK UNIT NUMBER
N/A

7. PERFORMING ORGANIZATION NAME(S) AND ADDRESS(ES)
Air Force Test Center
412th Test Wing
USAF Test Pilot School
Edwards AFB CA 93524-6485

8. PERFORMING ORGANIZATION REPORT NUMBER
USAFTPS-TIM-19B-03

9. SPONSORING / MONITORING AGENCY NAME(S) AND ADDRESS(ES)
Dr Zak (Zaher) M. Kassas
University of California, Irvine
Samueli School of Engineering
4200 Engineering Gateway Building, Room 3233
Irvine, CA 92697

10. SPONSOR/MONITOR'S ACRONYM(S)
UCI

11. SPONSOR/MONITOR'S REPORT NUMBER(S)

12. DISTRIBUTION / AVAILABILITY STATEMENT
Distribution A. Approved for public release; distribution is unlimited.

13. SUPPLEMENTARY NOTES
SC: 012100 CA: 412th Test Wing Edwards AFB CA Print this document in COLOR.

14. ABSTRACT

This report documents results of testing a system for collecting signals of opportunity that can be utilized to generate a navigation solution, under the project name Have Signals of opportunity for Navigation In Frequency-Forbidden EnviRonments (Have Sniffer). Testing was requested by University of California, Irvine (UCI), Irvine, California, in support of research sponsored by the Office of Naval Research (ONR). The executing test organization was Class 19B of the USAF Test Pilot School, Edwards AFB. Testing was conducted from 09 March 2020 to 13 March 2020 and comprised of 2 ground test hours and 4 sorties totaling 11.8 flight test hours. The first general test objective was to characterize the performance of the UCI Opportunistic Navigation system using LTE and CDMA signals. The second general test objective was to collect LEO satellite SOPs for system development and research by UCI. All test objectives were met or partially met.

15. SUBJECT TERMS
Have SNIFFER, TMP(Test Management Project), EGI(Embedded Global Navigation Satellite System/Inertial Navigation System), GNSS, INS, OpNav(Opportunistic Navigation), SOP(Signals of Opportunity), UCI(University of California, Irvine), Cellular Signals, LTE(Long Term Evolution), CDMA(Code-Division Multiple Access), BTS(Base Transceiver Station), PNT(Position, Navigation, and Timing), PVT(Position, Velocity, Time), SDR(Software Defined Radio), Kalman Filter, C-12J, Mable, Flight Test

16. SECURITY CLASSIFICATION OF:			17. LIMITATION OF ABSTRACT	18. NUMBER OF PAGES	19A. NAME OF RESPONSIBLE PERSON
a. REPORT	b. ABSTRACT	c. THIS PAGE			Dr. Zak Kassas
U	U	U	Same as Report	74	19B. TELEPHONE NUMBER (INCLUDE AREA CODE) (949) 824-5855

STANDARD FORM 298 (REV. 8-98)
PRESCRIBED BY ANSI STD. Z39.18

This page was intentionally left blank.

PREFACE

A special thank-you goes to Mr. Eric Whitaker from Los Angeles District TWLA-South Airspace Coordination Center. His extra help allowed this test to be a success.

An additional thank-you goes to the Office of Naval Research, especially Dr. Tommy Willis, for sponsoring the research that allowed this project to become a reality.

This page was intentionally left blank.

EXECUTIVE SUMMARY

This report presents the results of the *Have Signals of opportunity for Navigation in Frequency-Forbidden EnviRonments (Have SNIFFER)* test management project (TMP). The lead developmental test organization (LDTO) was the Air Force Test Center, Edwards AFB, California. The executing test organization (ETO) was Class 19B of the United States Air Force Test Pilot School (USAF TPS), Edwards AFB working in partnership with the University of California, Irvine (UCI). Testing was requested by University of California, Irvine (UCI), Irvine, California, in support of research sponsored by the Office of Naval Research (ONR). Testing was conducted by the *Have SNIFFER* Test Team IAW the *Have SNIFFER* Test Plan (reference 1) and comprised of 2.0 ground test hours and four sorties totaling 11.8 flight test hours. Testing was performed in a 586th Flight Test Squadron C-12J, serial number 86-0080 from 09 March 2020 to 13 March 2020 within the R-2515 airspace and in the civil airspace near Palmdale and Riverside, CA under the Job Order Number MT19B700.

Nearly every military aircraft today is equipped with an Embedded Global Navigation Satellite System/Inertial Navigation System (Embedded GNSS/INS, or EGI). However, in GNSS-denied environments, a drifting INS-only solution can degrade mission effectiveness. *Have SNIFFER* tested UCI's Opportunistic Navigation (OpNav) algorithm, associated software, and the hardware needed to passively collect signals of opportunity (SOPs) and generate a navigation solution without the aid of traditional GNSS signals. The system under test (SUT) collected Code-Division Multiple Access (CDMA) and Long-Term Evolution (LTE) cellular signals as well as some Low Earth Orbit (LEO) satellite signals. Previous work by UCI had demonstrated this system on a small unmanned aerial vehicle at 200 ft Above Ground Level (AGL). *Have SNIFFER* was the first test of this system on a full-scale aircraft.

The general test objectives (GTOs) were:
1) Characterize the performance of the UCI OpNav system using LTE and CDMA signals.
2) Collect LEO satellite SOPs for system development and research by UCI.

The SUT was flown in three different geographic regions: R-2515 (near Edwards Air Force Base), airspace over Palmdale, CA, and airspace over Riverside, CA. These regions were selected to expose the SUT to varied levels of SOP density. Testing was accomplished from 500 ft AGL up to 25,000 ft MSL at approximately 160 KIAS. Maneuvers included segmented teardrop climbs to characterize signals in the vertical spectrum, and racetracks and grid maneuvers at selected altitudes to characterize navigation performance. Data collected included carrier-to-noise ratio, emitter geometry, and aircraft position. From these data, the presence of signals at various altitudes, the theoretical best performance, and the Root Mean Square (RMS) error of the navigation solution were used to characterize the SUT over the different geographic regions. Due to the developmental nature of this technology, a navigation solution was not generated real-time during the test sorties. Instead, the data collected was post-processed by UCI to generate a map of detected SOP emitters and a navigation solution.

The SUT was able to detect signals in all tested regions and altitudes. CDMA signals were found to be much stronger than LTE signals and provided a more useful source for OpNav; however, CDMA is primarily used in the US and is being phased out by many cellular carriers. Analysis of theoretical performance metrics showed that vertical theoretical variance must be much larger than the horizontal variance. The navigation error was on the same order of magnitude as previous testing accomplished by UCI with a small UAV. The OpNav system, with further development, could provide military utility in a number of applications subject to GNSS denial. With a more mature system, future testing should focus on real-time navigation and the use of more relevant SOPs, like LTE.

This page was intentionally left blank.

TABLE OF CONTENTS

Page No.

LIST OF FIGURES

LIST OF TABLES

This page was intentionally left blank.

INTRODUCTION

This report presents the results of the Have Signals of opportunity for Navigation in Frequency-Forbidden EnviRonments (*Have SNIFFER*) test management project (TMP). The lead developmental test organization (LDTO) was the Air Force Test Center, Edwards AFB, California. The executing test organization (ETO) was Class 19B of the United States Air Force Test Pilot School (USAF TPS), Edwards AFB working in partnership with the University of California, Irvine (UCI). Testing was requested by University of California, Irvine (UCI), Irvine, California, in support of research sponsored by the Office of Naval Research (ONR). Testing was conducted by the *Have SNIFFER* Test Team IAW the *Have SNIFFER* Test Plan (reference 1) and comprised of 2.0 ground test hours and four sorties totaling 11.8 flight test hours. Testing was performed in a 586th Flight Test Squadron C-12J, serial number 86-0080 from 09 March 2020 to 13 March 2020 within the R-2515 airspace and in the civil airspace near Palmdale and Riverside, CA under the Job Order Number MT19B700.

BACKGROUND

Most military aircraft are equipped with an Embedded Global Navigation Satellite System/Inertial Navigation System (EGI). In the age of precision warfare and autonomous systems, accurate Positioning, Navigation, and Timing (PNT) are essential for nearly every military operation. However, Global Navigation Satellite System (GNSS) signals may be limited due to masking by terrain or buildings, inadvertent jamming by other signals, or deliberate jamming or spoofing by an adversary. Without frequent GNSS updates, the EGI can be forced to navigate solely with the Inertial Navigation System (INS). Over time, the INS solution drifts, and the accumulated error can prevent the system from performing its mission (reference 2).

Opportunistic Navigation (OpNav)

An alternative approach to traditional navigation is to exploit Radio Frequency (RF) Signals of Opportunity (SOPs), such as cellular, Wi-Fi, AM/FM, television, and satellite data links, for navigation purposes. These signals are abundant, geometrically diverse, large in bandwidth, and relatively high-powered compared to GNSS (reference 2). Navigation with SOPs is referred to as Opportunistic Navigation (OpNav). The main challenge that OpNav systems face is a lack of knowledge of the transmitter's position and clock error. This information is provided in the navigation message from GNSS satellites, but not in the transmission from a cellular Base Transceiver Station (BTS, informally known as a "cell phone tower"). This means that the OpNav system must either have a-priori knowledge of the emitter's location or make an estimate of the emitter's location. The a-priori method relies on either a system of multiple networked receivers or a database of emitters. The estimation method is referred to as Simultaneous Localization and Mapping, or "SLAM" (reference 2). From a military utility perspective, the SLAM approach has obvious benefits and tremendous potential. However, it is the more technically challenging of the two methods, requiring the a-priori method to be matured first. This test only investigated the a-priori method.

Previous Work

With the sponsorship of the Office of Naval Research (ONR), UCI has demonstrated the use of Code Division Multiple Access (CDMA), Long-Term Evolution (LTE), and Low Earth Orbit (LEO) satellite downlink signals to produce SOP-aided INS solutions for a small Unmanned Aerial Vehicle (UAV) (references 2 and 3). With CDMA and LTE signals, 3D navigation error was demonstrated on the order of 5 m, but the experiment was conducted for only 50 seconds of GPS unavailability at a maximum airspeed of 30 knots at 200 ft AGL (reference 2). *Have SNIFFER* was the first test of this system on a full-scale aircraft. For brevity, the term "System Under Test" (SUT) refers to UCI's OpNav software and hardware.

Observables

In general, the SUT exploited three BTS observables for OpNav: pseudorange, carrier-to-noise ratio, and Doppler. The following sections will further describe these exploitable observables.

Pseudorange

Pseudorange is traditionally used to describe the distance between a satellite and a receiver, but the concept applies similarly to ground-based emitter/receiver pairs. By measuring the time delay between the signal leaving the emitter and reaching the receiver, the pseudorange, ρ, can be calculated from the following equation:

$$\rho = c * (\Delta t + \tau) + \varepsilon$$

where c is the speed of light, Δt is the time delay, τ is the receiver clock error, and ε is zero-mean white Gaussian noise. Due to the scaling provided by c, a very short timing error can translate to hundreds or even thousands of meters (reference 4).

Carrier-to-Nose Ratio (C/N_0)

Carrier-to-noise ratio is defined as the ratio of the total carrier signal power to the noise power. This metric is crucial because it directly related to the variance of the pseudorange, and therefore to the variance of the BTS location estimate and the navigation solution estimate (reference 5). A higher C/N_0 correlates to a smaller (better) variance.

Doppler

The Doppler Effect is the change in observed frequency due to relative motion between a transmitter and receiver. This change, known as the "Doppler shift," is directly proportional to the relative velocity between the transmitter and receiver. The frequency of the shift is described by:

$$\nu = \frac{V_r}{\lambda}$$

where v is the Doppler shift, V_r is the relative velocity between the transmitter and receiver, and λ is the wavelength of the transmission (reference 4). In the context of OpNav, by measuring the Doppler shift, the receiver can estimate its motion relative to the emitter.

Cellular Signals

Of the many "ambient" signal types available for OpNav, cellular signals are among the most useful. Most cellular modulation techniques are time-sensitive and therefore contain a time synchronization component. OpNav systems can use the available time information to estimate a timing difference between when the signal was sent from the BTS and when it was received. This test focused primarily on OpNav with LTE and CDMA signals. At the time of this test execution there were 14 countries, including the United States and China, using CDMA networks. Six of those 14 networks were scheduled to transition to LTE or shut down completely by 2024 (reference 6). Additionally, the majority of the countries around the world currently make use of an LTE network in some fashion (reference 7).

Long-Term Evolution (LTE) (reference 12)

LTE is a fourth-generation (4G) communication standard for many cellular providers. LTE uses Orthogonal Frequency Division Mutliplexing (OFDM) to transmit signals from BTS to receivers. Frequency division multiplexing means that LTE receivers must tuned to the exact frequency of the subcarriers to use LTE signals. This operational characteristic also implies that LTE signals are sensitive to frequency interference. In the aerial environment, some of this interference may come from neighboring BTSs because there is less environmental signal attenuation in the air than on the ground. On another note, the orthogonality among subcarriers in OFDM signals is only maintained if the receiver uses an oscillator that is synchronous with the carrier signal in the received signal. A mismatch in carrier frequency, also known as carrier frequency offset (CFO), can result in inter-carrier interference, thereby reducing the C/N_0 of the received signal. While CFO algorithms can estimate the amount of offset and compensate for it, some residual CFO may continue to exist. Doppler Effect is another example that can cause CFO.

Code-Division Multiple Access (CDMA) (reference 13)

CDMA is a third-generation (3G) wireless communication system that uses a technique called direct sequence spread spectrum modulation to enable multiplexing over the same channel. CDMA signals are spread with maximal-length pseudorandom noise (PN) sequences and receivers must have the same PN sequence to demodulate the signal. This modulation technique means that multiple users and BTSs can use the same carrier frequency without interfering much with one another. To distinguish the received data from different BTSs, each station uses a shifted version of the PN sequence, also known as PN offset. This operational characteristic means that the an OpNav system needs only a single antenna to receive signals from multiple CDMA BTSs. CMDA receivers also benefit from processing gain as the actual signal is demodulated from wider bandwidth carrier signal. This processing gain means CDMA signals are less susceptible to electrical noise and interference from other radio signals, and thus, may have longer range than LTE signals for OpNav systems.

Low Earth Orbit (LEO) Satellites

LEO satellite signals may also be useful SOPs for OpNav for several reasons. First, LEO satellites' downlink signals are generally more powerful than GNSS signals, as LEO satellites orbit at about 1/20 the distance of GNSS satellites. Second, LEO satellites orbit the earth at much faster speed as compared to GNSS satellites, making LEO satellites' Doppler measurements more useful to exploit. Third, commercial use of LEO satellites continues to grow, increasing the number and diversity of available sources of OpNav information. However, the error model of signals from LEO satellites signals for OpNav was not well defined at the point for this test. Hence, the signals from LEO satellites were collected solely for further research and development and no analysis of these signals were presented in this report.

Cramér-Rao Lower Bound (CRLB)

The CRLB is a theoretical expression of the best (lowest) possible variance of an estimated parameter, which is based on the estimation model and probability of the system errors. For the SUT, CRLB was a function of SOP emitter geometry and C/N_0. CRLB is introduced here because it will be utilized to describe the theoretical lower bound of the variance of the OpNav navigation solution. A full explanation of the CRLB metric is found in Appendix A.

TEST ITEM DESCRIPTION

The SUT was the UCI-developed OpNav algorithm, associated software, and RF collection system. The core of the SUT was a Software-Defined Receiver (SDR) called MATRIX (Multichannel Adaptive TRansceiver Information eXtractor), originally developed at the Autonomous Systems Perception, Intelligence, and Navigation (ASPIN) Laboratory at the University of California, Riverside. The ASPIN Lab had since relocated to UCI. The SUT hardware was provided by UCI and installed on the test aircraft at Holloman AFB, NM, where it underwent environmental testing prior to arrival at Edwards AFB, CA. Environmental testing included a vibration test to ensure the rack and its contents would not become hazards inside the C-12 cabin.

MATRIX was capable of both extracting pseudorange and estimating the Doppler shift of the acquired signal. With the appropriate antennas and SDR modules, the system could collect SOPs in each of the bands shown in Table 1.

Table 1: SOP Emitter and Frequency Bands

Frequency Band	Emitter
137 – 138 MHz	Orbcomm LEO satellites
720 – 900 MHz	LTE & CDMA
1900 – 2200 MHz	LTE
2300 – 2600 MHz	LTE & Globalstar LEO satellites

The SUT could provide either real-time monitoring or recording of received signals during flight. Post-flight, in-phase and quadrature components of the data was extracted and post-processed to create a PVT (Position, Velocity, Time) solution. With further development, aided by the results of this test, the PVT solution was expected to be made available real-time. An overview of the system is shown in Figure 1.

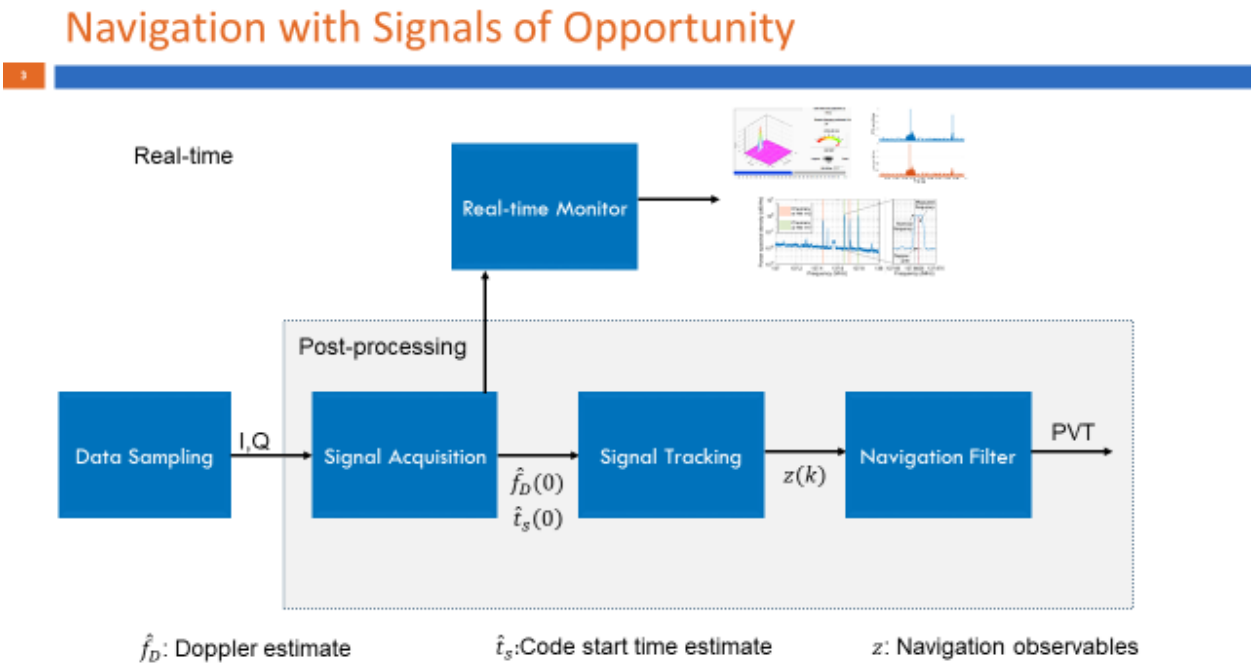

Figure 1: SUT Overview

The MATRIX LTE module used a four-stage process to generate observables from the carrier signals: acquisition, system information extraction, tracking, and timing information extraction. The result was a Time Of Arrival (TOA) estimate, which was then converted to a pseudorange. Figure 3 describes the architecture of the LTE module (reference 2). The CDMA module functioned similarly.

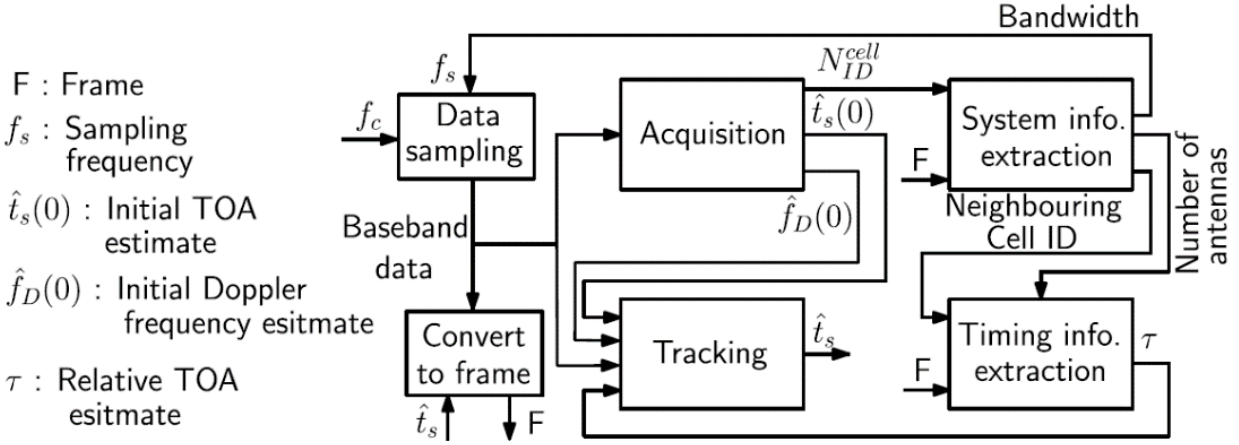

Figure 3: LTE Module of the MATRIX SDR

Once a pseudorange was generated, it was passed to an Extended Kalman Filter (EKF), similar to a Kalman Filter used in a tightly-coupled EGI. The main difference was that it estimated the states (position and clock error) of the emitter(s) while simultaneously estimating the navigating vehicle's states (position, velocity, Inertial Measurement Unit [IMU] measurement error, and receiver clock error). Figure 2 shows the framework of the filter (reference 2). $\hat{x}^-$ and $\hat{P}^-$ represent state and error covariance predictions, respectively, while $\hat{x}^+$and $\hat{P}^+$ represent state and covariance updates.

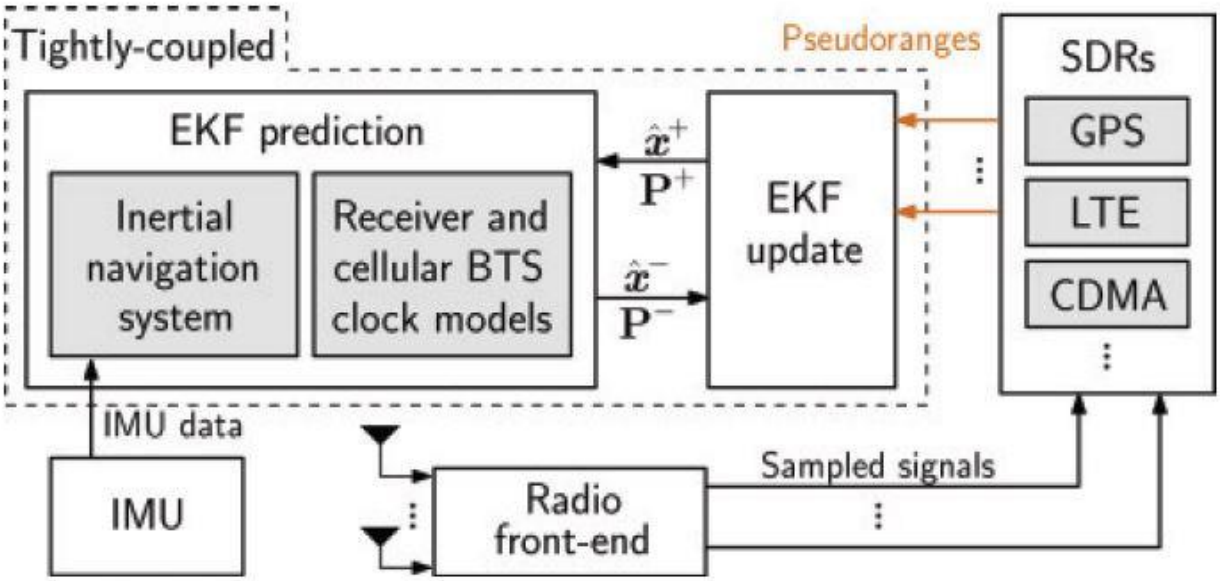

Figure 2: Tightly-Coupled Cellular-Aided INS Framework

The SUT also included a Vectornav IMU, however, due to the tight reporting timeline of this report, a physics-based IMU model was used in the EKF instead to generate PVT solution.

TEST AIRCRAFT

The SUT was installed on the 586th Flight Test Squadron's C-12J "Mable" aircraft (USAF S/N 86-0080), shown in Figure 4. A VHF antenna for receiving Orbcomm signals was mounted at the Dorsal Controlled Reception Pattern Antenna (CRPA) port. The Globalstar antenna was mounted on the cockpit dashboard while an array for four cellular antennas was mounted in the ventral interchangeable mission antenna port. A more detailed description of the antennas used for this test can be found in Appendix B.

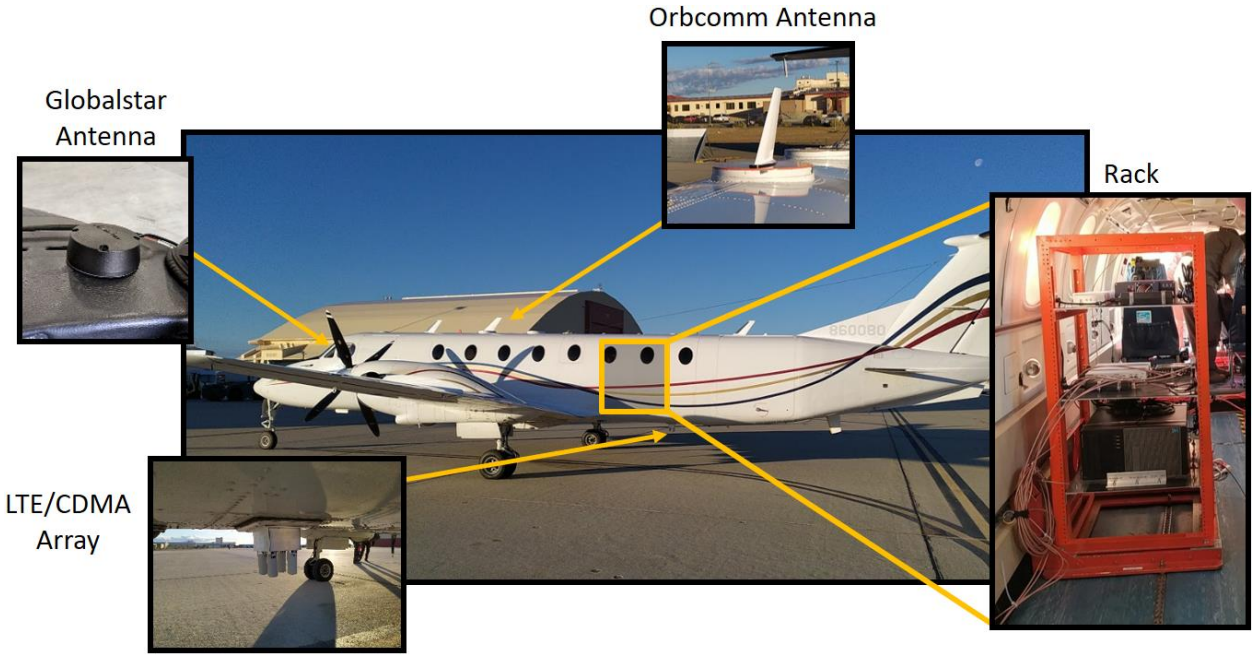

Figure 4: SUT Installed on C-12J "Mabel"

Mable was equipped with a Fighter Instrumentation Navigation System (FINS) rack, which houses all of the aircraft's Time-Space-Position Information (TSPI) sources, including a Honeywell H764-ACE EGI capable of providing TSPI at a 1Hz data rate. Accuracy specifications for the EGI are found in Table 2.

Table 2: Honeywell H764-ACE EGI Accuracy

	Blended INS/GPS Specs
Position	5m SEP
Velocity	0.01 m/s (0.03 ft/sec)
Heading	0.015 deg
Pitch/Roll	0.01 deg

For this test, the navigation solution was generated post-flight. For a real-time OpNav system, the BTS state estimates and pseudoranges would be used to correct INS errors when GNSS signals are unavailable. BTS state estimates would be continually refined as the vehicle navigates (reference 2).

TEST OBJECTIVES

The first general test objective was to characterize the performance of the UCI OpNav system using LTE and CDMA signals. The first general test objective was partially met because oceanic flights were not flown. The Specific Test Objectives (STOs) were as follows:

1. Demonstrate in-flight functionality of the SUT
2. Determine the best theoretical performance of the SUT
3. Determine the navigation performance of the SUT

The second general test objective was to collect LEO satellite SOPs for system development and research by UCI. The second general test objective was met.

Table 3 shows the objective status after testing was complete.

Table 3: Test Objectives Status

GTO 1	**Partially Met**
STO 1	Met
STO 2	Partially Met
STO 3	Partially Met
GTO 2	**Met**

LIMITATIONS AND CONSTRAINTS

There were several test limitations that prevented the general test objectives from being fully met.

Several constraints to testing limited the scope of the activities in the test.

The SUT was unable to simultaneously monitor and record signals, so the test team was limited to either recording or monitoring the signals present. Originally, the test team had planned to record signals in both climbing and descending flight over a specific geographic point. Because of the SUT's inability to monitor while recording, signals were recorded either during climbing or descending flight. Any hysteresis within the SUT was not formally measured.

The test team planned to characterize four geographic regions from 500 ft AGL to 25,000 ft Pressure Altitude (PA). A diagram of proposed regions for testing can be found in Appendix C. Not all of these altitudes and regions were attainable during this test, primarily due to scheduling and air traffic control constraints.

Due to air traffic control constraints, the test team was not able to perform all the maneuvers planned in region B and D. In execution, the maximum altitude attained in region B was 17,500 ft MSL and therefore, the SUT was only characterized to approximately 15,000 ft AGL in region B. In region D, two

primary altitudes of 6,000 ft MSL and 17,000 ft MSL were flown. Hence, the SUT was primarily characterized at two altitudes of 5,100 ft AGL and 16,100 ft AGL.

Due to the nationwide response to the COVID-19 pandemic, the C-12J was recalled back to Holloman AFB after only four test flights. With only four flights flown out of eight flights planned for this test, there was no opportunity to attempt a flight to region C. Hence, no data were obtained in region C.

The aircraft flight dynamics presented challenges previously unseen by the UCI team because this was the first time the SUT had been implemented on a full-scale aircraft. Because of the relatively high speeds flown in this test compared to previous research, tracking signals was more difficult than previously experienced. The Doppler shift observed during testing was higher than previously seen, and the high speeds meant that the signal strength was constantly changing throughout flight. The SUT had difficulty tracking LTE signals, and a navigation solution was unable to be generated from them. Although LTE signals were recorded and analyzed, all navigation solutions were generated from CDMA data only.

At its current maturity level, the SUT was not able to generate a 3D navigation solution. Only 2D navigation solutions are presented in this report. This constraint only affected the third specific test objective. The best theoretical performance in both 2D and 3D was still calculated.

A timing error was identified between the SUT and FINS position estimates for one of the data sets collected at low altitude in Region B. This error was corrected, but, due to low consistency metrics, other data sets are suspected to have a similar error. Due to the reporting timeline of this test, this error remains unverified. The remaining suspect data sets are the high altitude Region A data set and the remainder of the low altitude Region B data. For completeness, the data are reported as-is.

Even with these constraints to testing, the performance of the SUT could be characterized using the signals collected, and LEO satellite SOPs were collected for future research. Therefore, the general objectives of this test were partially met, and the primary questions presented in the test plan were answered.

TEST AND EVALUATION

The 2D Square Root of the Trace (SROT) of the CRLB, an indicator of best theoretical performance, had a mean across all regions of 11.8 meters and the 2D condition number of the CRLB had a mean across all regions of 18.0. The post-processed navigation solutions had a mean accuracy of 13.6 ± 5.8 meters. Overall, with CDMA signals, the SUT scaled well from previous testing on a small UAV to full-scale testing on the C-12J. **Future development and test of the OpNav system should include real-time navigation solution generation. (R1)**[1]

TEST METHODS AND CONDITIONS

Three flight test techniques (FTTs) were used to collect LTE, CDMA, and LEO satellite signal data for SUT characterization. A climbing or descending teardrop maneuver, as shown in Figure 5, was accomplished while monitoring or recording data to demonstrate in-flight functionality of the SUT. Three maneuvers were used to determine best theoretical performance and navigation performance of the SUT: the teardrop, the racetrack (Figure 6) and the Sniffer Straight and Level Grid (Figure 7). Collection of LEO satellite SOPs was accomplished during all three maneuvers, or during transit, as necessary.

The configuration of the SUT prohibited simultaneous monitoring and recording of signals, therefore, prior to the start of a maneuver, one pass was dedicated to identifying the desired cellular signals. The SUT was then configured to record up to four of the identified cellular frequencies, based on the highest-strength signals observed during the identification pass. In addition, the customer provided known frequencies of interest for some regions. Because the mounted cellular antennas were omni-directional, there was no requirement to remain on a specific heading while passing over the geographic points. The teardrop maneuver was flown to the lowest altitude achievable based on visual flight rules, Air Force Instructions (AFI), or the test safety plan and highest practical altitude based on Air Traffic Control (ATC) considerations or the aircraft flight envelope. LTE and CDMA carrier to noise ratios (CNR or C/N_0) were computed post-flight.

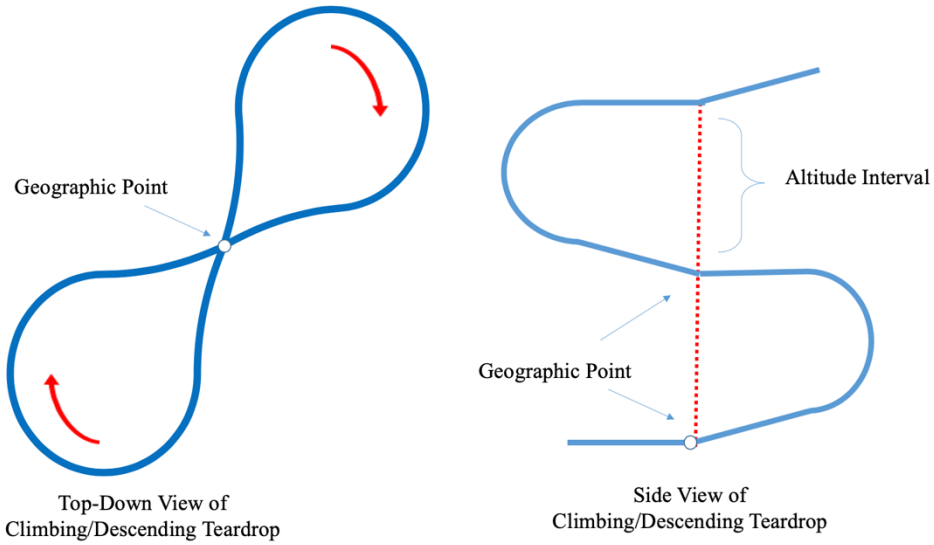

Figure 5: Climbing/Descending Teardrop

[1] Numerals following an "R" represent recommendation numbers.

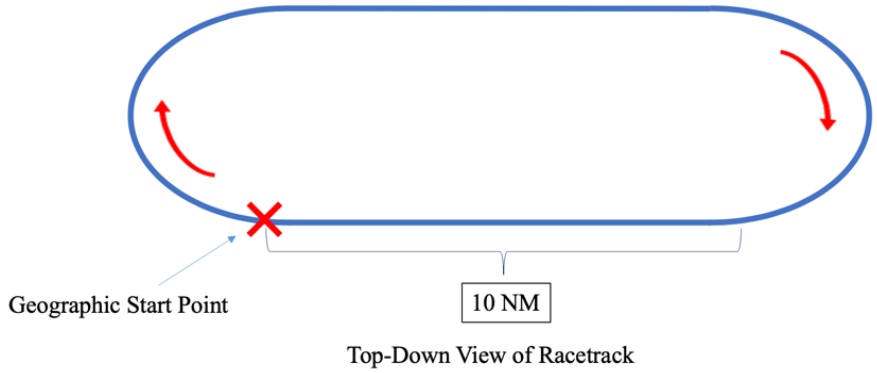

Figure 6: Racetrack Maneuver

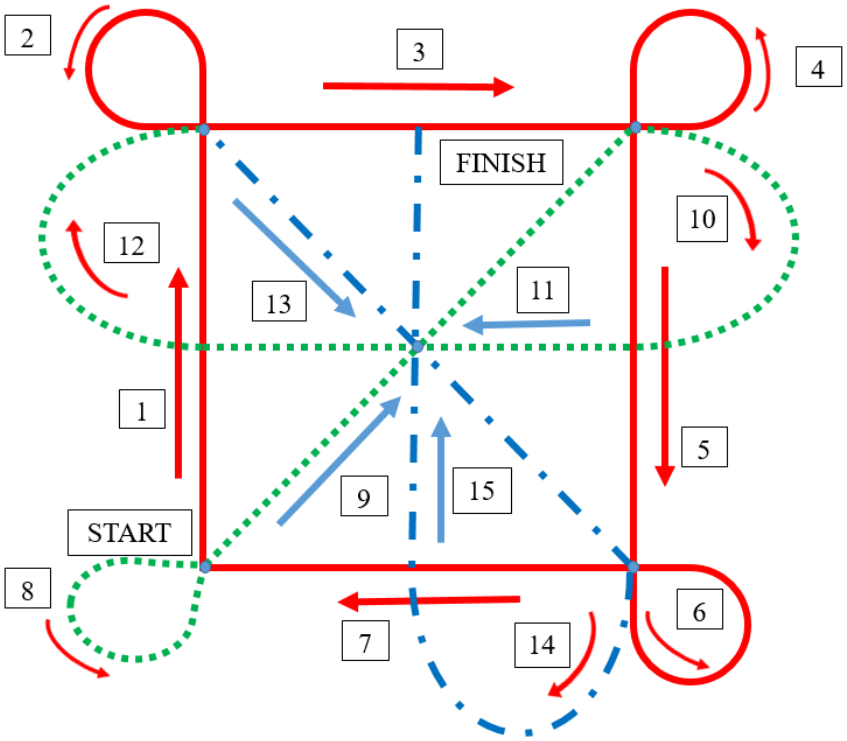

Figure 7: Sniffer Straight and Level Grid Maneuver

The Sniffer Straight and Level Grid and the racetrack maneuvers were flown at altitudes determined after preliminary analysis of signal strength versus altitude from the teardrop maneuver in each region. The geographic center point coordinates, maneuver, and altitude flown for each region are shown in Table 4 and Figure 8. UCI determined the two altitudes to conduct the Sniffer Straight and level flight at a low altitude to similar to an aircraft on approach. The higher altitude was determined for the highest altitude at which UCI expected they could produce a navigation solution.

Table 4: Geographic Point Coordinates and Maneuvers per Region

Region	Latitude	Longitude	Elevation	Maneuver	Altitude Flown
A (R-2515)	N 35° 03.21’	W 117° 57.09’	2,800 ft	Teardrop	3,300 ft MSL – 25,000 ft MSL
				Sniffer S&L Grid	7,500 ft MSL & 20,000 ft MSL
B (Palmdale)	N 34° 41.11’	W 118° 09.60’	2,500 ft	Teardrop	3,500 ft MSL – 17,500 ft MSL
	N 34° 40.86’	W 118° 04.27’	2,500 ft	Racetracks	5,500 ft MSL & 10,000 ft MSL
D (Riverside)	N 33° 55.42’	W 117° 24.14’	945 ft	Racetracks	6,000 ft MSL & 17,000 ft MSL

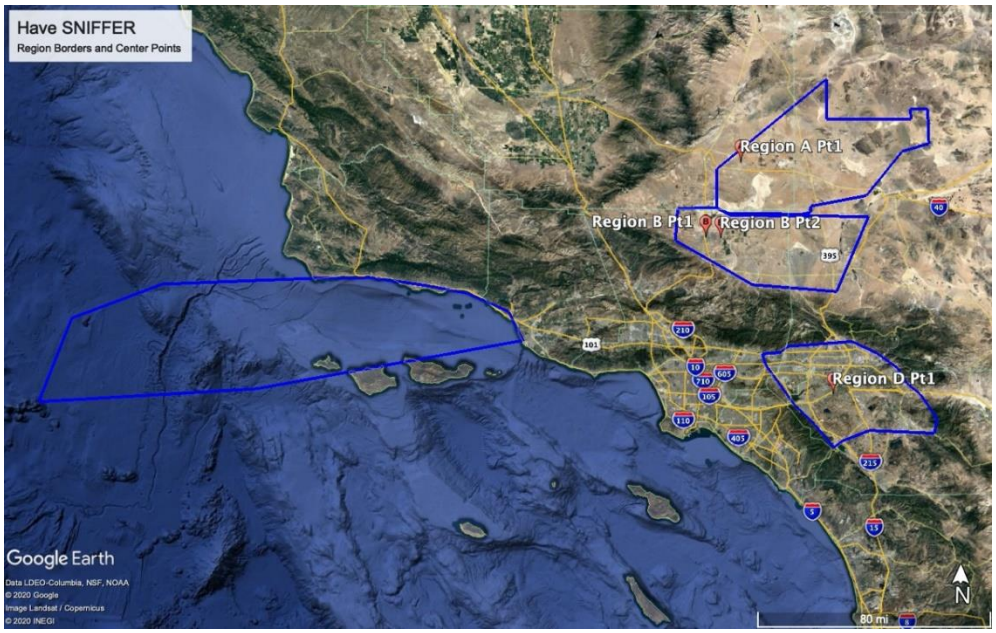

Figure 8: Geographic Regions and Center Points

The functionality of the SUT was demonstrated by first observing that the SUT was detecting SOPs. The SUT was then configured to record SOP C/N_0 with increasing altitude. To accomplish this, a teardrop FTT was flown while continuously recording data in Regions A and B.

The CRLB was used to describe the theoretical lower bound of the variance of the OpNav navigation solution. Two metrics were used to analyze the calculated CRLB: the square root of the trace of the CRLB and the condition number of the CRLB. The square root of the trace of the CRLB characterizes the size of the error ellipse, while the condition number characterizes its shape. Both the square root of the trace and condition number can only take on positive values.

The trace of a square matrix is defined as the sum of its diagonal entries. In the case of a CRLB matrix, the diagonal entries represent the variance in the estimation of each of the parameters in question. Namely, the first two or three diagonal entries (σ_{11}, σ_{22}, and σ_{33}) in the CRLB matrix represent the variance around the estimation of the vehicle’s two-dimensional (2D) or three-dimensional (3D) position respectively. Therefore, the square root of the trace yields a succinct metric for the total 2D or 3D position uncertainty in units of distance. For brevity, the square root of the trace will be referred to as “SROT."

The condition number represents the ratio of the largest over the smallest axes of the 3D (2D) error ellipsoid (ellipse) derived from the CRLB matrix. A large condition number means the ellipsoid (ellipse) is elongated along the major axis. As the condition number trends towards a value of 1 (the condition number is at least 1 by definition), the major and minor axes become equal and the ellipsoid (ellipse) becomes a sphere (circle), which is ideal for a navigation solution.

The SROT and the condition number were calculated for both the 2D (ignoring altitude variance) and 3D cases from the SUT-collected 8 Hz sample data as stated in Appendix A. Partial autocorrelation analysis was then preformed on the SROT, the condition number, and each element of the CRLB matrix in order to determine the necessary sample spacing to ensure sample correlation was limited to no more than 10%. A sample correlation of 10% is a 412th TW common standard for considering samples independent.

The SUT did not provide real-time navigation data. Instead, UCI post-processed the collected data to generate a navigation solution using the CDMA SOPs. C-12J FINS data were considered "truth" for this investigation. SUT accuracy and consistency were calculated in each geographic region and altitude block where data were collected. Accuracy was calculated by first finding the 2D radial position error, using the Root Sum Square (RSS) of the North and East position error components of the 8 Hz sample data. Partial autocorrelation analysis was then performed on the 2D radial position error to determine the necessary sample spacing to limit sample correlation to no more than 10%. Finally, the Root Mean Square (RMS) error was calculated from the resulting independent samples. The reader should note that the down sampling rate required for independent navigation error samples was not necessarily the same as the rate required for independent CRLB samples.

Consistency was calculated to determine the SUT's ability to estimate its own error statistics. A 95% confidence ellipse was drawn at each time step corresponding to the independent position error samples. The FINS truth position was then compared to the ellipse. Figure 9 shows an inconsistent data sample, where the truth position falls outside of the within the ellipse. Figure 10 shows an example of a consistent data sample, where the truth position falls within the uncertainty ellipse. The number of consistent samples was divided by the number of total samples to determine a consistency percentage.

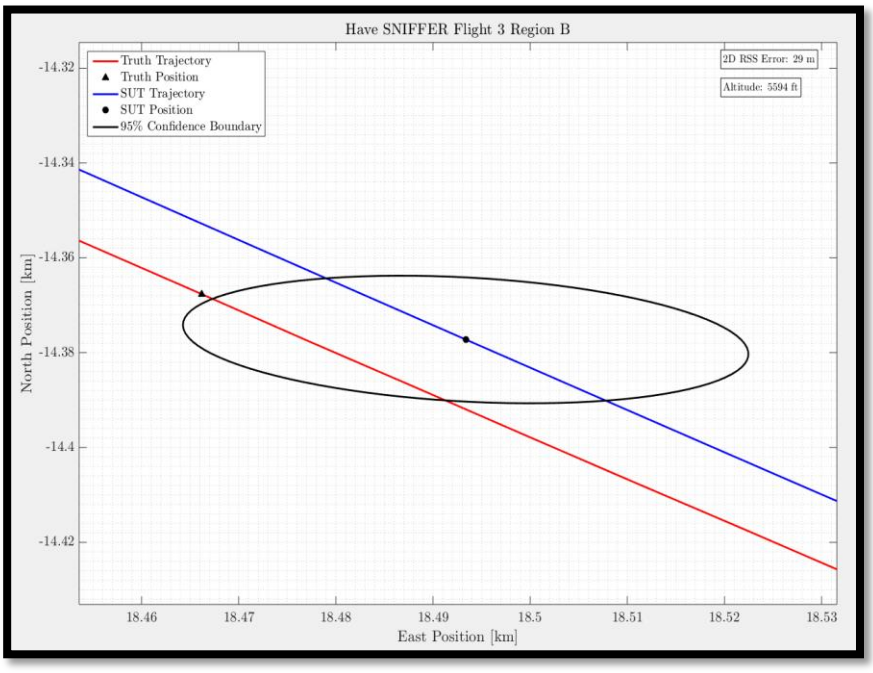

Figure 9: Inconsistent Data Sample

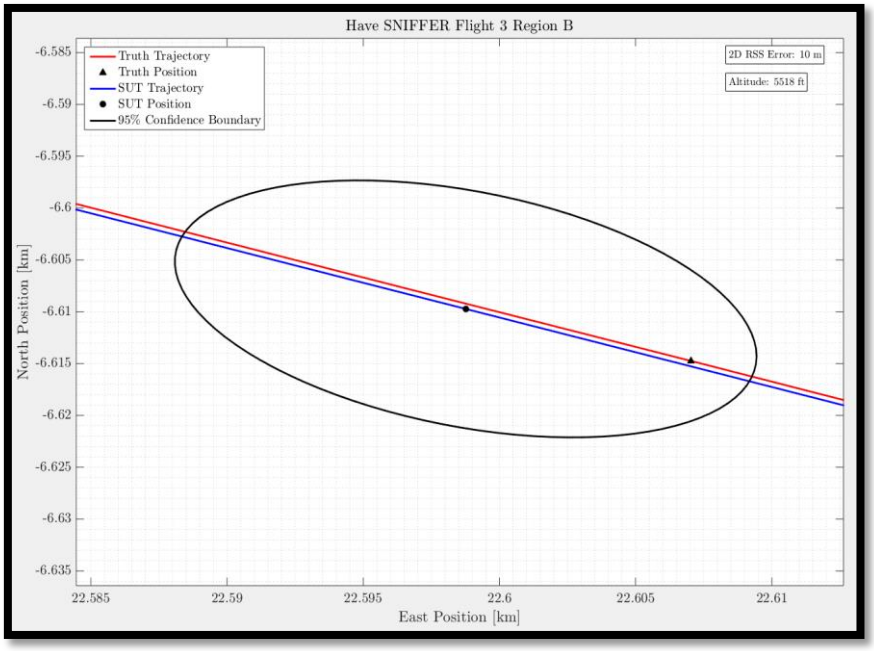

Figure 10: Consistent Data Sample

Finally, SUT accuracy (2D radial position error) was plotted against the SROT of the CRLB. Since the CRLB represents the theoretical lower bound of performance, it was expected that the accuracy of the system would vary directly with the SROT of the CRLB. 2D radial position error was calculated at each of the positions where the independent CRLB samples were taken.

UCI OPNAV SYSTEM PERFORMANCE

The first general test objective was to characterize the performance of the UCI OpNav system using LTE and CDMA signals. Throughout testing, a list of BTSs that the SUT detected was maintained. That list and the accompanying map of BTSs can be found in Appendix D. Once the SUT mapped the towers, the UCI team was able to use them to generate a post-flight navigation solution.

In-Flight Functionality Demonstration

The specific test objective was to demonstrate in-flight functionality of the SUT. The SUT needed to detect a single signal to demonstrate functionality. This specific test objective was met.

Test Results

CDMA and LTE Signals were recorded during a climbing teardrop FTT in Regions A and B. The results can be found in Table 5. Green "Y" cells indicate that a signal was detected at the corresponding altitude and region. Red "N" cells indicate that a signal was not detected. Unfilled cells indicate that testing was not accomplished at that particular altitude and region.

Region A was a region of low SOP density and Region B was a region of high SOP density. The test team expected signals from regions of lower SOP density to extend higher into the atmosphere because of the increased power from the transmitted towers. Transmit power is lower in higher density regions to avoid interference between towers (reference 8). Table 5 shows the test results from the climbing or descending teardrop. A single signal detection was the only requirement to place a "Y" in the corresponding altitude cell. As expected, signals in lower density regions were detected at a higher altitude when compared to higher density regions. The increase in detection altitude in low density areas was attributed to the increased power of each individual transmitter.

As shown in Table 5, LTE signals in regions with higher transmitter density tended to decay faster with altitude when compared to regions with lower transmitter density. CDMA signals were detected at each altitude flown, and at times up to distances of 68 NM away from the transmitting tower (see Figure D1). The higher detection altitude of CDMA suggests it may be an easier source to utilize for OpNav than LTE. This trend was observed in all the regions tested. At the conclusion of testing, the team was unable to determine the maximum altitude for the CDMA signals, because the signals were detected up to and including the service ceiling of the C-12J. The service ceiling was 25,000 feet pressure altitude, which corresponded to 22,000 feet AGL in Region A.

Table 5: CDMA and LTE SOP Detection

	Region A		Region B	
Altitude (ft AGL)	CDMA	LTE	CDMA	LTE
0	-	-	-	-
500	Y	Y	-	-
1000	Y	Y	Y	Y
2000	Y	Y	Y	Y
3000	Y	Y	Y	Y
4000	Y	Y	Y	Y
5000	Y	Y	Y	Y
6000	Y	Y	Y	Y
7000	Y	Y	Y	Y
8000	Y	Y	Y	Y
9000	Y	Y	Y	Y
10000	Y	Y	Y	Y
11000	Y	Y	Y	Y
12000	Y	Y	Y	Y
13000	Y	Y	Y	Y
14000	Y	Y	Y	N
15000	Y	Y	Y	N
16000	Y	Y	-	-
17000	Y	Y	-	-
18000	Y	Y	-	-
19000	Y	Y	-	-
20000	Y	N	-	-
21000	Y	N	-	-
22000	Y	N	-	-

Figure 11 and Figure 12 show strength of CDMA and LTE signals as a function of altitude in Region A. The CDMA signal in Figure 11 is one example of the CDMA signals detected. PN240 is the pseudorandom noise offset from the tower. In the case of PN240, the signals were all detected from the same tower. Figure 12 shows the LTE signals collected in Region A. The 751 MHz signal came from a single tower, while the 731.5 MHz signal was collected from only the highest power tower of several available, at times switching towers throughout the FTT.

UCI's previous research determined that LTE signals, when compared to CDMA signals, required a higher C/N_0 to generate reliable navigation solutions. Similarly, the SUT had a lesser ability to detect the presence of an LTE signal than a CDMA signal. LTE signals were not identifiable below approximately 40 dB-Hz, while CDMA signals were observed to as low as 25 dB-Hz. For the SUT, the detection threshold for LTE signals was approximately 15 dB-Hz higher than the CDMA threshold. In other words, the LTE required 32 times the power of the CDMA C/N_0 to detect the signal. Both LTE and CDMA

signals were collected using the same antennas, cable types, amplifiers, and radio receiver. Because the SUT used the same hardware for the collection of both signals, the results from this limited test show a higher C/N_0 required for LTE navigation versus CDMA.

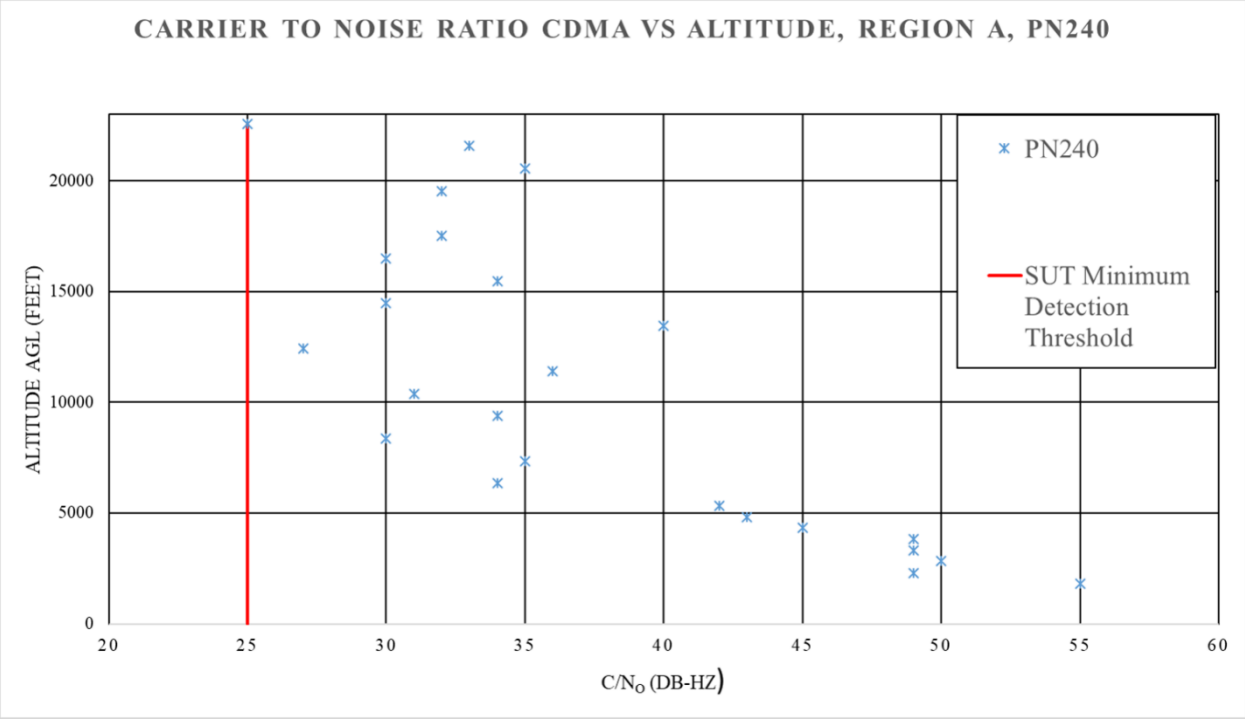

Figure 11: C/N_0 vs Altitude for CDMA Signals

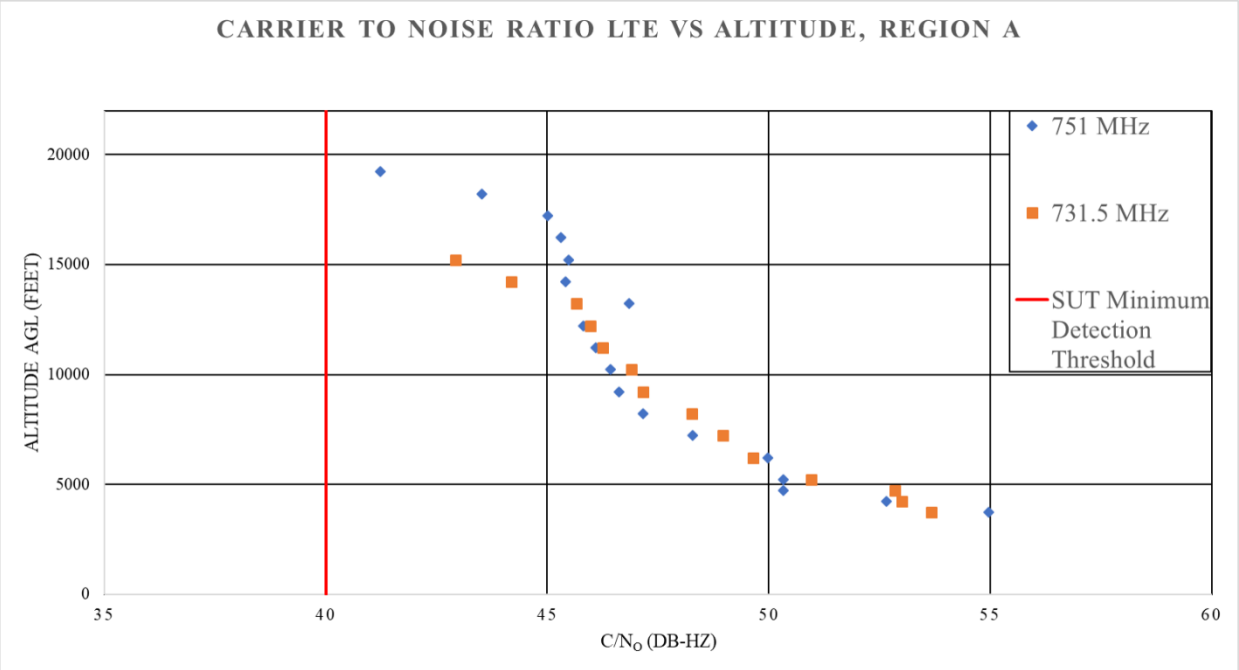

Figure 12: C/N_0 vs Altitude for LTE Signals

Theoretical Performance of the SUT

The specific test objective was to determine the best theoretical performance of the SUT. The specific test objective was partially met. Though enough independent data samples were collected for performance characterization in regions A, B, and D for CDMA signals, no data were collected in region C, and no valid LTE data were collected in any region due to the aforementioned test constraints.

Test Results

A histogram of CRLB metrics in Region B at 10,000 ft MSL (approximately 7,600 ft AGL) is shown as a representative example of the data in Figure 17. The y-axis represents the percentage of data in each bin and the x-axis represents values of the data in that bin. Bin widths and number of bins were standardized across all graphs. The median is plotted on the histogram as a vertical red dashed line and the mean is plotted on the x-axis as a black diamond. Additional histograms of the independent sample data are shown grouped by metric and also region are shown in Appendix E. The mean and 2.5 and 97.5 percentile values (giving a 95% sample envelope) of the data were calculated from the resulting independent samples and are reported in Table 6, Table 7, Table 8, and Table 9 below.

The data are characterized by a large positive skew as seen in Figure 17. A large number of samples are concentrated below the mean, and a long tail extends with a small number of samples with values several times larger than the mean. This is also seen in the tables below, as the relative distance from the mean to the 2.5 and 97.5 percentile values of the data and its value with respect to the median. In all data samples and metrics the mean is greater than the median and closer in value to the 2.5 percentile than the 97.5 percentile. These data indicate that majority of conditions have a relatively low consistent value (lower theoretical positioning variance). Larger values were observed with decreasing occurrence as they increased in value, but these large values had enough prominence to substantially increase the mean of the data in most data sets.

As shown in Figures 13-16, there are several smaller peaks in the histograms following the main one in both the 2D and 3D SROTs. A similar pattern of smaller peaks is also seen in the 2D SROT of region A. The distribution of 2D and 3D SROT samples indicates a possible multimodal distribution. The source of multimodal results was not investigated and is outside the scope of this test.

The 2D SROT is the only metric that shows a consistent trend with altitude across all regions, a lower altitude correlates with a smaller mean SROT. Other metrics did not have an identifiable trend with changes in altitude. The relationship between the 2D and 3D metrics in the tables show the relative theoretical performance of the horizontal vs. vertical position accuracy. The 3D Condition Number is more than an order of magnitude much larger than the 2D condition number at every tested region and altitude in all four calculated statistical measures. Since the condition number is related to the ratio between the largest and smallest variances in the CRLB, this large difference means that the vertical variance in the CRLB is either much larger or much smaller than either horizontal variance. In addition, the fact that the mean of the 3D SROT is much larger than the mean of the 2D SROT indicates that the addition of the vertical variance in the trace significantly increases the total variance. This leads to the conclusion that the vertical theoretical variance calculated in the CRLB must be much larger than the horizontal variance.

The most striking change in the data in a particular region occurs in Region A. The data become more widely distributed from the mean, the histogram peaks reduce in height, and the mean, median, and percentiles all increase substantially at the higher altitude compared to the lower altitude. This is true for the 2D SROT, 3D SROT, and 3D condition number. Although this trend is not observed in the mean and 97.5 percentiles in the 2D condition number, its median does increase and the height of the main peak in its histogram is noticeably reduced. This indicates a lower concentration of samples around a single value. A similar change also occurs in Region D, but with the lower percentile and median not increasing as much. In this case the 2D condition number does follow the trend with the other metrics. The trend for the different altitudes in Region B is not as clear although it also had less than half change in height between the two sample altitudes as the other two regions.

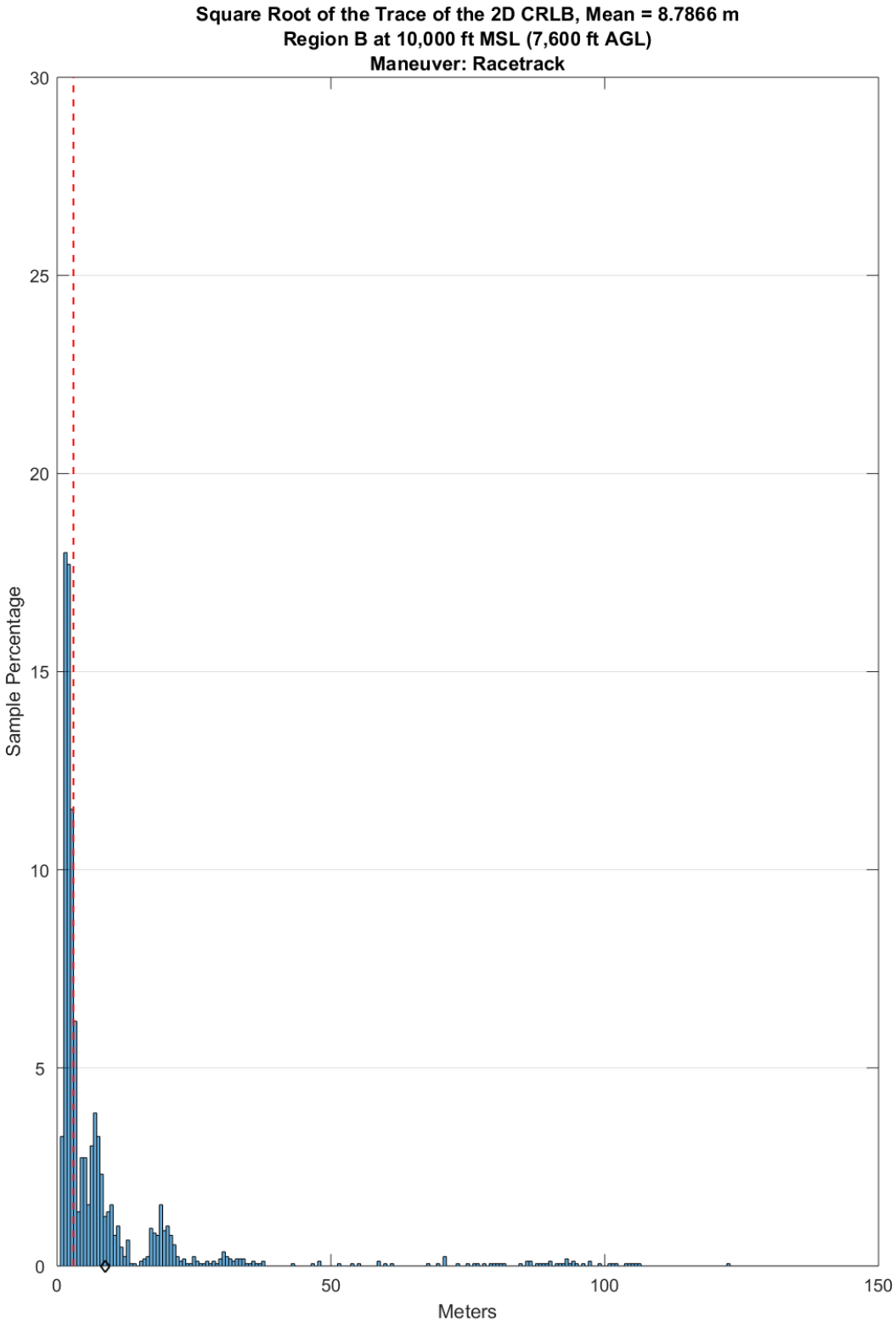

Figure 13: SROT of the 2D CRLB, Region B at 10,000 ft MSL

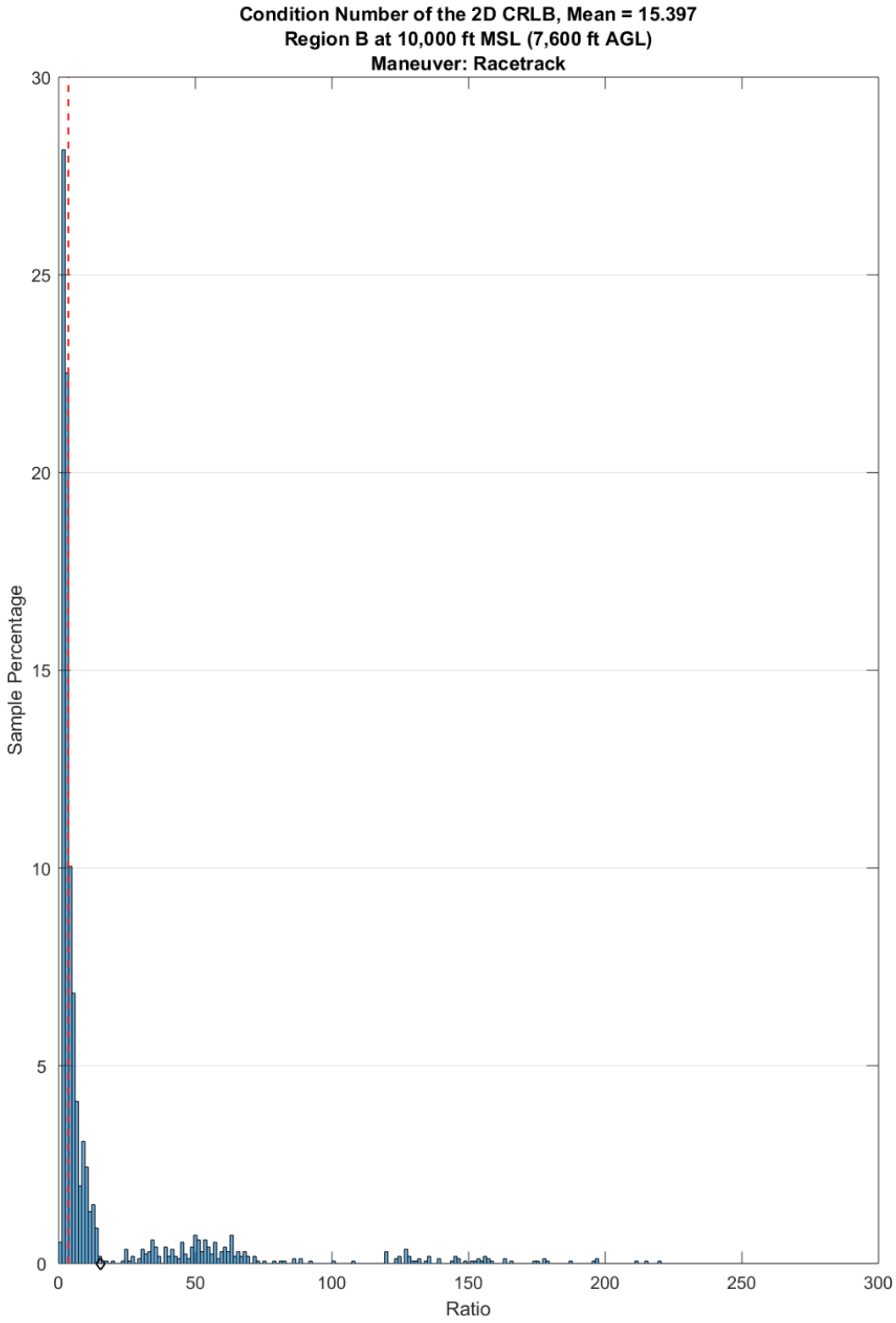

Figure 14: Condition Number of the 2D CRLB, Region B at 10,000 ft MSL

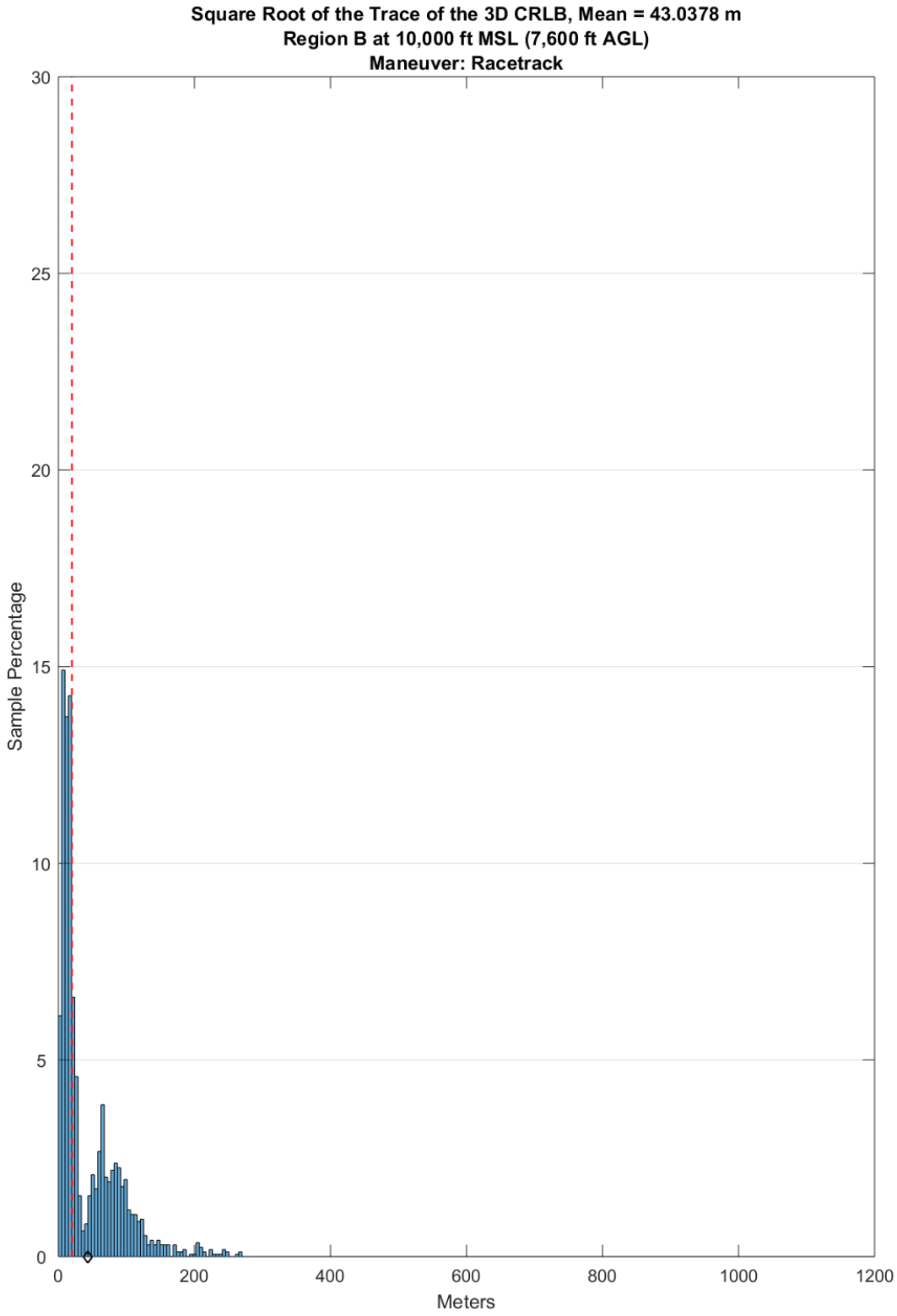

Figure 15: SROT of the 3D CRLB, Region B at 10,000 ft MSL

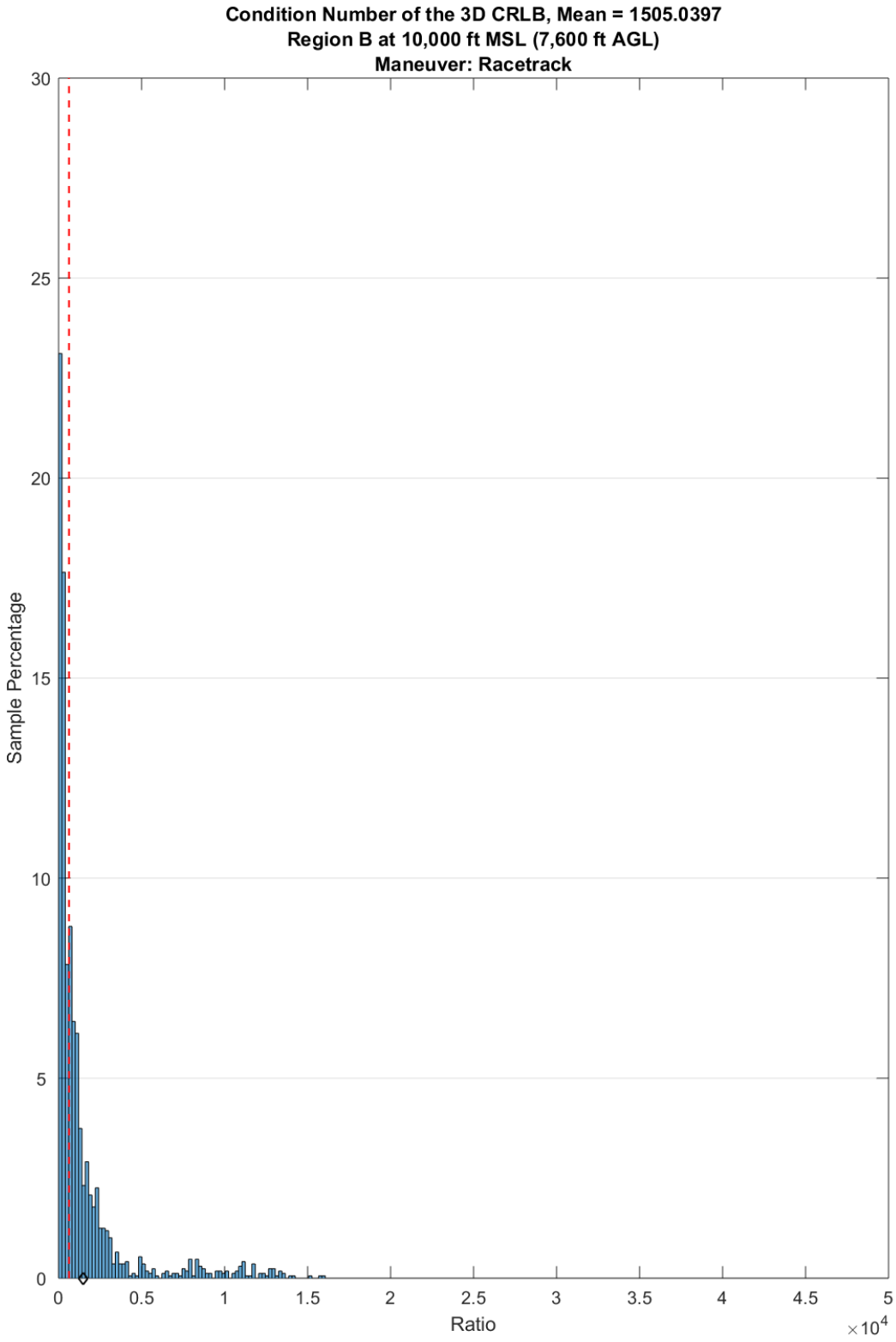

Figure 16: Condition Number of the 3D CRLB, Region B at 10,000 ft MSL

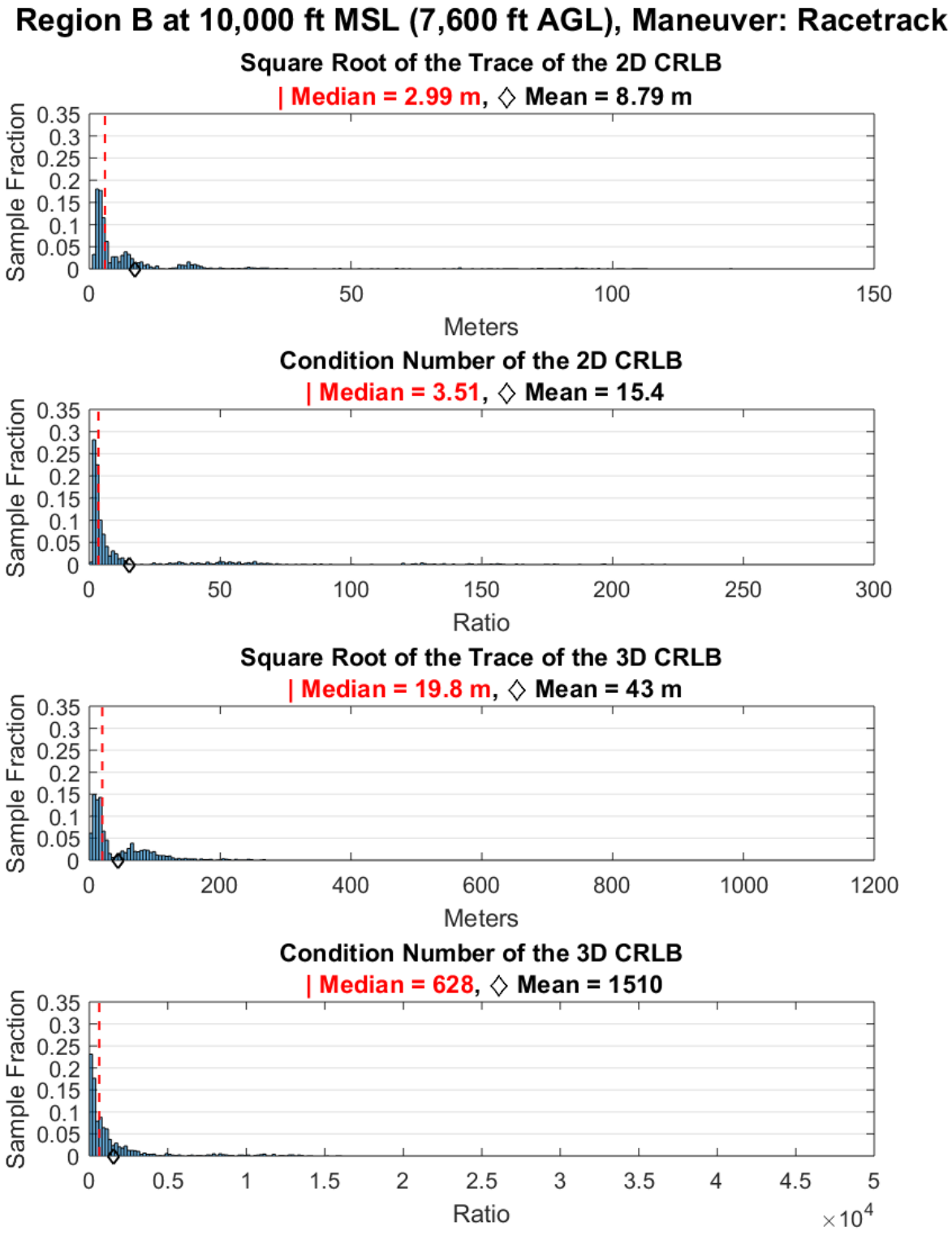

Figure 17: Histogram of Metrics from Region B at 10,000 ft MSL

Table 6: 2D SROT

2D Square Root of the Trace of the CRLB (meters)						
Region	Approximate AGL Altitude (ft)	Independent Samples	2.5 Percentile	Median	Mean	97.5 Percentile
A	19200	421	5.5	24.1	28.8	70.5
	4700	711	1.2	4.5	8.3	40.5
B	7600	1683	1.2	3.0	8.8	75.7
	3100	1730	0.9	3.1	4.3	23.0
D	16100	675	4.1	11.6	43.8	245.7
	5100	716	3.0	5.5	5.9	11.2
Overall			1.2	4.6	11.8	88.7

Table 7: 2D Condition Number

2D Condition Number of the CRLB (ratio)						
Region	Approximate AGL Altitude (ft)	Independent Samples	2.5 Percentile	Median	Mean	97.5 Percentile
A	19200	421	5.0	12.6	27.5	131.4
	4700	711	1.3	4.6	51.1	616.8
B	7600	1683	1.5	3.5	15.4	130.1
	3100	1730	1.4	4.4	9.3	46.7
D	16100	675	1.6	9.9	35.9	266.6
	5100	716	1.4	3.1	4.3	13.7
Overall			1.5	4.6	18.0	127.0

Table 8: 3D SROT

3D Square Root of the Trace of the CRLB (meters)						
Region	Approximate AGL Altitude (ft)	Independent Samples	2.5 Percentile	Median	Mean	97.5 Percentile
A	19200	421	36.4	149.4	199.1	532.1
	4700	711	7.2	15.0	19.0	61.4
B	7600	1683	3.3	19.8	43.0	161.4
	3100	1730	5.2	28.0	52.3	454.1
D	16100	675	6.7	22.4	295.3	1936.9
	5100	716	10.3	22.8	25.8	60.2
Overall			4.7	23.9	76.7	609.9

Table 9: 3D Condition Number

3D Condition Number of the CRLB (ratio)						
Region	Approximate AGL Altitude (ft)	Independent Samples	2.5 Percentile	Median	Mean	97.5 Percentile
A	19200	421	1197	4237	7810	35854
	4700	711	53	646	810	2677
B	7600	1683	17	628	1505	10962
	3100	1730	117	1592	4007	24713
D	16100	675	10	64	10838	61308
	5100	716	38	102	154	590
Overall			17	586	3356	31078

Navigation Performance

The specific test objective was to determine the navigation performance of the SUT. The specific test objective was partially met. Though enough independent data samples were collected for performance characterization in Regions A, B, and D for CDMA signals, no data were collected in region C, and no valid LTE data were collected in any region due to the aforementioned test constraints.

SUT data were compared to the C-12J FINS data, which were considered "truth" with zero error. However, per FINS specifications, position data were accurate to 5m spherical error probable.

Test Results

Across all regions and altitudes, the mean 2D RMS error was 13.6 ± 5.8 m. Consistency was 89.7% with a standard deviation of 16.8%. Results are broken out by region and altitude in Table 10 below.

Table 10: CDMA Navigation Performance

Region	Approximate AGL Altitude (ft)	Independent Samples	2D RMS Error (m)	Consistency (%)
A	19200	843	9.9	100.0
	4700	1185	13.8	77.0
B	7600	3929	18.1	100.0
	3100	3633	11.4	61.0
D	16100	1349	22.1	100.0
	5100	1909	6.0	100.0
Mean			13.6	89.7
Standard Deviation			5.8	16.8

These error values are promising for future OpNav research and use for navigation purposes. The error values observed during this test are along the same order of magnitude as GNSS-based enroute navigation solutions. For context, open source GPS information from the official website lists cellular phone accuracy as typically a 4.9 m radius (reference 14). The Federal Aviation Administration (FAA) requires that aircraft navigation systems achieve lateral navigation accuracy of 1.0 nautical mile at least 95 percent of the flight time while in the arrival and terminal phases of flight (reference 15). OpNav systems, if able to provide a real-time navigation solution, have the potential to approach the accuracy and utility of GPS today.

Consistency results varied widely. In most regions, consistency was 100%, but the mean was heavily influenced by some outliers, as indicated by the large standard deviation. It should be noted that consistency was, by definition, expected, to be about 95% for each region and altitude, since a 95% confidence ellipse was used for this evaluation. Instances where consistency was 100% suggest that the SUT was too conservative in estimating its error statistics. In regions/altitudes where poor consistency was demonstrated, the suspected cause is the timing error discussed in Limitations and Constraints.

Six plots were generated to examine the relationship between navigation error and the SROT of the CRLB at each of the six test conditions. Two are shown here in Figure 18 and Figure 19. The remainder can be found in Appendix E. The reader should note that the scale varies between figures.

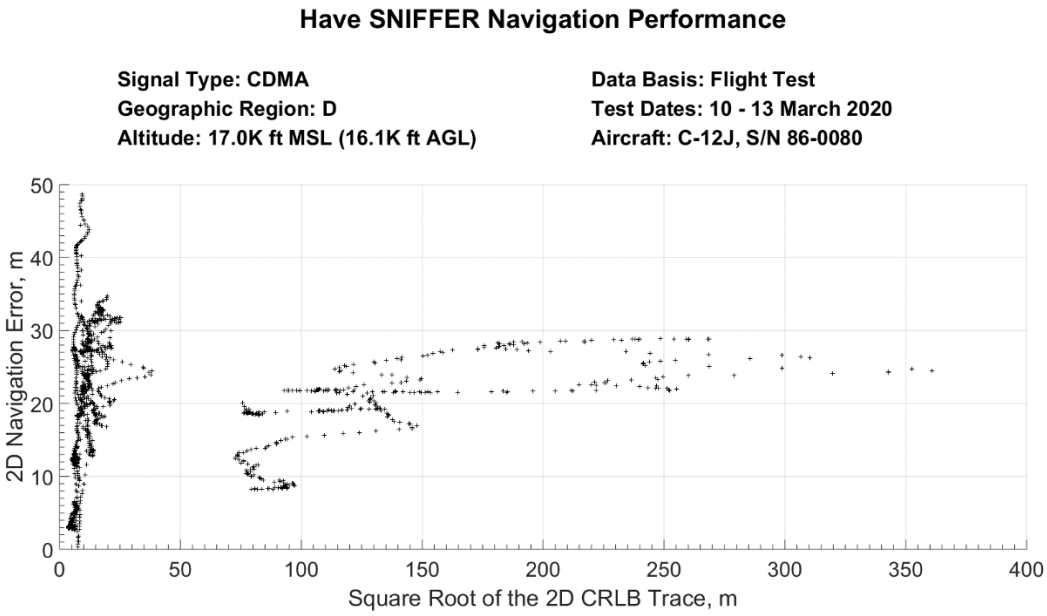

Figure 18: Navigation Error vs SROT of CRLB, Region D, High Altitude

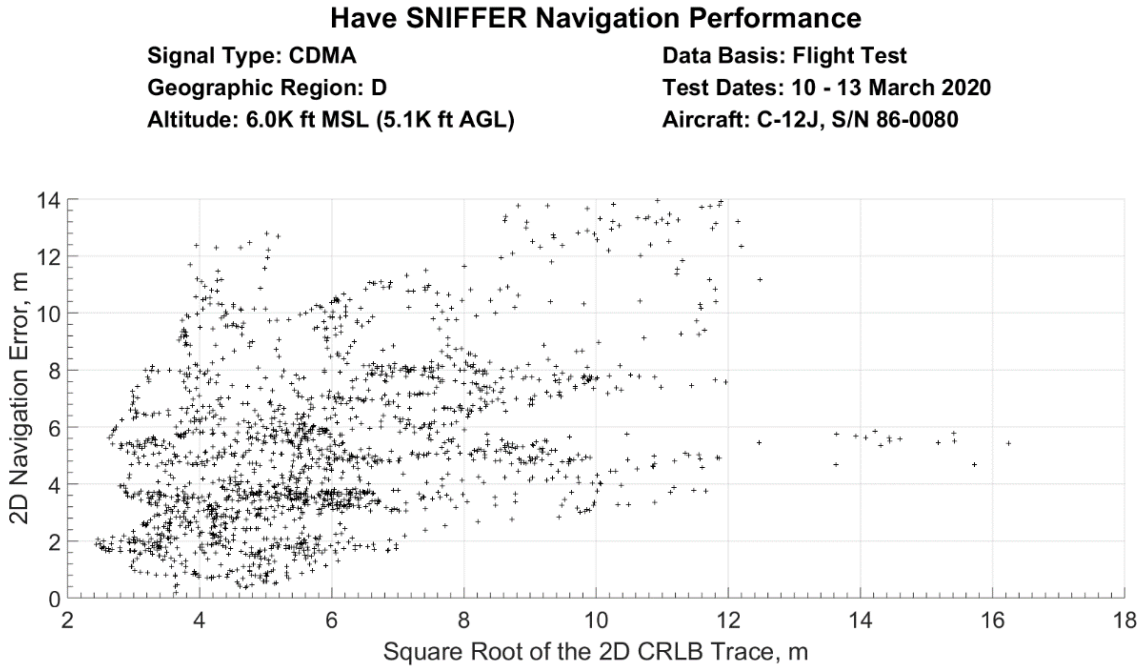

Figure 19: Navigation Error vs SROT of CRLB, Region D, Low Altitude

While no direct correlation was apparent, some interesting observations can be made. Figure 10 shows a distinct bifurcation in the data, while Figure 11 displays a relatively tight grouping. The bifurcation is suspected to be due to the system moving out of range of a tower (or multiple towers), or possibly being masked by terrain, throughout the course of the test point. The loss of a SOP source could cause the SROT of the CRLB to increase significantly between one data sample and the next. However, the navigation error did not reflect the same large jump in magnitude, indicating that the Extended Kalman Filter (EKF) and the Inertial Measurement Unit (IMU) performed as expected. **Investigate the source of the large changes in magnitude of the SROT of the CRLB (R2).**

Additional Findings

Some interesting findings were made that warrant additional discussion but do not fit elsewhere within the structure of this report.

First, CDMA signal strength at altitude came as a surprise to the entire test team. CDMA signals were present at every altitude/region combination flown, so the upper altitude limit on CDMA signals was never actually found. While this is an encouraging result, it should also be noted that CDMA is not widely used outside of the US, and is in fact being phased-out even within the US (reference 9). Therefore, the military utility of CDMA OpNav may be limited. **Focus further development on more relevant SOPs, including LTE. (R3)**

Second, while this test was planned to only investigate the "a-priori" navigation method, tower mapping was not completed prior to the flight test window. Instead the SUT, with GPS data, was used to

map the emitters, whose locations were confirmed with open-source information, such as Google Earth. Anecdotally, many of these emitters were mapped to within 10m of their actual (open-source derived) locations. This is another encouraging finding, as accurate mapping from a known position is an important technical maturity step before moving on to SLAM. A formal test of this mapping function is a logical next step. **Continue to pursue SLAM by formally evaluating the ability of the SUT to map SOP emitters. (R4)**

COLLECT LEO SATELLITE SOPS

The second general test objective was to collect LEO satellite SOPs for system development and research by UCI. LEO satellite SOPs were collected on flight 4. The test objective was met. Signals were collected from both the Globalstar and Orbcomm constellations. Data was provided to the customer.

TEST RESULTS SUMMARY

The SUT was able to detect signals in all tested regions and altitudes. CDMA signals were found to be much stronger than LTE signals and provided a more useful source for OpNav; however, CDMA is primarily used in the US and is being phased out by many cellular carriers. Analysis of theoretical performance metrics showed that vertical theoretical variance calculated in the CRLB must be much larger than the horizontal variance. The navigation error was on the same order of magnitude as previous testing accomplished by UCI with a small UAV. The OpNav system, with further development, could provide military utility in a number of applications subject to GNSS denial. With a more mature system, future testing should focus on real-time navigation and the use of more relevant SOPs, like LTE.

Additional lessons learned are captured in Appendix F.

This page was intentionally left blank.

REFERENCES

1. USAF-TP-19B-03, *Have SNIFFER Test Plan*, USAF TPS, Edwards AFB, California, February 2020.

2. Kassas, Zaher M, Joshua J Morales, Kimia Shamaei, and Joe Khalife. "LTE Steers UAV." *GPS World* 28, no. 4 (April 2017): 18–25. www.gpsworld.com.

3. Kassas, Zaher M, Joshua J Morales, and Joe J Khalife. "STAN: Simultaneous Tracking and Navigation with LEO Satellite Signals." *Inside GNSS*, 2019, 56–65. www.insidegnss.com.

4. Kayton, Myron, and Walter R Fried. *Avionics Navigation Systems*. 2nd ed. New York, NY: Wiley, 1997.

5. Morales, Joshua J. 'Re: CRLB Computations.' Email, January 2020.

6. "List of CDMA2000 Networks," Wikipedia. Wikimedia Foundation, May 28, 2020. https://en.wikipedia.org/wiki/List_of_CDMA2000_networks.

7. "List of LTE Networks." Wikipedia. Wikimedia Foundation, June 2, 2020. https://en.wikipedia.org/wiki/List_of_LTE_networks.

8. Markgraf, Bert. "How far can cell tower cellphone pick up signal" *Small Business-Chron.com* 26 October 2016. smallbusiness.chron.com/far-can-cell-tower-cellphone-pick-up-signal-32124.html. Accessed 9 Apr. 2020.

9. "CDMA Network Retirement." Verizon. Accessed May 16, 2020. https://www.verizonwireless.com/support/knowledge-base-218813/.

10. Kay, Steven M. *Fundamentals of Statistical Signal Processing*. Upper Saddle River: Prentice Hall PTR, 2017.

11. Sunga, David I. *Inertial Navigation Basics.* PDF, December 2019

12. "LTE Tutorial." Tutorialspoint. Tutorials Point, June 2, 2020. https://www.tutorialspoint.com/lte/index.htm

13. "CDMA Tutorial." Tutorialspoint. Tutorials Point, June 2, 2020. https://www.tutorialspoint.com/cdma/index.htm

14. "GPS Accuracy." GPS.gov. Accessed June 3, 2020. https://www.gps.gov/systems/gps/performance/accuracy/

15. "Flight Operations Group: Performance Based Navigation (PBN) Guidance & Approval." Federal Aviation Administration. Accessed June 3, 2020. https://www.faa.gov/about/office_org/headquarters_offices/avs/offices/afx/afs/afs400/afs410/pbn/

This page was intentionally left blank.

APPENDIX A – CRLB AND DATA ANALYSIS

CRLB DEFINITION (REFERENCES 5 AND 10)

Characterizing a navigation system and its solution is usually a statistically heavy process. The branch of statistics that deals with estimating the values of certain parameters from a data sample that has a random component is known as Estimation Theory. A useful metric in Estimation Theory for determining the utility of a navigation solution is the Cramer-Rao Lower Bound (CRLB). The CRLB uses a probability distribution to determine the best (lowest) possible variance in the estimation of parameters. This is done by finding the curvature or sharpness of the Probability Distribution Function (PDF) (as a function of the parameters to be estimated) around the mean using its second derivative. To provide an intuition for how a CRLB works, a simplified derivation for the one dimensional case is shown in the next section.

The generic vector form of a CRLB of *x*, *y*, *z*, and receiver clock error is represented by a matrix

$$CRLB = \begin{pmatrix} {\sigma_{xx}}^2 & \sigma_{xy} & \sigma_{xz} & \sigma_{xt} \\ \sigma_{yx} & {\sigma_{yy}}^2 & \sigma_{yz} & \sigma_{yt} \\ \sigma_{zx} & \sigma_{zy} & {\sigma_{zz}}^2 & \sigma_{zt} \\ \sigma_{tx} & \sigma_{ty} & \sigma_{tz} & {\sigma_{tt}}^2 \end{pmatrix}$$

The diagonal entries of this matrix represents the variance of each estimated variable, while the off-diagonals represent the covariance between the respective variables. The trace of this matrix, therefore, is an estimate of the total variance in the best possible estimation; the square root of the trace can be thought of as a total standard deviation across all dimensions and variables. This metric was chosen as a succinct metric to help characterize the potential accuracy of the navigation solution for a particular point in time.

The CRLB for the SUT is found by using:

$$CRLB = [P^T * W^{-1} * P]^{-1}$$

$$P^T = \begin{pmatrix} \frac{\Delta x_1}{\sqrt{{\Delta x_1}^2 + {\Delta y_1}^2 + {\Delta z_1}^2}} & \frac{\Delta x_2}{\sqrt{{\Delta x_2}^2 + {\Delta y_2}^2 + {\Delta z_2}^2}} & \cdots & \frac{\Delta x_n}{\sqrt{{\Delta x_n}^2 + {\Delta y_n}^2 + {\Delta z_n}^2}} \\ \frac{\Delta y_1}{\sqrt{{\Delta x_1}^2 + {\Delta y_1}^2 + {\Delta z_1}^2}} & \frac{\Delta y_2}{\sqrt{{\Delta x_2}^2 + {\Delta y_2}^2 + {\Delta z_2}^2}} & \cdots & \frac{\Delta y_n}{\sqrt{{\Delta x_n}^2 + {\Delta y_n}^2 + {\Delta z_n}^2}} \\ \frac{\Delta z_1}{\sqrt{{\Delta x_1}^2 + {\Delta y_1}^2 + {\Delta z_1}^2}} & \frac{\Delta z_2}{\sqrt{{\Delta x_2}^2 + {\Delta y_2}^2 + {\Delta z_2}^2}} & \cdots & \frac{\Delta z_n}{\sqrt{{\Delta x_n}^2 + {\Delta y_n}^2 + {\Delta z_n}^2}} \\ 1 & 1 & \cdots & 1 \end{pmatrix}$$

$$W = \begin{pmatrix} \frac{c^2 B_{dll} t_{eml} T_c^2}{2 (C/N_0)_1}\left(1 + \frac{1}{(T)(C/N_0)_1}\right) & 0 & \cdots & 0 \\ 0 & \frac{c^2 B_{dll} t_{eml} T_c^2}{2 (C/N_0)_2}\left(1 + \frac{1}{(TCO)(C/N_0)_2}\right) & \cdots & 0 \\ \vdots & \vdots & \ddots & 0 \\ 0 & 0 & 0 & \frac{c^2 B_{dll} t_{eml} T_c^2}{2 (C/N_0)_n}\left(1 + \frac{1}{(T)(C/N_0)_n}\right) \end{pmatrix}$$

The first three rows of the *P* matrix represent the *x, y, z* unit vector to each of *n* towers that were detected by the system while the fourth row is the estimated clock error. The *W* matrix is the variance due to the system bandwidth and time delays. The terms in the *W* matrix are: c^2 is the speed of light, squared (m^2/s^2), B_{dll} is the bandwidth caused by the systems delay lock loop method of synchronizing tower signals (0.5 Hz), t_{eml} is the chip spacing factor (1 chip), T_c is the chip clock interval between cycles (1/1.2288e6 s), *TCO* is the system's coherent integration time (1/37.5 s), and C/N_0 is the received carrier-to-noise ratio. All values in the *W* matrix except for C/N_0 were considered characteristics of the system itself and were held constant.

The CRLB combines the effects of SOP geometry represented by the *P* matrix and the SOP pseudorange, represented by the *W* matrix, to produce an error ellipsoid based on the minimum possible location estimation variance given the above parameters. While the trace of the CRLB describes what can be considered a total variance, the shape of the ellipsoid (ellipse in 2D) is characterized by its condition number. The condition number describes the ratio of the eigenvalues of the CRLB matrix, which are also related to the shape of the 3D error bound ellipsoid. The ellipsoid major axis is controlled by the largest eigenvalue and the minor axis is controlled by the smallest eigenvalue of the matrix. The condition number describes how "stretched" an ellipse is, similar to an eccentricity by taking ratios of the largest and smallest eigenvalues of the matrix. The condition number helps to characterize how the geometry of the SOPS affects the shape of the CRLB error bound.

The CRLB was calculated for each time step available in the system observables delivered by UCI. The entries in the CRLB matrix were then be run through an autocorrelation filter to find the necessary sample spacing to consider the measurements independent, which for the purpose of this test was defined as <10% correlated. A mean and standard deviation of the condition number and square root of the trace were then calculated from the independent CRLB samples to determine the theoretical performance of the SUT based on the test environment.

ONE-DIMENSIONAL CRLB DERIVATION (REFERENCE 10)

The first step in deriving the CRLB is to create a model for how the random component is characterized and how it affects the system's measurements. The model often used is one of additive Gaussian noise:

$$\boldsymbol{x} = \theta(a, b, c, \dots) + \boldsymbol{w}$$

where $\boldsymbol{x}$ is a vector of the recorded measurements, and θ is the noise free value of the measurements and depends on the parameters *a,b,c,...* that are to be estimated. $\boldsymbol{w}$ is the vector of Gaussian noise that is measured along with our intended measurement θ. The Gaussian distribution is normally used as a model for the measurements' PDF as it has wide applicability due to the Central Limit Theorem. The Central Limit Theorem states that the sum of *N* independent random variables pulled from an identical but unspecified distribution has a PDF that tends to be Gaussian as *N* goes to infinity. In simpler terms, the aggregate distribution in noise from a large number of samples tends to be Gaussian. For this reason, in this test, and most data analysis, the noise was modeled using the Gaussian distribution.

Another assumption that is made for data analysis is that the noise has a mean of zero, which implies that the mean of the recorded measurements $\boldsymbol{x}$ is the mean of the noise-free measurement. The Gaussian PDF of each individual measurement can then be represented as:

$$p(x[i]; \theta(a, b, c, \dots)) = \frac{1}{\sqrt{2\pi\sigma^2}} \exp\left[-\frac{(x[i] - \theta(a, b, c, \dots)])^2}{2\sigma^2}\right]$$

where σ^2 is the variance of the noise. The assumption of independent samples allows the PDF of the total measurement vector to be computed from the product of the individual PDFs:

$$p(\boldsymbol{x};\theta(a,b,c,\dots)) = \prod_{i=0}^{N-1} \frac{1}{\sqrt{2\pi\sigma^2}} \exp\left[-\frac{(x[i]-\theta(a,b,c,\dots))^2}{2\sigma^2}\right]$$
$$= \frac{1}{(2\pi\sigma^2)^{N/2}} \exp\left[-\frac{\sum_{i=0}^{N-1}(x[i]-\theta(a,b,c,\dots))^2}{2\sigma^2}\right]$$

This PDF is then used to derive the CRLB formula to determine the minimum possible variance in an estimation of the parameters *a,b,c,…* given the measurements $\boldsymbol{x}$ with the assumption that an unbiased estimator is being used. The first step in deriving a CRLB is to recognize the PDF can be thought of as a function of the noise free measurement θ. This function of θ is known as the likelihood function. The natural logarithm of the likelihood function is known as the log likelihood function (LLF).

$$\ln\big(p(\boldsymbol{x};\theta(a,b,c,\dots))\big) = \ln\left(\frac{1}{(2\pi\sigma^2)^{N/2}}\right) + \left[-\frac{\sum_{i=0}^{N-1}(x[i]-\theta(a,b,c,\dots))^2}{2\sigma^2}\right]$$

To determine the curvature of the LLF, its second derivative is taken with respect to the parameters that are of interest (*a,b,c,…*). For illustrative purposes, assume the function θ is given by $\theta(a,b,c,\dots) = a$. Then the second derivative of the LLF can be taken with respect to the parameter a to determine its curvature as follows:

$$\frac{\partial^2}{\partial a^2}\left[\ln\big(p(\boldsymbol{x};\theta(a,b,c,\dots)=a)\big)\right] = \frac{\partial^2}{\partial a^2}\left[\ln\left(\frac{1}{(2\pi\sigma^2)^{N/2}}\right)\right] + \frac{\partial^2}{\partial a^2}\left[-\frac{\sum_{i=0}^{N-1}(x[i]-a)^2}{2\sigma^2}\right]$$

$$\frac{\partial^2}{\partial a^2}\left[\ln\big(p(\boldsymbol{x};a)\big)\right] = \frac{\partial}{\partial a}\left[\frac{\sum_{i=0}^{N-1}(x[i]-a)}{\sigma^2}\right]$$

$$\frac{\partial^2}{\partial a^2}\left[\ln\big(p(\boldsymbol{x};a)\big)\right] = \frac{\partial}{\partial a}\left[\frac{N}{\sigma^2}(\bar{x}-a)\right]$$

$$\frac{\partial^2}{\partial a^2}\left[\ln\big(p(\boldsymbol{x};a)\big)\right] = -\frac{N}{\sigma^2}$$

Now that the curvature of the PDF is known with respect to the parameter to be estimated, the formula for the CRLB is:

$$CRLB = \frac{1}{-E\left(\frac{\partial^2}{\partial a^2}\left[\ln\big(p(\boldsymbol{x};a)\big)\right]\right)_{a=true\ value}} = var(\hat{a}) \geq \frac{\sigma^2}{N}$$

The *E* function takes the expected value of the curvature with respect to $\boldsymbol{x}$, but since the curvature in this example did not depend on $\boldsymbol{x}$ the curvature remains unchanged.

This formula shows that for a constant parameter, the best estimates of parameter *a*, shown as $\hat{a}$, has a variance that decreases with increasing sample size and increases with increasing noise variance. This derivation can be done using measurements that are more complex functions of noiseless measurements

and extended into a vector of measurements, but this full derivation was outside the scope of this test plan.

RMS ERROR DATA ANALYSIS (REFERENCE 11)

To calculate the navigation performance of the SUT, the RMS (Root Mean Square) error was calculated through the following process. Navigation solutions were provided by UCI in either a Latitude-Longitude-Height or North-East-Down format. For the latter, the process began at Step 4.

1. Transform both coordinates [SUT position (ϕ, λ, H) and truth position (ϕ_T, λ_T, H_T)] from ellipsoid coordinates into Cartesian coordinates (*U, V, W*):

$U = (N + h)cos\phi \cos l$

$V = (N + h)cos\phi \sin l$

$W = (N(1 - e^2) +) \sin \phi$

, where $N = \frac{a}{\sqrt{1 - e^2 \sin^2 \phi}}$

Equatorial radius "a" = 20,925,646.32546 ft

Polar radius "b" = 20,855,486.58136 ft

f = (a-b) / a = 0.003352810665

$e^2 = 2f - f^2 = 0.00669437999$

2. Calculate delta vector (*Δu, Δv, Δw*) between the two Cartesian coordinate points:

$\Delta u = U - U_T$

$\Delta v = V - V_T$

$\Delta w = W - W_T$

3. Transform differences (*Δu, Δv, Δw*) into local differences (*n, e, h*):

$n = -\sin\phi \cos l * Du - \sin\phi \sin l * Dv + \cos\phi * Dw$

$e = -\sin\phi * Du + \cos l * Dv$

$h = \cos\phi \cos l * Du - \cos\phi \sin l * Dv + \sin\phi * Dw$

4. Calculate the RSS (Root Sum Square) 2D radial position error using just the north and east errors:

$r = \sqrt{n^2 + e^2}$

5. Calculate the Root Mean Root mean square error of each region will be calculated by the following:

$RMS = \sqrt{\frac{\Sigma r^2}{n}}$, where *n* = number of samples for each region

APPENDIX B – TEST ITEM DESCRIPTION (CONTINUED)

The following is a continuation of the test item description from the body of this report.

LTE/CDMA Antennas

Four consumer-grade Laird Technologies 800/1900/2700 MHz "Phantom Tri-Band" vertically polarized omnidirectional antennas were utilized to collect and record LTE and CDMA signals. The Laird Technologies part number for these antennas was TRA8063M3 or similar. Each antenna was 3.25 inches tall, 1.44 inches in diameter, and weighed 0.18 lb. In addition, the antennas were coated in plastic. The maximum power was 100 Watts, and the impedance was advertised as 50 Ohms.

Four LTE/CDMA antennas were arranged in a two-by-two uniform planar array where each side had a length of approximately 7cm from center to center of the array. A picture of the antennas arranged on a wooden platform can be found in Figure B1. This array was mounted on the ventral interchangeable mission antenna port on the C-12J.

Figure B1: Laird Technologies LTE Antennas Prior to Installation on the C-12J

Orbcomm Antenna

The very high frequency (VHF) antenna used to collect and record Orbcomm satellite signals was a commercial-off the shelf option purchased from Sensor Systems Incorporated. The part number for the antenna used in this test was S65-8280-68. The antenna was 11.85 inches tall, 10.87 inches long, 3.25 inches wide, and weighed 3.3 lb. Power and impedance advertised for this antenna were 250 watts and 50 Ohms respectively. The antenna was aluminum-cast and enamel-coated with grounding for lightning protection. The Orbcomm antenna operates between 116 MHz to 156 MHz, and is interchangeable with other various VHF communications antennas.

The product photograph for the Orbcomm antenna utilized for this test is shown in Figure B2. The Orbcomm antenna was mounted at the Dorsal Controlled Reception Pattern Antenna (CRPA) port on the C-12J in order to best capture Orbcomm signals.

Figure B2: VHF Orbcomm Antenna

A dimensional drawing of the Orbcomm antenna from Sensor Systems Incorporated is included in Figure B3. This particular model was flight rated by the manufacturer.

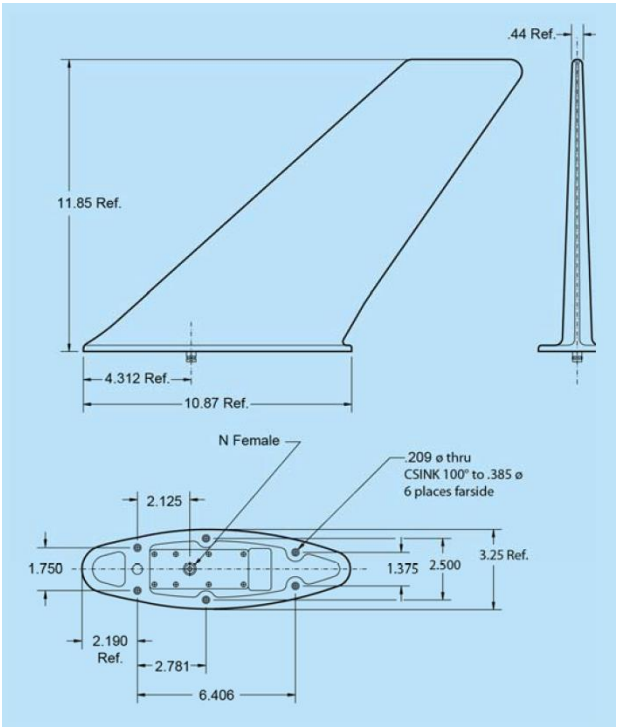

Figure B3: Orbcomm Antenna Dimensional Diagram

Globalstar Antenna

A puck-style antenna was used to collect and record Globalstar signals. The particular model used for this test was the GAT-17MP. This antenna originally was intended for civilian use in automobiles, and included a magnetic patch for placement. Because the puck was not flight rated, it was placed on the glare shield on the right side of the cockpit instead of an external mounting location. The GAT-17MP could receive frequencies from 2483.5 to 2500 MHz. The antenna had an advertised power output of 100 milli-watts.

The following figure, Figure B*4*, is a diagram of the Globalstar antenna used in this test.

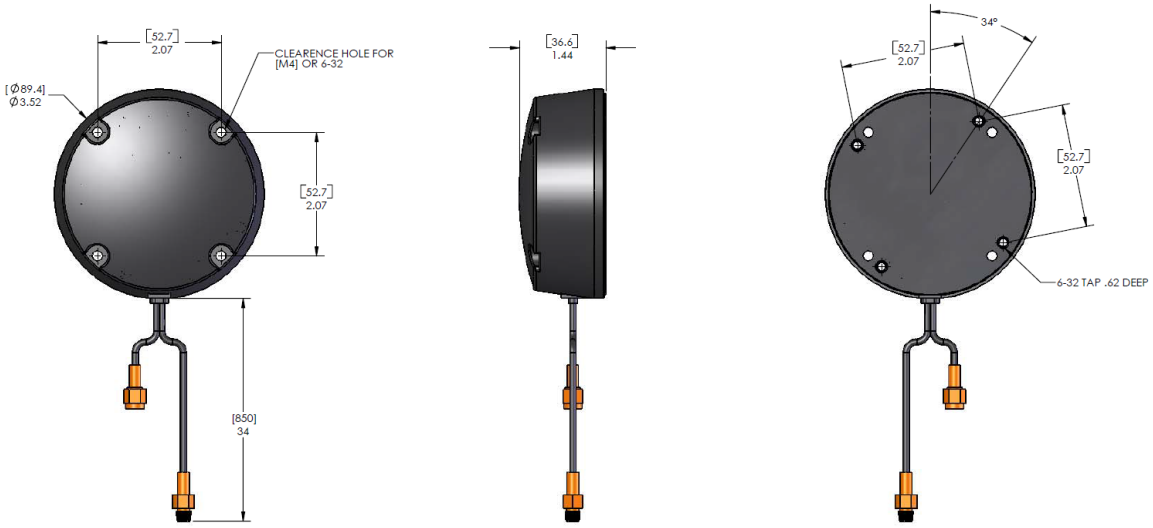

Figure B4: Globalstar GAT-17B Antenna Dimensions

This page was intentionally left blank.

APPENDIX C – TEST REGIONS

The Regions A, B, C, and D, as shown below in Figure C1, were regions of low signal density, expected high signal density, and oceanic signals. Region D was an additional high-density region where UCI's small UAV tests were conducted. One flight was flown to Region D to maximize a-priori knowledge of signal availability. Due to COVID-19, no flights to Region C were accomplished.

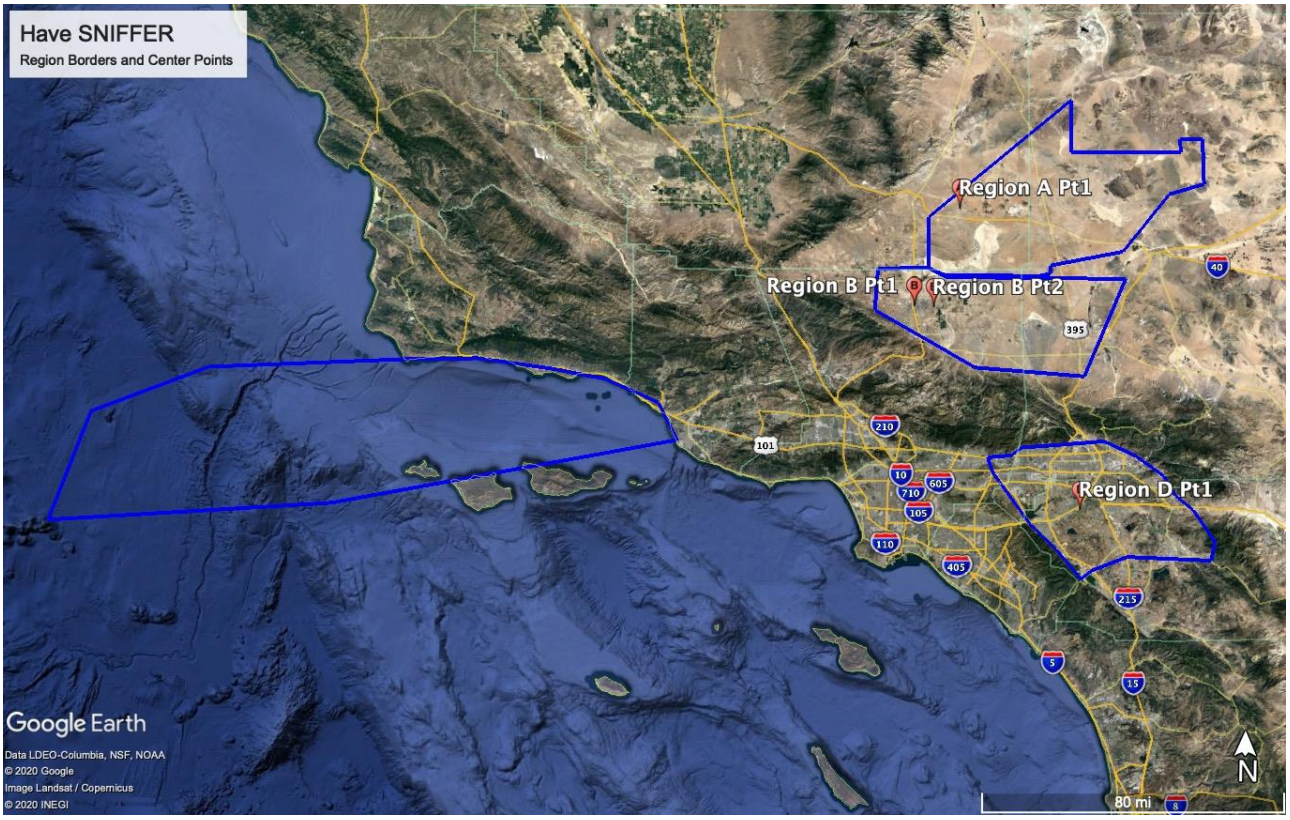

Figure C1: Approximate Geographic Regions

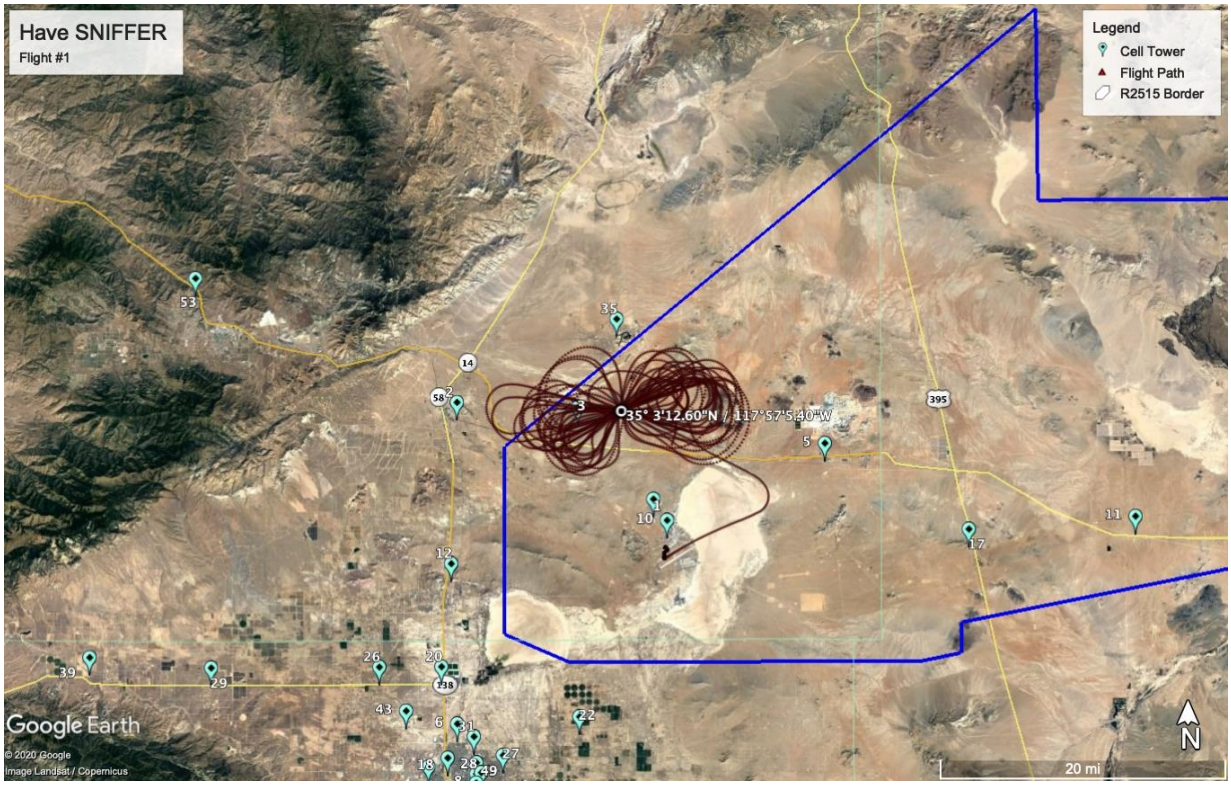

Figure C2: Climbing Teardrop at Region A

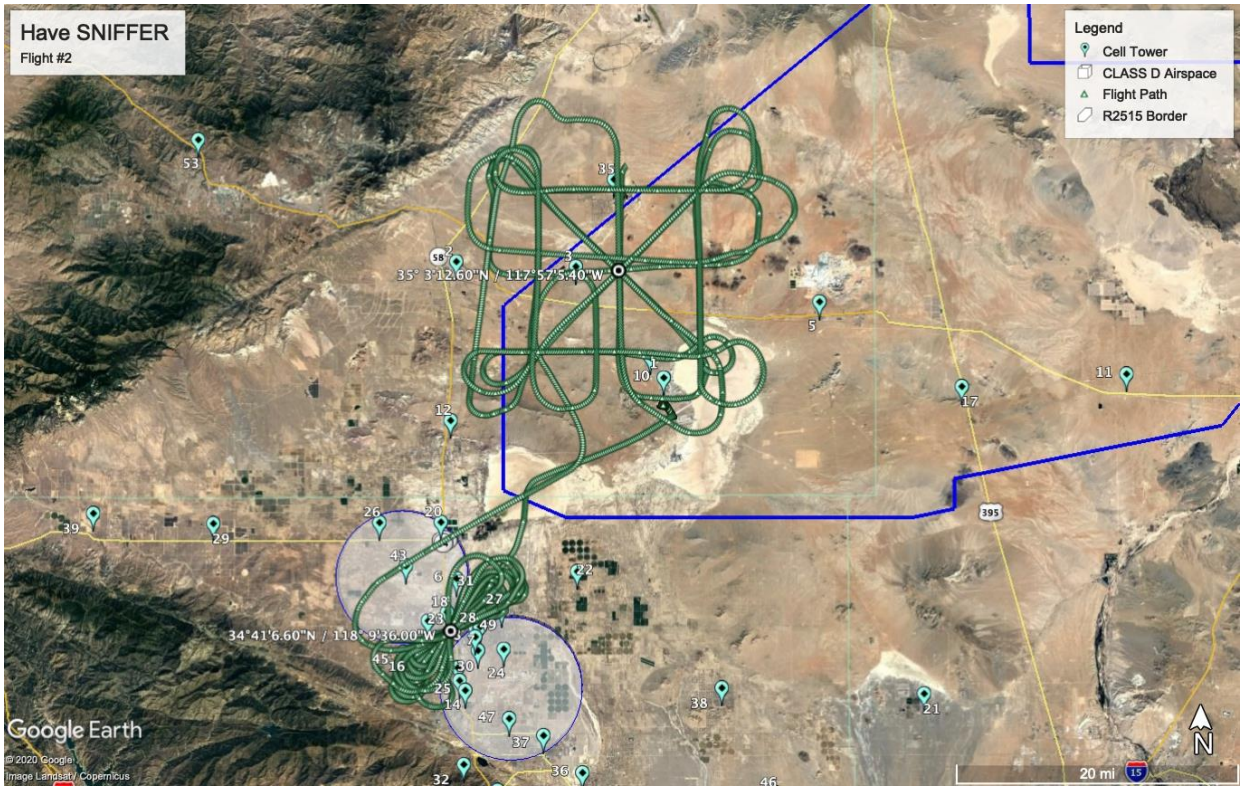

Figure C3: Climbing Teardrop at Region B and Sniffer Straight and Level Grid Maneuver at Region A

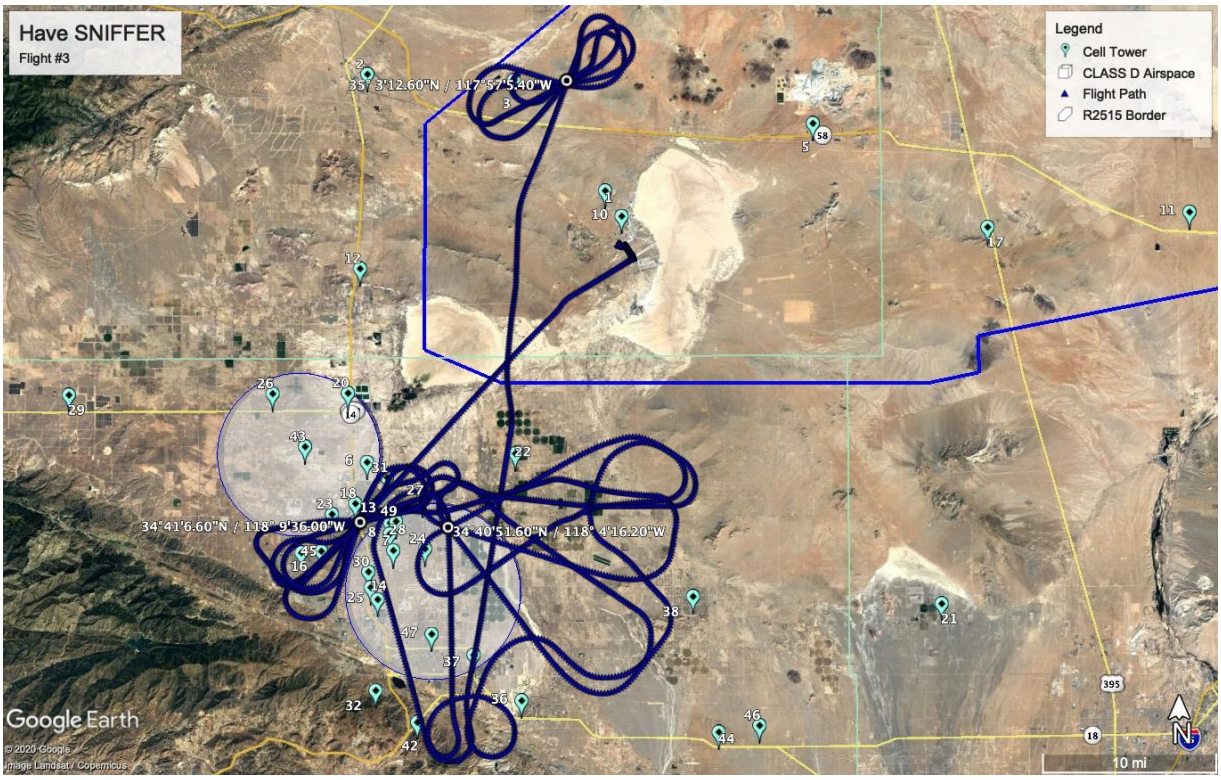

Figure C4: Descending Teardrop and Racetrack Pattern at Region B

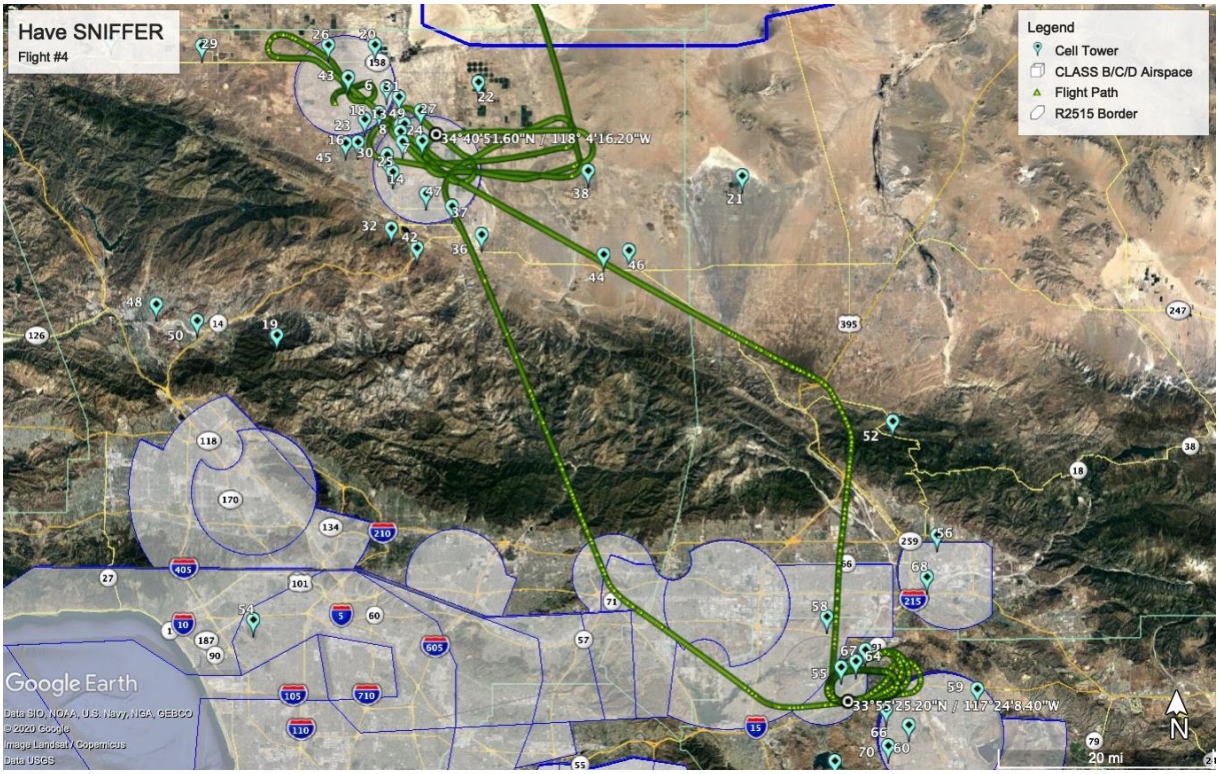

Figure C5: Racetrack Pattern at Region D

This page was intentionally left blank.

APPENDIX D – BTS LOCATION DATABASE

Throughout testing, a database of BTSs that the SUT detected was continually updated. Each tower was detected throughout normal operations of the SUT, but was not necessarily used to generate a navigation solution.

Figure D1 is a geographic map of the BTSs detected during testing, with number labels corresponding to Table D1. While not all of these towers were used to generate a navigation solution, the map demonstrates that the SUT could detect signals from significant distances.

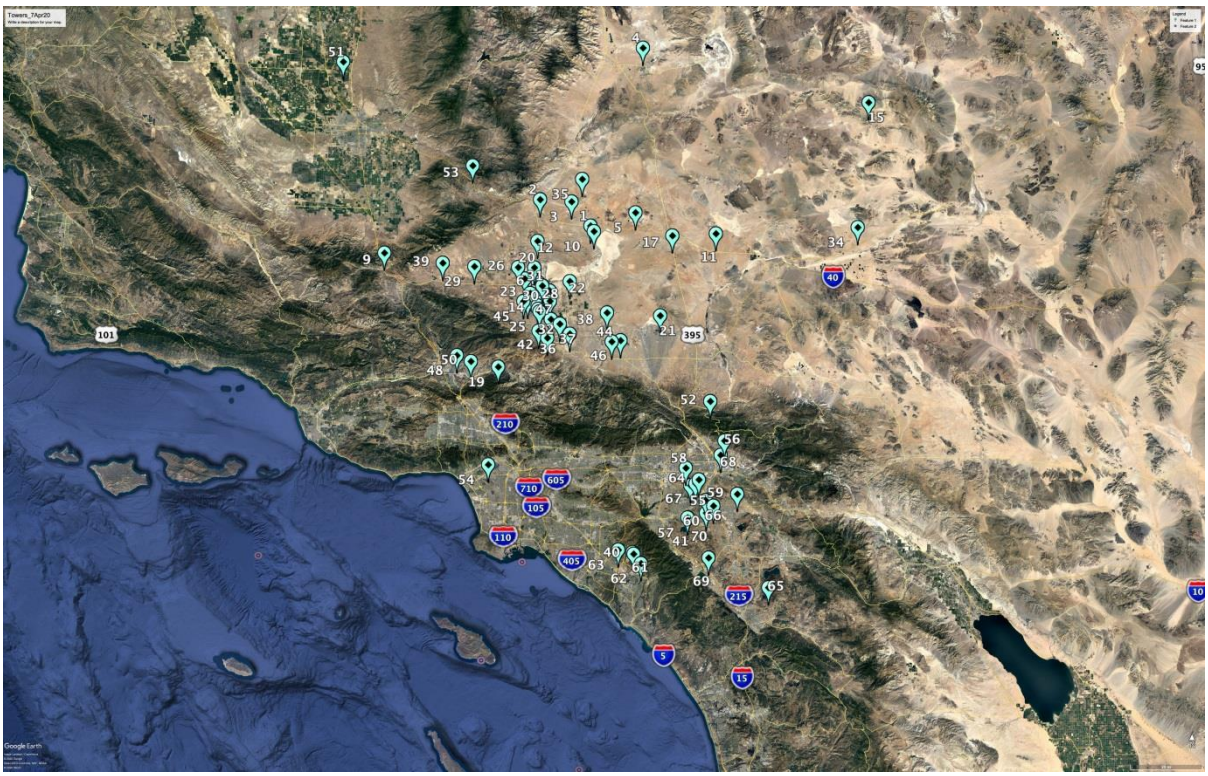

Figure D1: Map of the BTSs Detected by the SUT

The following tables, Table D1 and Table D2, are a list of those BTSs and their locations. The altitudes listed for each tower were found by using the signals received by the SUT, or utilizing commercial products such as Google Earth to determine the approximate altitudes. These are approximations only. Table D1 includes towers detected while flying over Regions A and B. Table D2 includes towers detected while flying over Region D.

Table D1: BTSs Detected Near Regions A and B

Tower #	N Latitude (deg)	W Longitude (deg)	Alt (ft)	Tower #	N Latitude (deg)	W Longitude (deg)	Alt (ft)
1	34.94577	-117.913391	2625	28	34.6691	-118.130821	2625
2	35.043272	-118.156086	2789	29	34.77442	-118.457614	2772
3	35.038347	-118.006434	2887	30	34.62854	-118.152508	2657
4	35.651312	-117.683824	2346	31	34.70665	-118.133861	2379
5	35.00196	-117.701638	2444	32	34.530269	-118.144632	4429
6	34.719459	-118.154346	2362	33	35.89087	-117.28289	3871
7	34.646271	-118.127423	2362	34	34.961963	-116.642576	1837
8	34.660112	-118.1309	2362	35	35.127765	-117.958788	2428
9	34.815404	-118.885237	2362	36	34.522126	-117.997657	2953
10	34.92444	-117.896621	2379	37	34.559892	-118.045977	2723
11	34.926719	-117.317833	2362	38	34.608264	-117.824913	2756
12	34.880584	-118.162449	2625	39	34.783997	-118.6078	3035
13	34.680458	-118.130715	2428	40	33.674139	-117.673109	869
14	34.615617	-118.15014	2690	41	33.819577	-117.425313	902
15	35.45334	-116.595315	5282	42	34.504045	-118.102637	4101
16	34.645524	-118.200242	2648	43	34.732262	-118.217253	2395
17	34.914775	-117.524302	3330	44	34.495982	-117.799268	3363
18	34.685113	-118.165945	2444	45	34.644199	-118.220369	2543
19	34.386199	-118.329304	4921	46	34.501435	-117.758248	3428
20	34.776821	-118.173971	2346	47	34.577063	-118.088441	2664
21	34.601685	-117.574008	2936	48	34.426138	-118.526619	1493
22	34.72683	-118.00435	2411	49	34.670447	-118.124756	2470
23	34.676252	-118.189547	2411	50	34.404584	-118.45945	1545
24	34.647737	-118.095402	2536	51	35.56517	-119.126403	689
25	34.605659	-118.143038	2707	52	34.273014	-117.3305	4199
26	34.776248	-118.250449	2461	53	35.16791	-118.481456	4068
27	34.687917	-118.098059	2461	54	34.005327	-118.363107	558

Table D2: BTSs Detected Near Region D

Tower #	N Latitude (deg)	W Longitude (deg)	Alt (ft)
55	33.944862	-117.415046	853
56	34.120838	-117.25952	1132
57	33.819596	-117.425313	1558
58	34.012259	-117.438071	984
59	33.915044	-117.195428	1640
60	33.867333	-117.306111	1755
61	33.680437	-117.678206	755
62	33.637928	-117.63756	869
63	33.688541	-117.745088	338
64	33.967907	-117.375948	932
65	33.554201	-117.042582	1640
66	33.888437	-117.342669	1640
67	33.952796	-117.391299	902
68	34.064894	-117.27629	1066
69	33.665703	-117.323835	1608
70	33.839693	-117.339425	1663

This page was intentionally left blank.

APPENDIX E – SUPPLEMENTAL DATA

C/N_0 VS ALTITUDE CHARTS

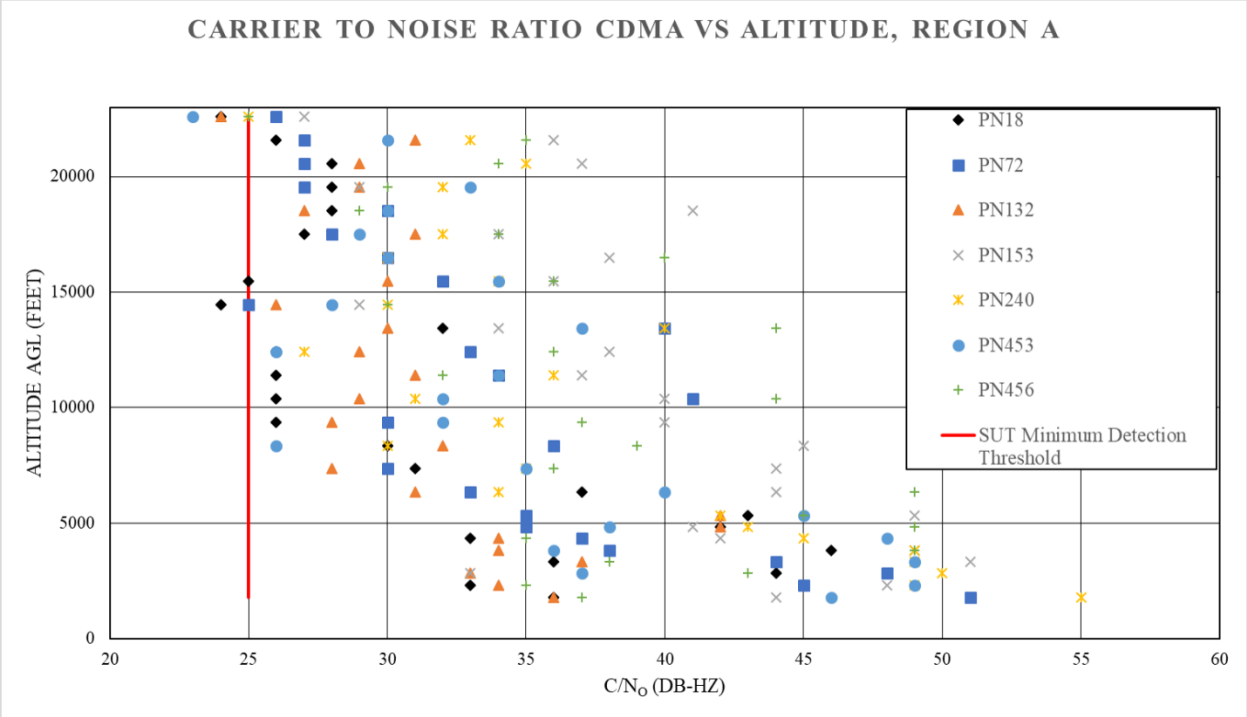

Figure E1: C/N_0 vs Altitude for CDMA Signals, Region A

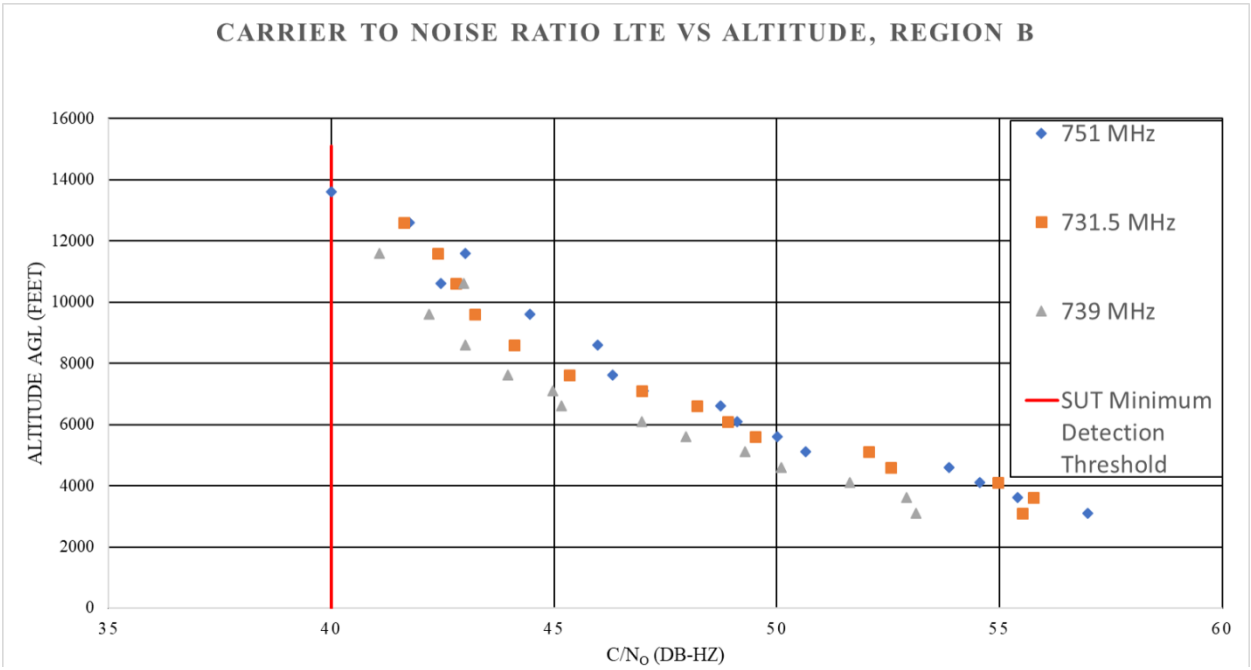

Figure E2: C/N_0 vs Altitude for LTE Signals, Region B

SQUARE ROOT OF THE TRACE AND CONDITION NUMBER HISTOGRAMS

The first set of histograms are linearly scaled such that the top of the chart represents 33% of the total independent samples recorded as noted on the right-hand axis. The median of the data is represented by a red dashed line through the chart and the mean is represented by the black diamond on the x-axis.

The second set of charts is scaled logarithmically so that individual samples can be viewed and the maximum value on the x-axis represents the largest 97.5 percentile in the data set across all flights and altitudes.

The third set of charts groups the metrics by region and altitude to make for better comparison against other regions and altitudes.

Table E1: 2D SROT

2D Square Root of the Trace of the CRLB (meters)								
Region	MSL Altitude (ft)	Approximate AGL Altitude (ft)	FTT	Independent Samples	2.5 Percentile	Median	Mean	97.5 Percentile
A	22000	19200	Teardrop	421	5.5	24.1	28.8	70.5
	7500	4700	Grid	711	1.2	4.5	8.3	40.5
B	10000	7600	Racetrack	1683	1.2	3.0	8.8	75.7
	5500	3100	Racetrack	1730	0.9	3.1	4.3	23.0
D	17000	16100	Racetrack	675	4.1	11.6	43.8	245.7
	6000	5100	Racetrack	716	3.0	5.5	5.9	11.2
Overall					1.2	4.6	11.8	88.7

Table E2: 2D Condition Number

2D Condition Number of the CRLB (ratio)								
Region	MSL Altitude (ft)	Approximate AGL Altitude (ft)	FTT	Independent Samples	2.5 Percentile	Median	Mean	97.5 Percentile
A	22000	19200	Teardrop	421	5.0	12.6	27.5	131.4
	7500	4700	Grid	711	1.3	4.6	51.1	616.8
B	10000	7600	Racetrack	1683	1.5	3.5	15.4	130.1
	5500	3100	Racetrack	1730	1.4	4.4	9.3	46.7
D	17000	16100	Racetrack	675	1.6	9.9	35.9	266.6
	6000	5100	Racetrack	716	1.4	3.1	4.3	13.7
Overall					1.5	4.6	18.0	127.0

Table E3: 3D SROT

3D Square Root of the Trace of the CRLB (meters)								
Region	MSL Altitude (ft)	Approximate AGL Altitude (ft)	FTT	Independent Samples	2.5 Percentile	Median	Mean	97.5 Percentile
A	22000	19200	Teardrop	421	36.4	149.4	199.1	532.1
	7500	4700	Grid	711	7.2	15.0	19.0	61.4
B	10000	7600	Racetrack	1683	3.3	19.8	43.0	161.4
	5500	3100	Racetrack	1730	5.2	28.0	52.3	454.1
D	17000	16100	Racetrack	675	6.7	22.4	295.3	1936.9
	6000	5100	Racetrack	716	10.3	22.8	25.8	60.2
Overall					4.7	23.9	76.7	609.9

Table E4: 3D Condition Number

3D Condition Number of the CRLB (ratio)								
Region	MSL Altitude (ft)	Approximate AGL Altitude (ft)	FTT	Independent Samples	2.5 Percentile	Median	Mean	97.5 Percentile
A	22000	19200	Teardrop	421	1197	4237	7810	35854
	7500	4700	Grid	711	53	646	810	2677
B	10000	7600	Racetrack	1683	17	628	1505	10962
	5500	3100	Racetrack	1730	117	1592	4007	24713
D	17000	16100	Racetrack	675	10	64	10838	61308
	6000	5100	Racetrack	716	38	102	154	590
Overall					17	586	3356	31078

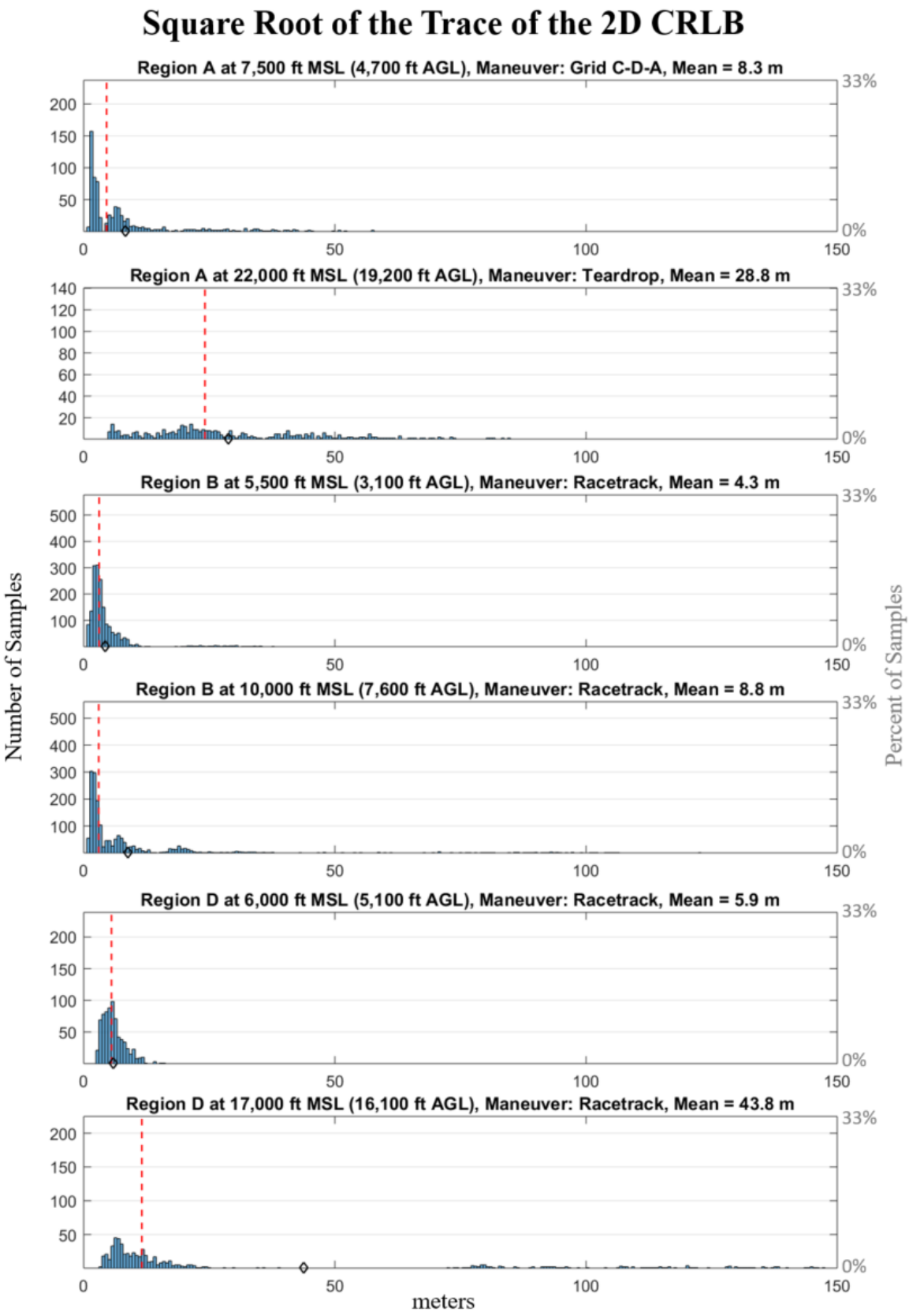

Figure E3: Square Root of the Trace of the 2D CRLB Histogram (Linear Scale)

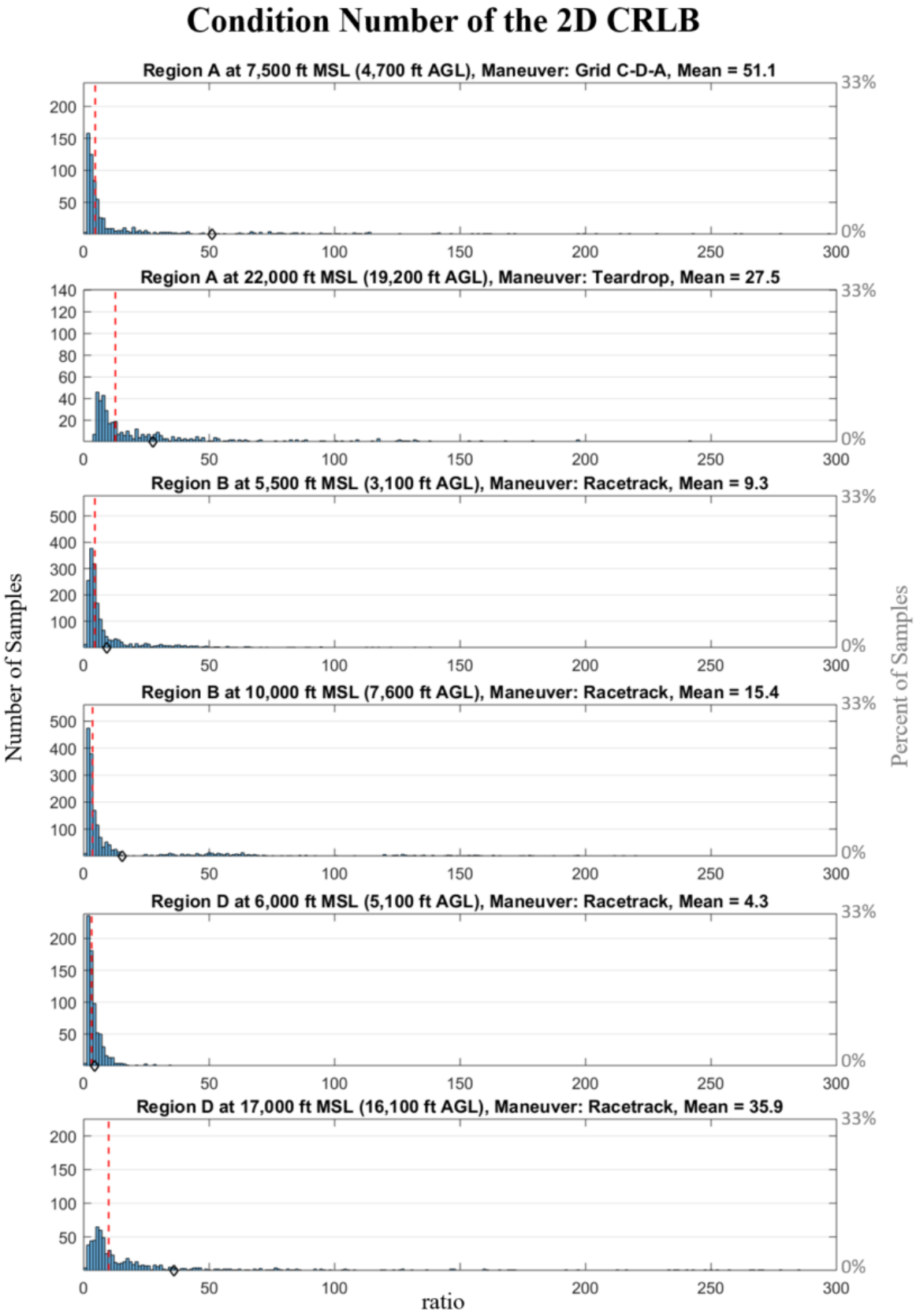

Figure E4: Condition Number of the 2D CRLB Histogram (Linear Scale)

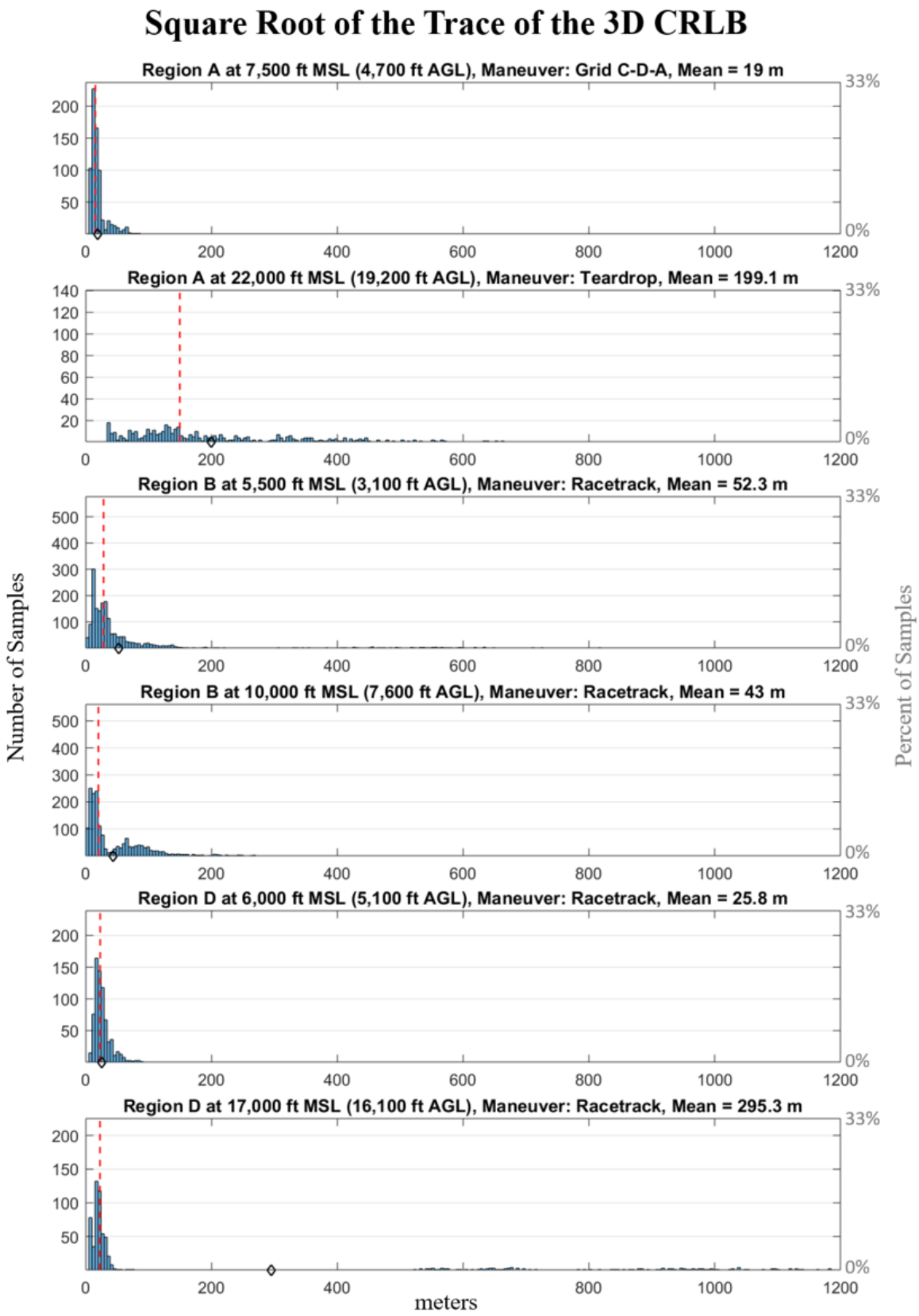

Figure E5: Square Root of the Trace of the 3D CRLB Histogram (Linear Scale)

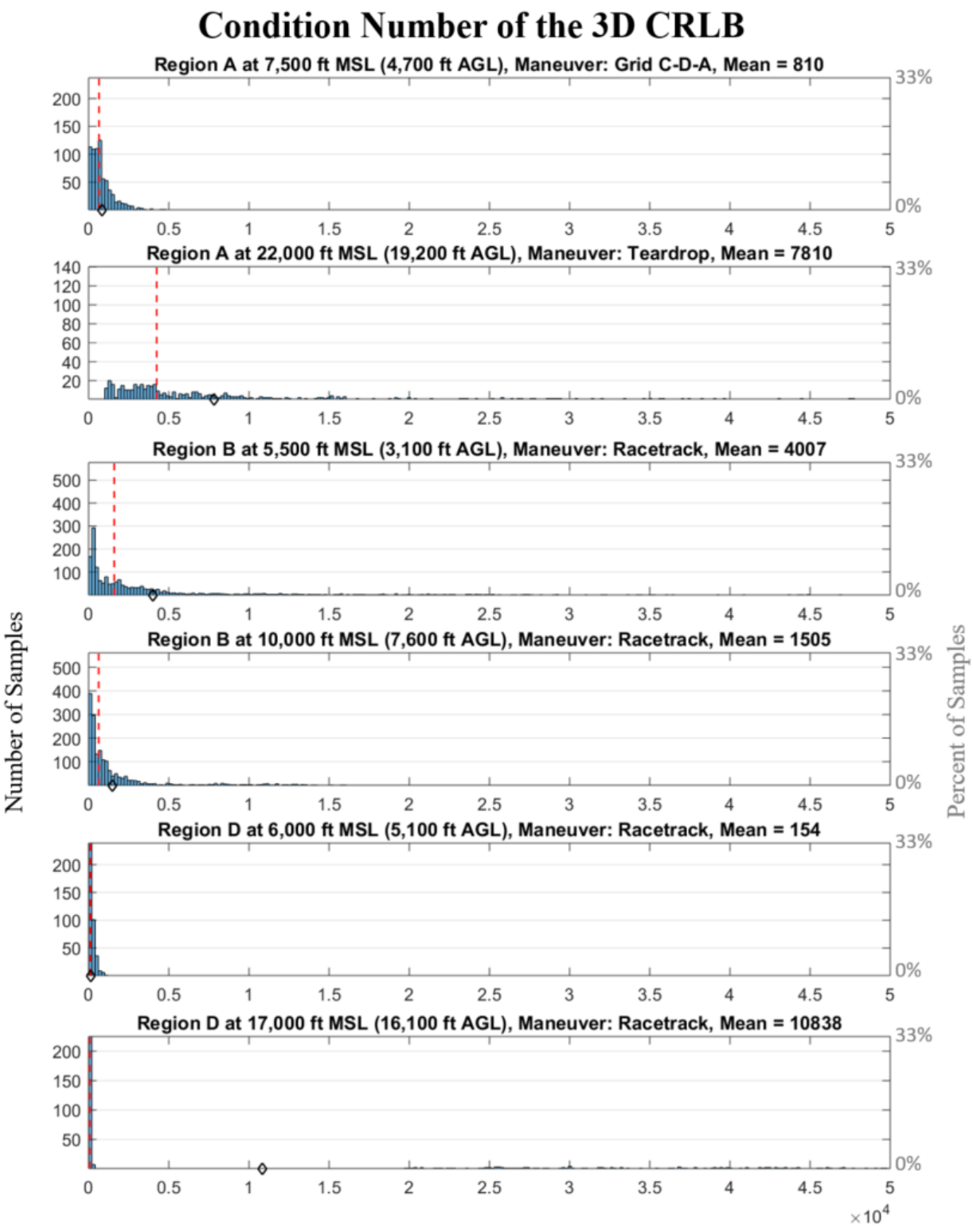

Figure E6: Condition Number of the 3D CRLB Histogram (Linear Scale)

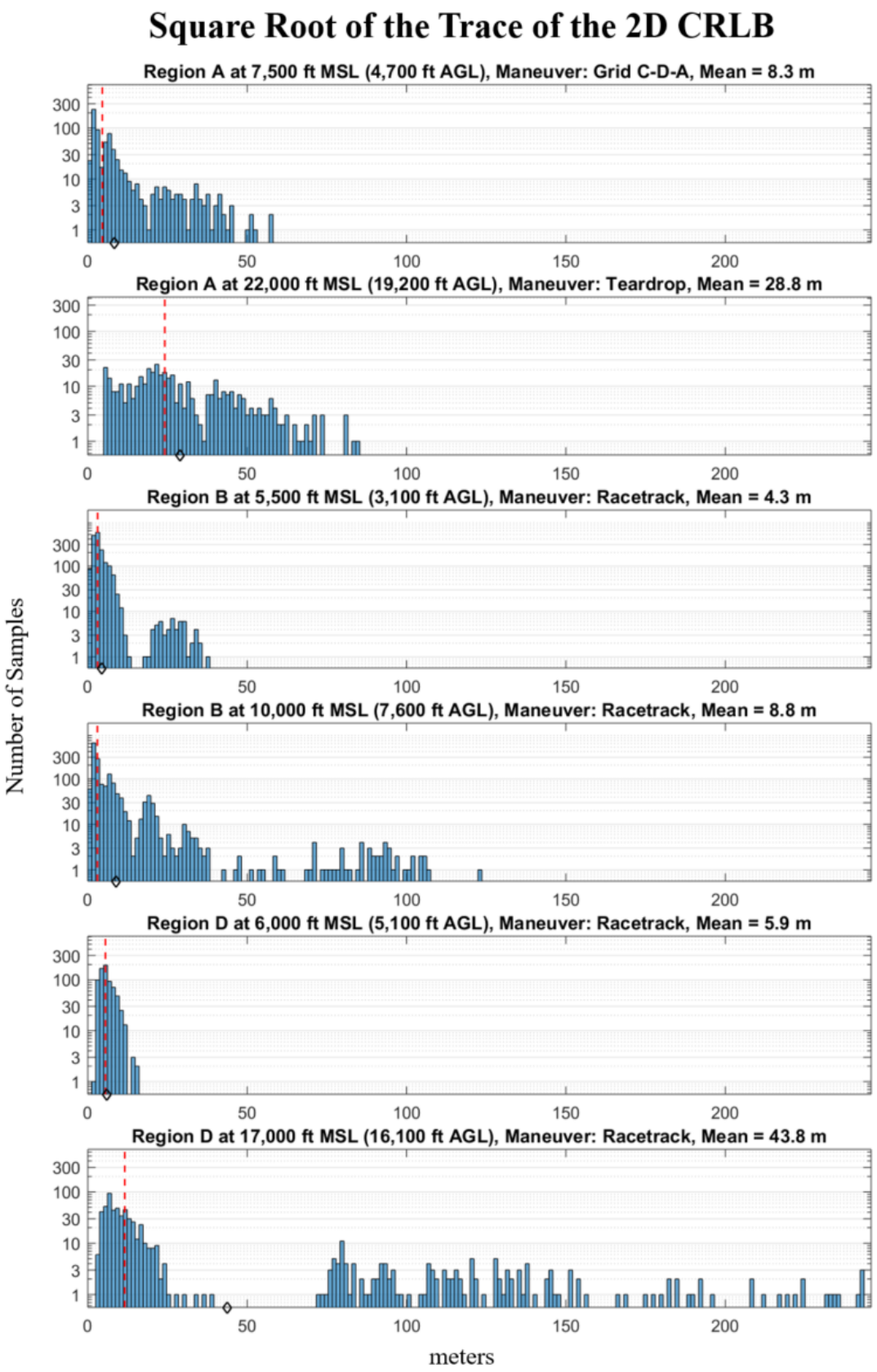

Figure E7: Square Root of the Trace of the 2D CRLB Histogram (Logarithmic Scale)

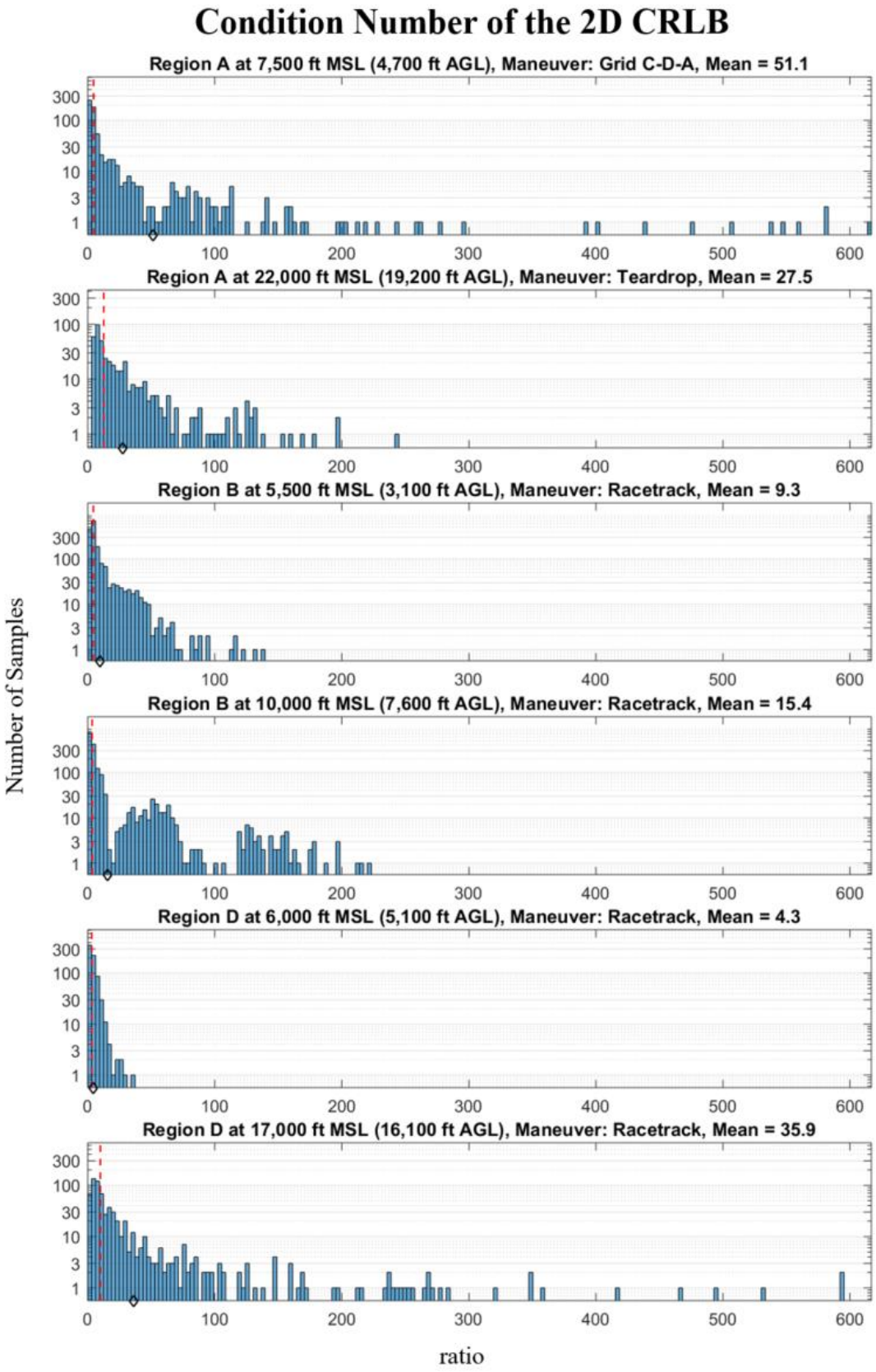

Figure E8: Condition Number of the 2D CRLB Histogram (Logarithmic Scale)

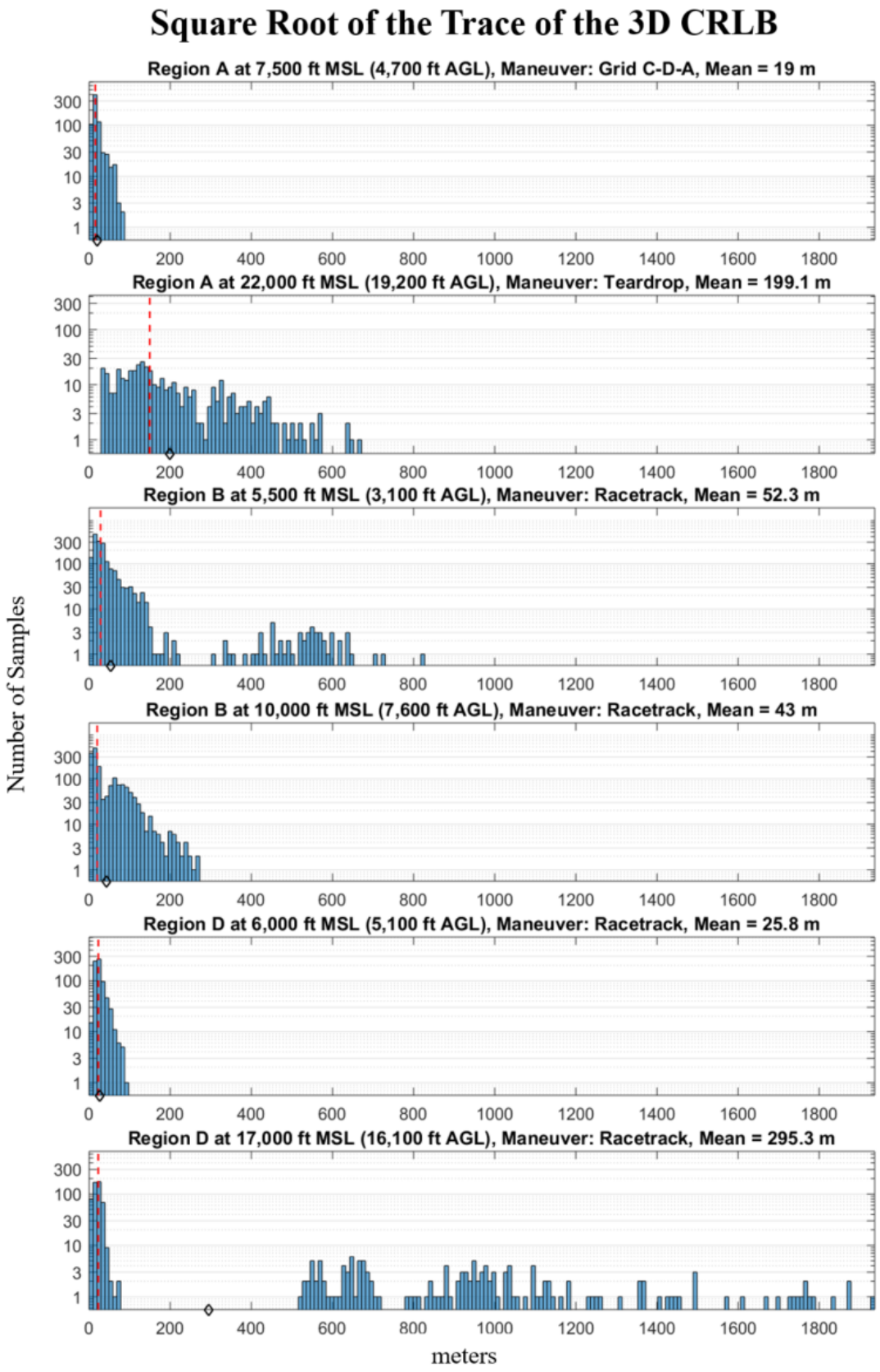

Figure E9: Square Root of the Trace of the 3D CRLB Histogram (Logarithmic Scale)

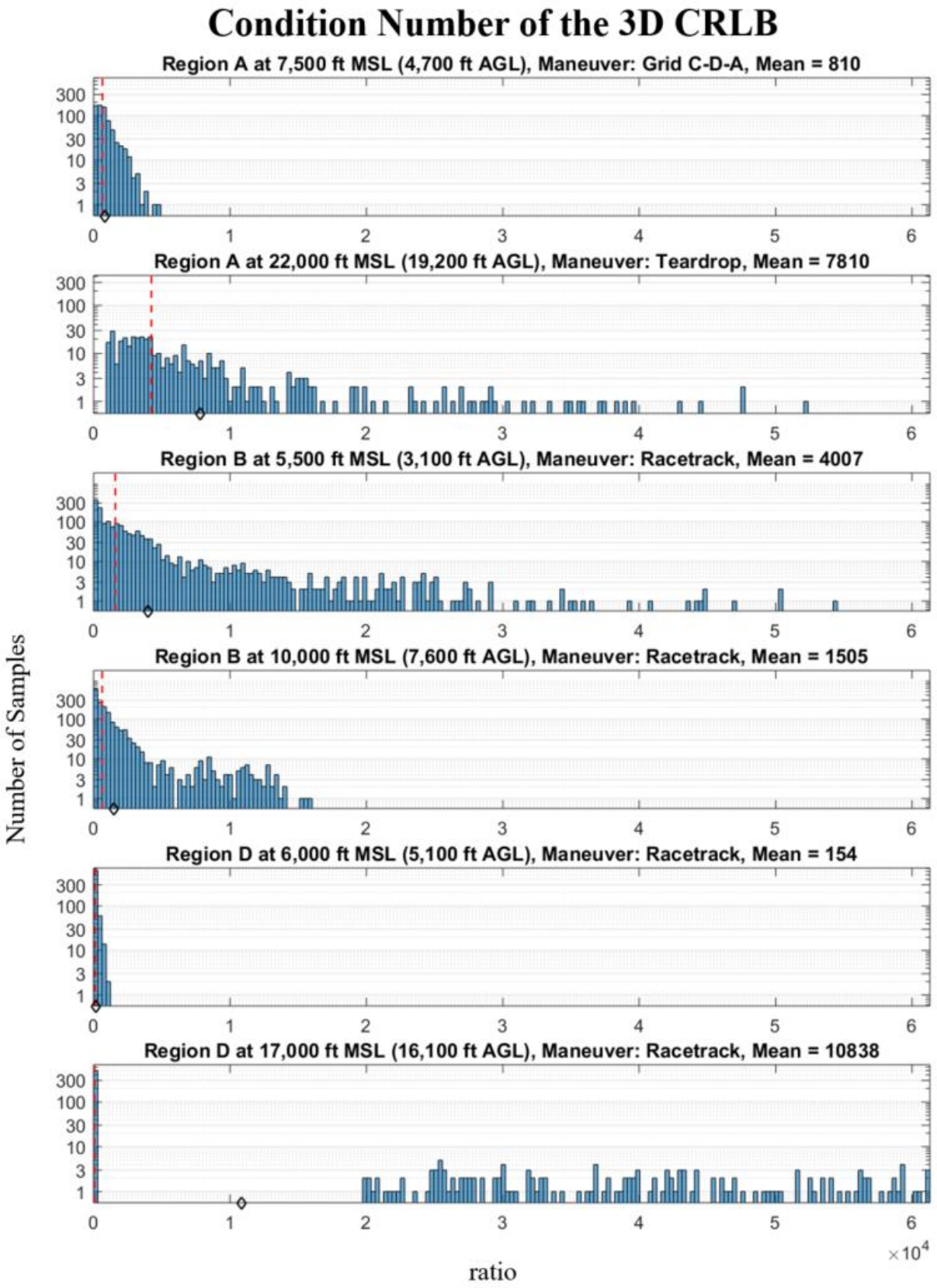

Figure E10: Condition Number of the 2D CRLB Histogram (Logarithmic Scale)

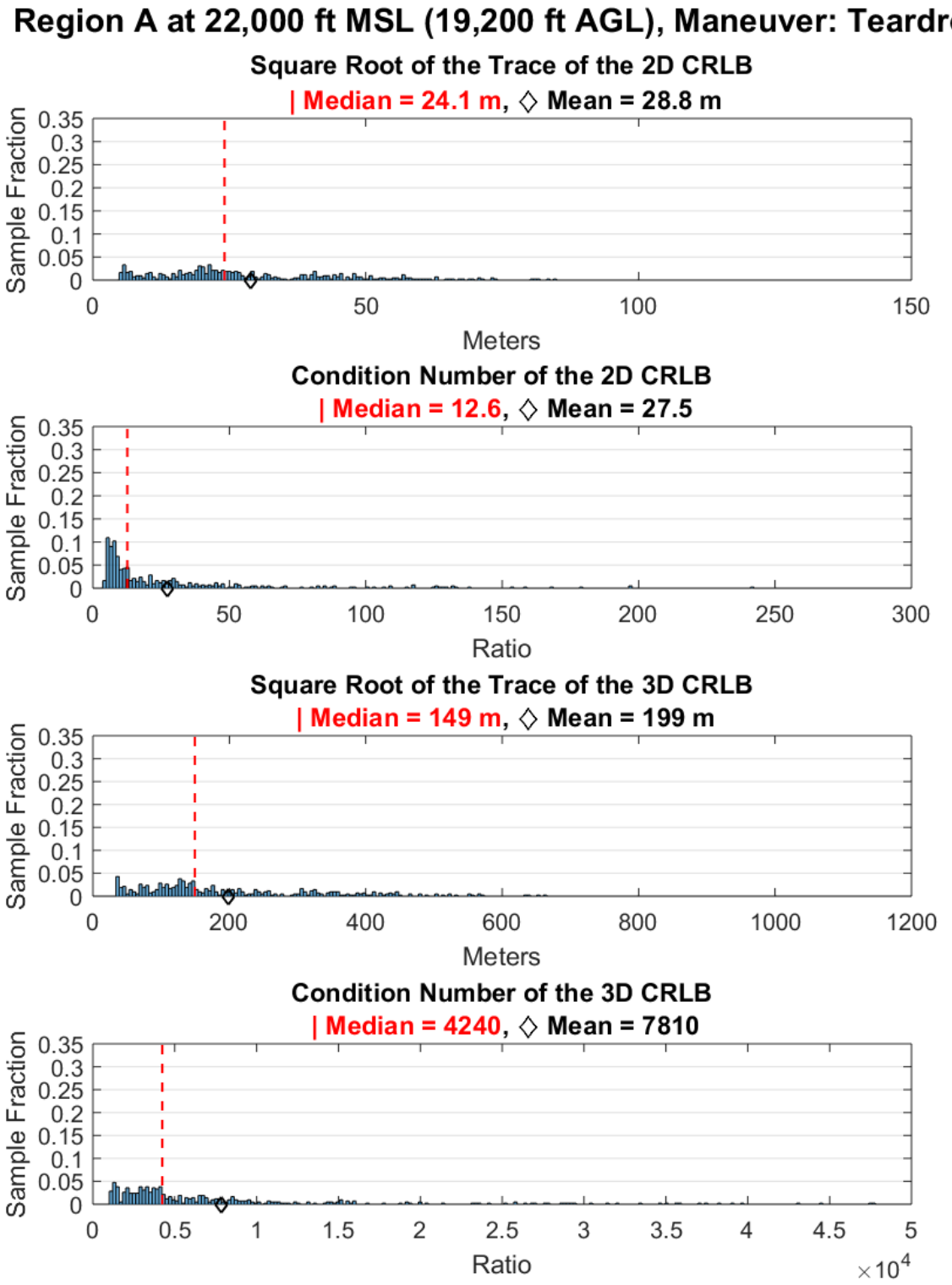

Figure E11: Metrics derived from CRLB for Region A at 22,000ft MSL

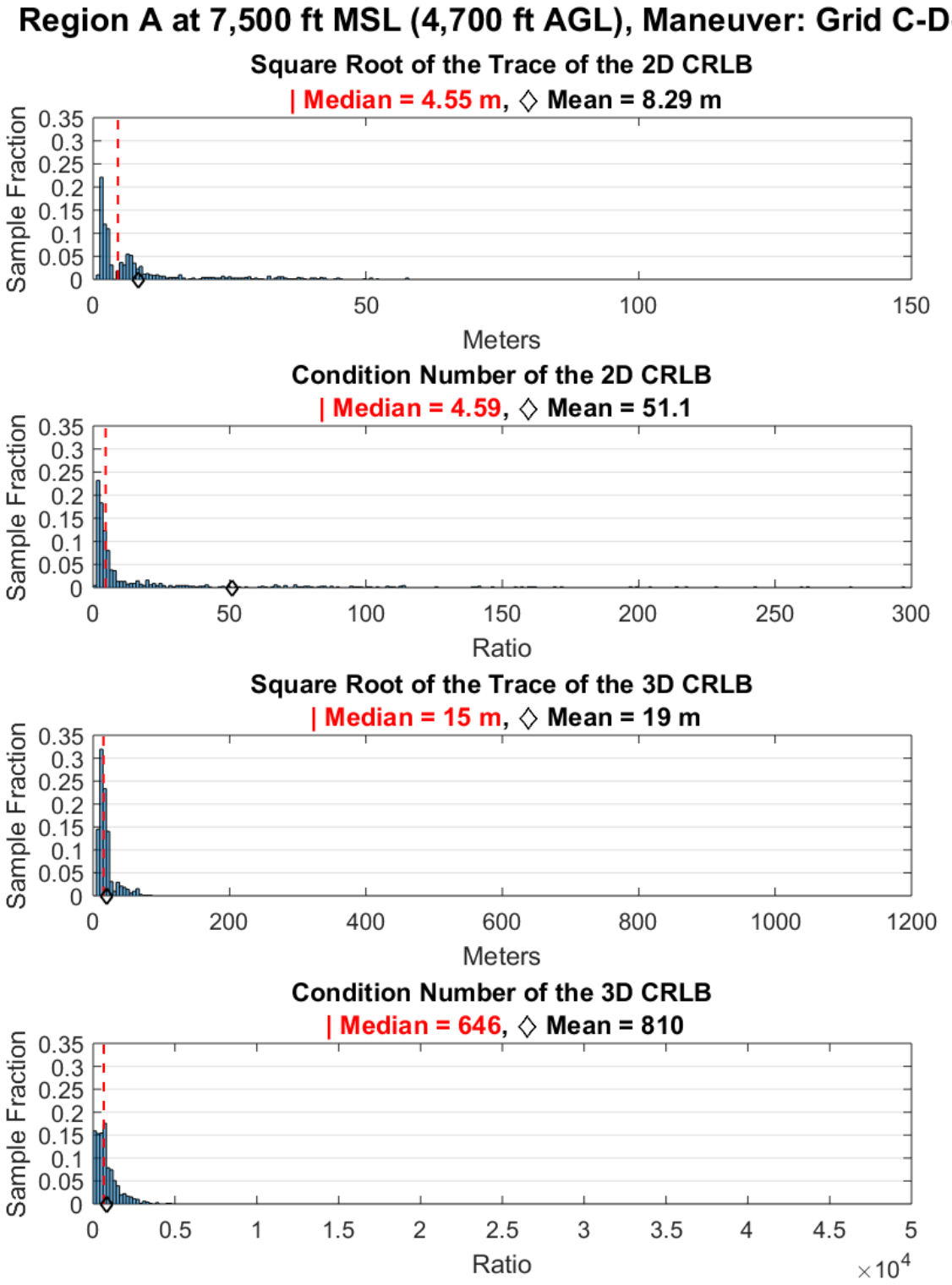

Figure E12: Metrics derived from CRLB for Region A at 7,500ft MSL

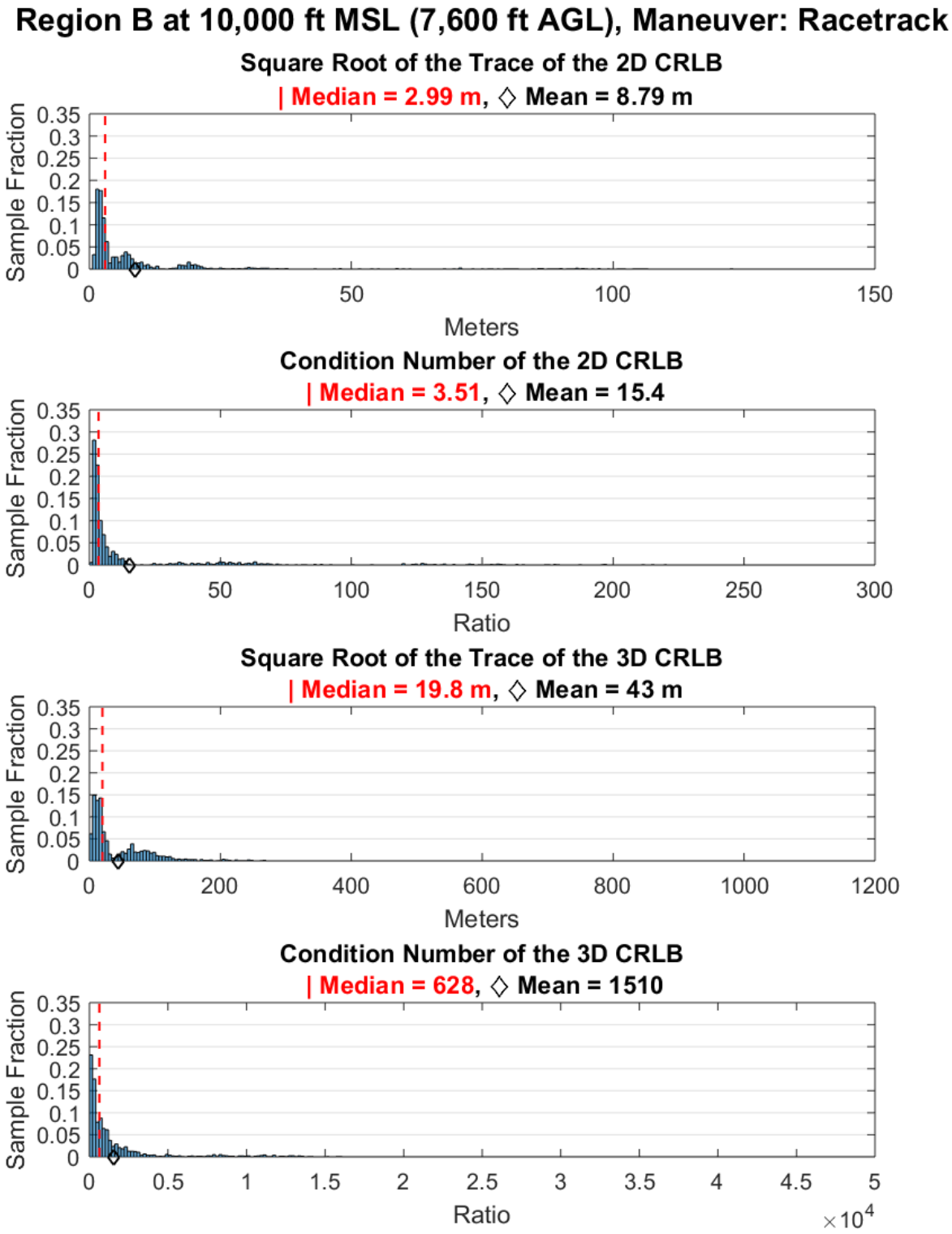

Figure E13: Metrics derived from CRLB for Region B at 10,000ft MSL

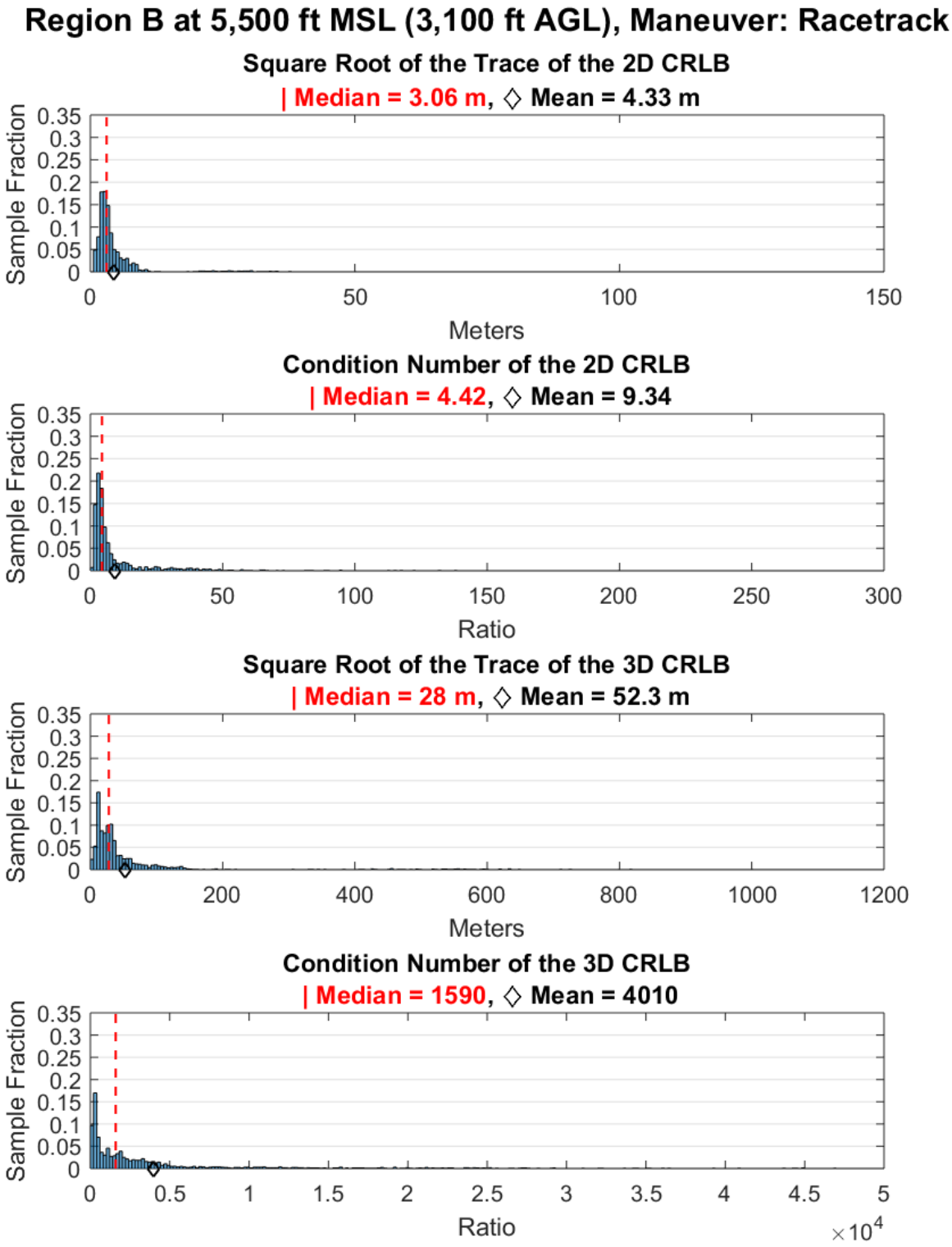

Figure E14: Metrics derived from CRLB for Region B at 5,500ft MSL

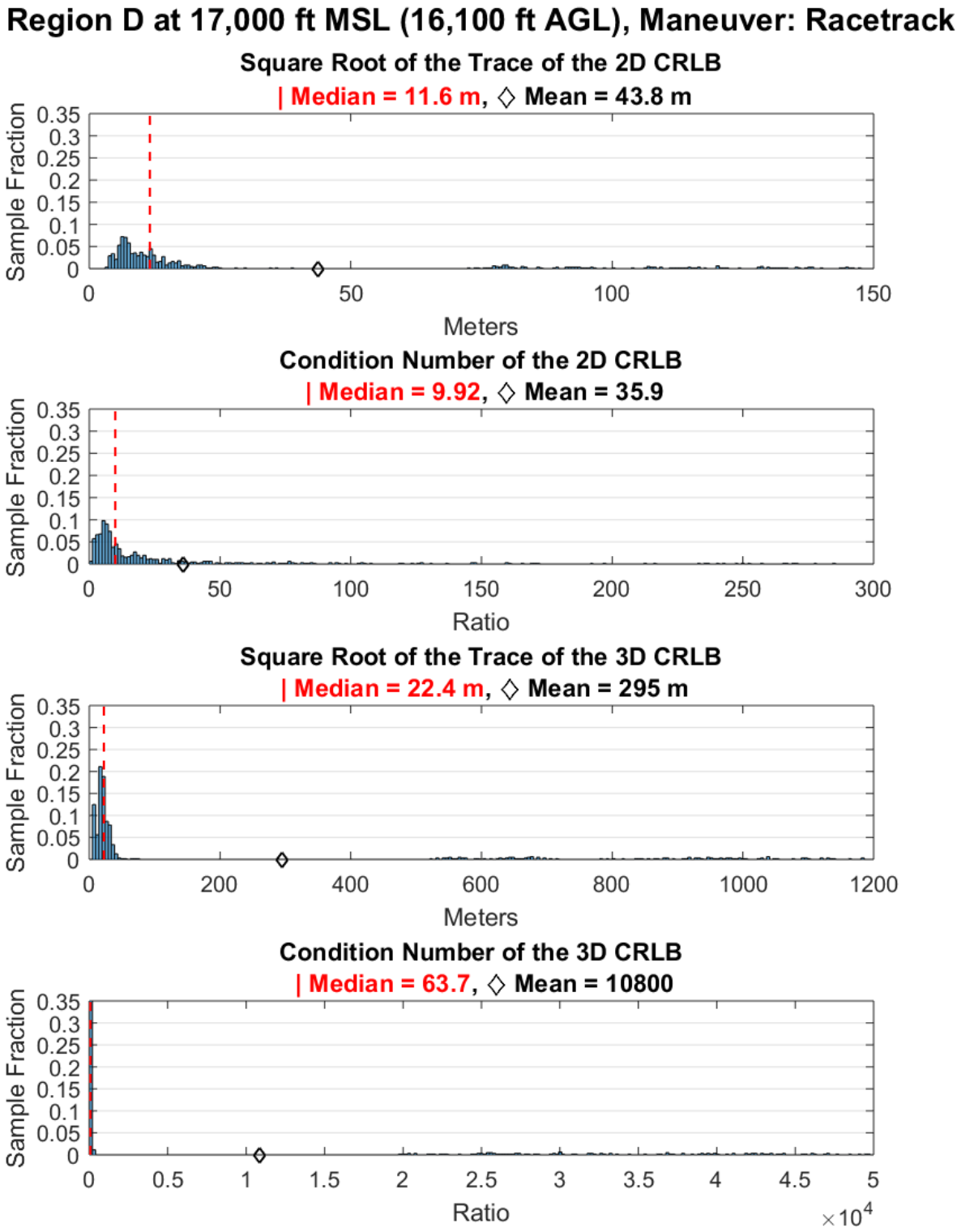

Figure E15: Metrics derived from CRLB for Region D at 17,00ft MSL

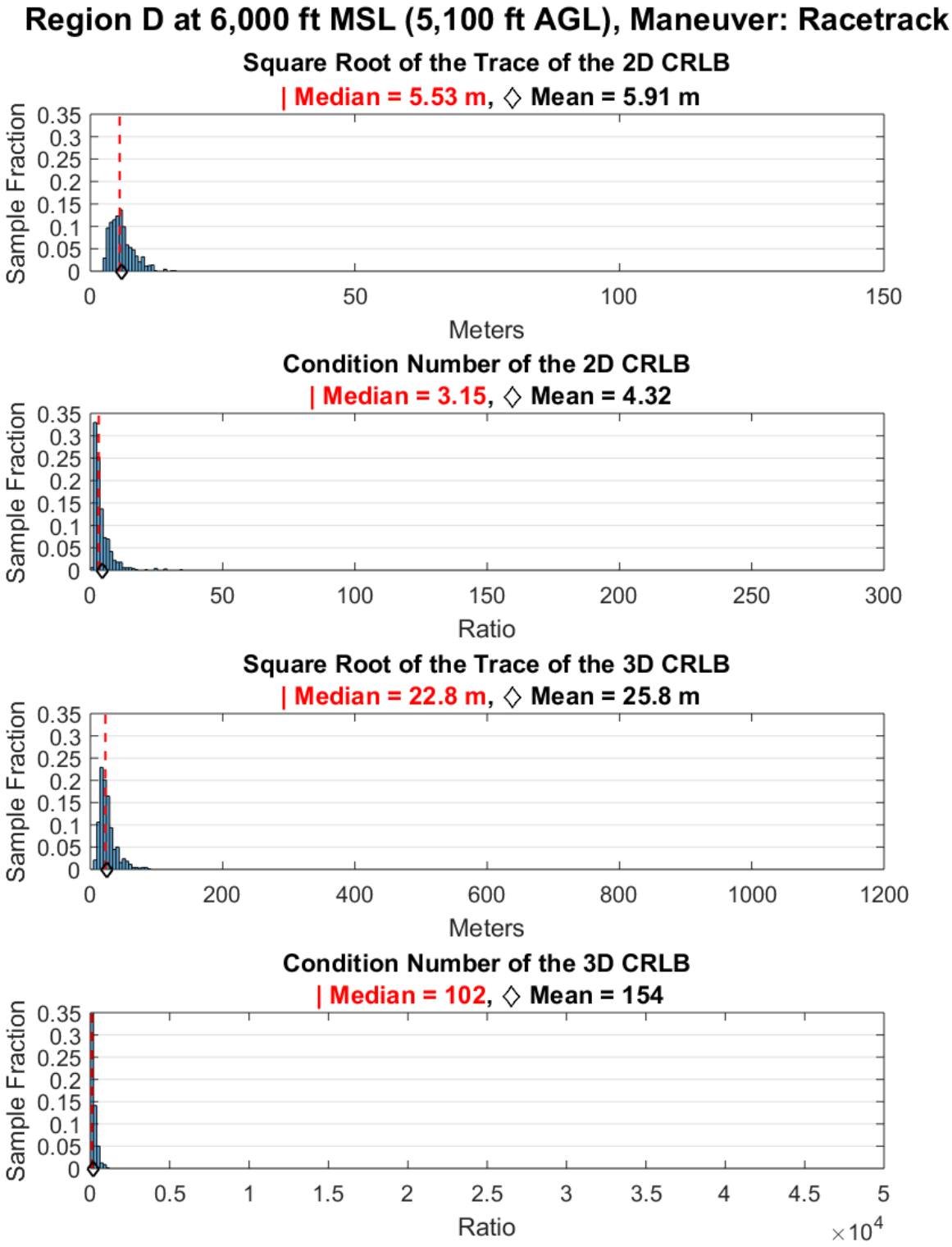

Figure E16: Metrics derived from CRLB for Region D at 6,000ft MSL

HAVE SNIFFER NAVIGATION PERFORMANCE CHARTS

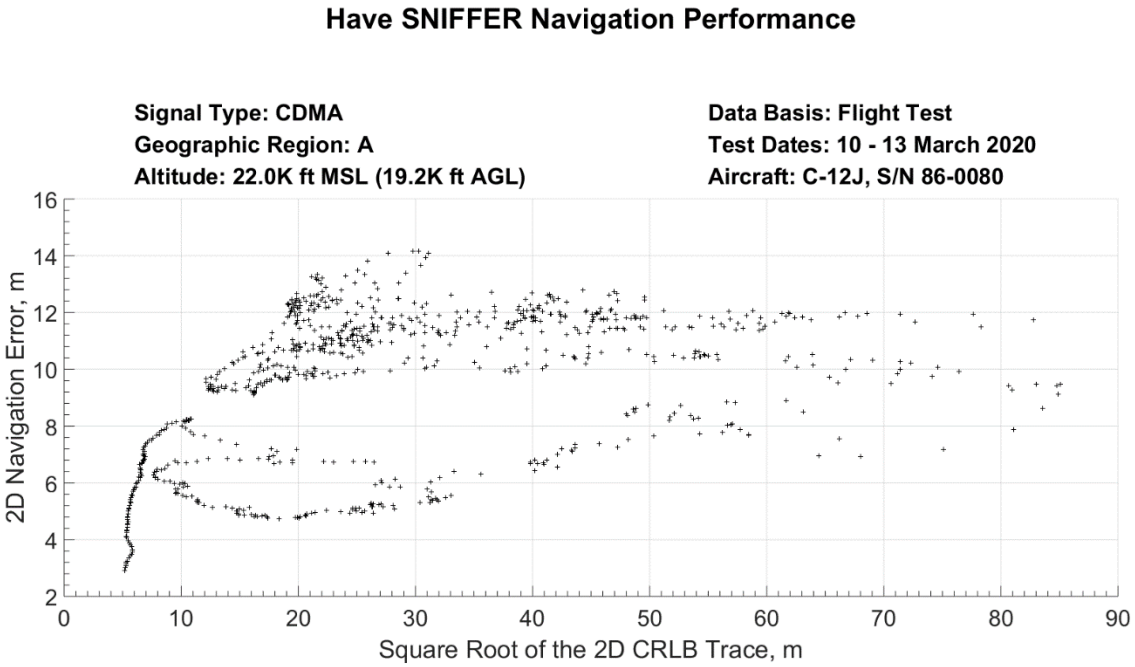

Figure E17: Have SNIFFER Navigation Performance, Region A at 22,000 ft MSL

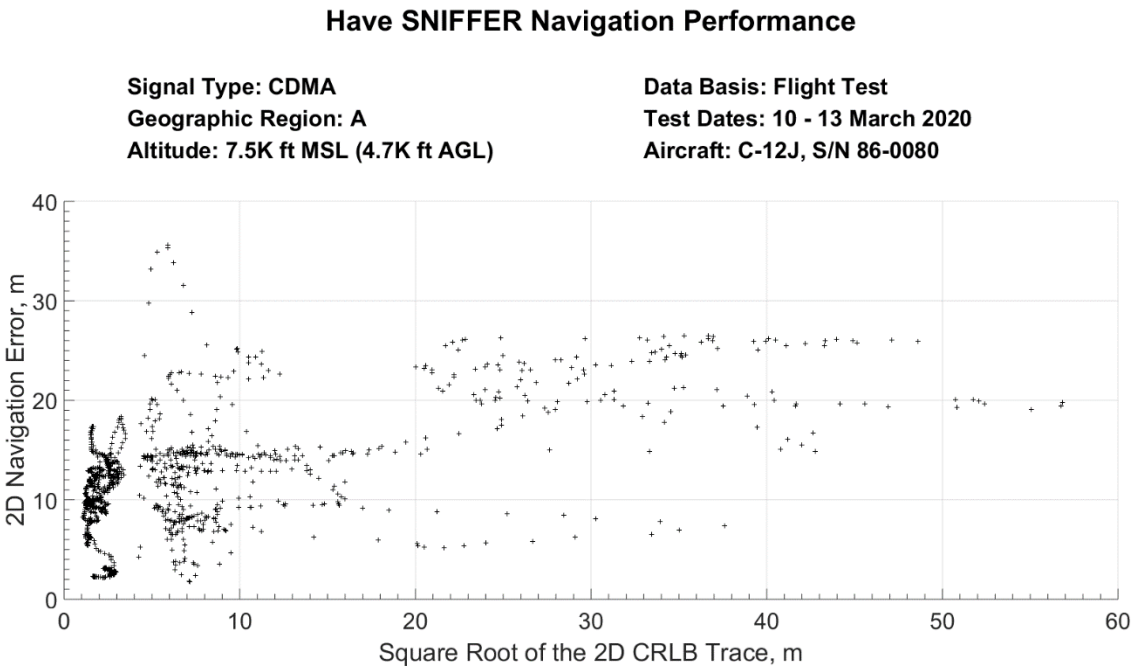

Figure E18: Have SNIFFER Navigation Performance, Region A at 7,500 ft MSL

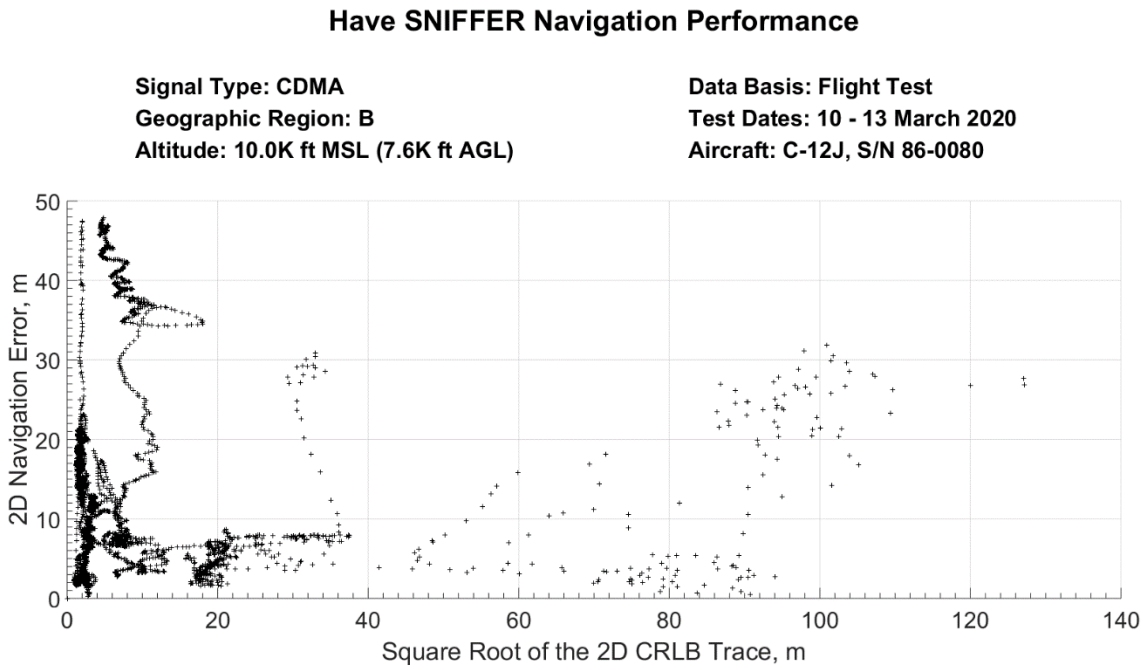

Figure E19: Have SNIFFER Navigation Performance, Region B at 10,000 ft MSL

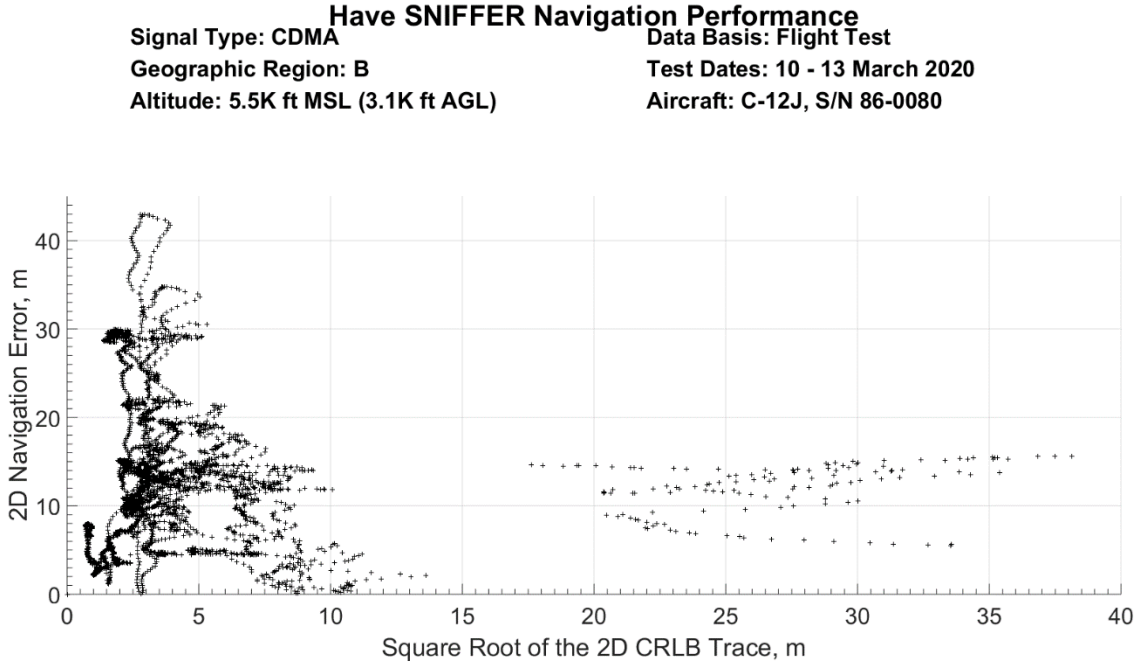

Figure E20: Have SNIFFER Navigation Performance, Region B at 5,500 ft MSL

This page was intentionally left blank.

APPENDIX F – LESSONS LEARNED

The following lessons learned were deemed important enough to share with future teams testing similar systems.

1) Hold environmental testing deadlines firm, especially if the test window is extremely limited. The system in this test passed environmental testing on timeline, however if the system had failed environmental testing, the whole test would have been jeopardized.

2) Consider the ramifications of data transfer early. If large data files are expected, ensure that the customer is ready to provide appropriately fast and capable data storage and transfer. For this test, the team had to purchase several 1TB hard drives from Best Buy the night before the test because of unforeseen data limitations. Previous communication and consideration could have prevented the last-minute flail.

3) If possible, accomplish as much testing as possible within R-2515, especially if the test requires complicated maneuvering. Coordinating with outside controlling agencies should be accomplished early, and often. A "Special Activity Alert" can be requested in advance to help coordinate with busy SoCal airspace.

   The following commercial phone numbers may prove useful for future testing:

   Joshua Approach: (661) 575-2100

   Los Angeles Center: (661) 265-8246

   Palmdale Tower: (661) 272-6730

   W.J. Fox Tower: (661) 948-0836

   SoCal Approach: (858) 537-5830

This page was intentionally left blank.

APPENDIX G – ABBREVIATIONS, ACRONYMS, AND SYMBOLS

Abbreviation	Definition	Units
2D	two-dimensional	---
3D	three-dimensional	---
4G	fourth generation	---
ADIZ	air defense identification zone	---
AFB	Air Force Base	---
AFI	Air Force Instruction	---
AFTC	Air Force Test Center	---
AFTCI	Air Force Test Center Instruction	---
AGL	above ground level	ft
ASPIN	Autonomous Systems Perception, Intelligence, and Navigation	---
BTS	base transceiver station	---
CDMA	code division multiple access	---
CFO	carrier frequency offset	---
CFR	code of federal regulations	---
CRLB	Cramér-Rao Lower Bound	---
CRPA	controlled reception pattern antenna	---
CRS	cell-specific reference signal	---
DOD	Department of Defense	---
DOP	dilution of precision	---
DTIC	Defense Technical Information Center	---
EGI	embedded GNSS/INS	---
EIAP	environmental impact analysis process	---
EKF	extended Kalman filter	---
FINS	fighter instrumentation navigation system	---
FLTS	flight test squadron	---
FTE	flight test engineer	---
FTT	flight test technique	---
GPS	global positioning system	---
GNSS	global navigation satellite system	---
GTO	general test objective	---

IAW	in accordance with	---
IMU	inertial measurement unit	---
INS	inertial navigation system	---
JON	job order number	---
KIAS	knots indicated airspeed	kts
LDTO	lead developmental test organization	---
LEO	Low-Earth orbit	---
LLF	log likelihood function	---
LLH	latitude, longitude, height	---
LTE	long-term evolution	---
MATRIX	Multichannel Adaptive TRansceiver Information eXtractor	---
MOP	measure of performance	---
MSL	mean sea level	ft
NTIS	National Technical Information System	---
OFDM	orthogonal frequency division mutliplexing	---
ONR	Office of Naval Research	---
PAR	program assessment review	---
PDF	probability distribution function	---
PN	pseudorandom noise	---
PNT	positioning, navigation, and timing	---
POC	point of contact	---
PRN	pseudo random noise	---
PRS	positioning reference signal	---
PSS	primary synchronization signal	---
PVT	position, velocity, time	---
RF	radio frequency	---
RMS	root mean square	---
RSAF	Republic of Singapore Air Force	---
SDR	software-defined receiver	---
SEP	spherical error probable	m
SLAM	simultaneous localization and mapping	---
S/N	serial number	---
SNIFFER	SOPs for Navigation In Frequency-Forbidden EnviRonments	---
SOP	signal of opportunity	---
SROT	square root of the trace	m

SSS	secondary synchronization signal	---
STO	specific test objective	---
SUT	system under test	---
TIM	technical information memorandum/meeting	---
TMP	test management project	---
T.O.	technical order	---
TOA	time of arrival	---
TP	test plan	---
TPS	Test Pilot School	---
TR	technical report	---
TS	test squadron	---
TSPI	time-space-position information	--
TW	test wing	---
UAV	unmanned aerial vehicle	---
UCI	University of California, Irvine	---
U.S.	United States	---
USAF	United States Air Force	---
U.S.C.	United States Code	---
UTSO	unit test safety officer	---
VHF	very high frequency	---
C/N_0	carrier-to-noise ratio	dB-Hz
V_r	relative velocity	m/s
Y	distribution shape coefficient	---
λ	wavelength	m
v	Doppler shift	Hz
ρ	pseudorange	m

This page was intentionally left blank.

APPENDIX H – DIGITAL APPENDIX

Raw data from the SUT and the FINS truth source data from the C-12J are available by contacting the USAF Test Pilot School.

At the root level, the Digital Appendix contains one Excel file and two folders. The Excel file, titled "BTS Locations," contains the location of the BTSs detected by the SUT in LLH coordinates. The two folders are titled "CN0 vs Altitude Data" and "CRLB & Navigation Data."

There are two Excel files inside "CN0 vs Altitude Data," one containing CDMA C/N_0 vs altitude and one containing LTE C/N_0 vs altitude.

There are four subfolders inside "CRLB & Navigation Data," one corresponding to each sortie flown. Each subfolder name also describes the region(s) where that day's sortie was flown. Within each subfolder are at least two files.

One of these is an Excel file titled "FINS," containing the truth source data from the C-12J. The header row gives a description of each column, as well as the units.

The other file or files within each subfolder contain the observables collected by the SUT and the post-processed navigation solution. These are .mat files with descriptive names representing the region, altitude, and type of maneuver. Each .mat file includes the following:

- emitter_locations_NED: 3x5 matrix of tower locations expressed in NED, each column corresponding to a tower location
- tVec: Reference time vector. This vector is a subset of the FINS time vector (in seconds of day, for that particular day)
- observables: 1xn cell array whose n^{th} element contains observables to the n^{th} emitter
    - observables{n}: Kx4 matrix containing time vector and observables to emitter n. Each row corresponds to one particular time-step and K is the total time index. The observables{n} matrix's columns are as follows:
        - Time vector (seconds of day)
        - Pseudorange (m)
        - Carrier-to-noise ratio (dB-Hz)
        - Doppler frequency (Hz)
- LLA_to_NED_reference_point: LLH of the reference point for NED transformation, with altitude in meters
- C12_estimated_position_NED: SOP-only based estimate of the C-12 position expressed in NED (initialized with FINS data)
- C12_estimated_position_Cov_NED: Kx3 matrix containing covariance ($\sigma_{11,}$ $\sigma_{12,}$ and σ_{22}) at time step K

This page was intentionally left blank.

APPENDIX I – DISTRIBUTION LIST

Onsite	Number of Copies		
	E-mail	Digital	Paper
TPS/CT Attn: Mr. David Vanhoy 220 S Wolfe Ave Edwards AFB CA 93524	0	1	0
TPS/ED Attn: Lt Col Juan Jurado 220 S Wolfe Ave Edwards AFB CA 93524	0	1	0
Edwards AFB Technical Research Library Attn: Darrell Shiplett 307 E Popson Ave Edwards AFB CA 93524	0	0	2
AFTC/HO Attn: AF Test Center/HO Mailbox 305 E Popson Ave Edwards AFB CA 93524	0	1	0
Offsite			
Defense Technical Information Center Submit per DTIC procedures Attn: DTIC-O 8725 John J. Kingman Rd, Ste 0944 Ft Belvoir VA 22060 Email: aq@dtic.mil	1	0	0
University of California, Irvine Samueli School of Engineering Attn: Dr. Zak (Zaher) M. Kassas 4200 Engineering Gateway Building, Room 3233 Irvine, CA 92697 Email: zkassas@uci.edu	1	0	0
Total	2	3	2

This page was intentionally left blank.